UNIVERSITA' DEGLI STUDI DI PAVIA

FACOLTA' DI INGEGNERIA
DIPARTIMENTO DI INGEGNERIA INDUSTRIALE E DELL'INFORMAZIONE

DOTTORATO DI RICERCA IN BIOINGEGNERIA E BIOINFORMATICA
XXX CICLO - 2017

DOES THE MODELING STRATEGY MAKE THE DIFFERENCE IN PHARMACOMETRICS? SOME EXAMPLES IN ONCOLOGY AND INFECTIOUS DISEASES

PhD Thesis by
LETIZIA CARRARA

Advisor:
Prof. Paolo Magni

PhD Program Chair:
Prof. Riccardo Bellazzi

A MariAngela e Giambattista

Acknowledgements

The very first acknowledgement goes to my PhD advisor, Prof. Paolo Magni, for inspiring me to work hard every day and for always giving me his valuable help. I am very grateful to you for the great opportunity to pursue this PhD.

A special thank goes to Prof. Oscar Della Pasqua, who gave me the chance to spend six months at University College of London and work in a very formative environment. You led me into the system pharmacology! Thanks to Frank Kloprogge, who wrote a very exciting and challenging project -I really enjoyed it- and thanks to Donato Teutonico for sharing his knowledge on PBPK models. Thank you to all the colleagues of Oscar's team. Morris, it was a pleasure to exchange our views on PBPK; Salvo, you definitely know the mystery of R codes; Sean and Paul for letting me be a part of the team.

Of course, a very big thank to all the BMS Lab: Prof. Riccardo Bellazzi; Prof. Giuseppe De Nicolao; Lorenzo, for his great suggestions, Elisa my english mate and colleague in the DDMoRe project, the two mathematicians Silvia L. and Elena, Silvia G. for the very deep

lung knowledge; Maiara, for the work we did together; Italo, for his irreplaceable experience. Thanks to Susanna, Ilaria, Roberta, Nicola, Ivan, Ettore, Elisabetta, Francesca, Massimo, Maria Luisa, Enrica, Giulia.

It is an honor to have Massimo Cella and Stefano Zamuner as reviewers of this PhD thesis, thank you.

There are no words to give thanks to Lorenzo, always at my side. You are my better half!

Finally, the biggest thank goes to my parents, MariAngela and Giambattista, for everything you have done in these years. This thesis is for you!

Abstract (Italiano)

L'utilizzo di modelli matematici in grado di descrivere e predire sia la farmacocinetica (pharmacokinetics, PK), ossia cosa il corpo fa al farmaco, sia la farmacodinamica (pharmacodynamics, PD), ossia cosa il farmaco fa al corpo, è fondamentale durante tutte le fasi di sviluppo di un farmaco. Tra le altre cose, questi modelli permettono di identificare i candidati più promettenti durante lo sviluppo preclinico, guidano la scelta del dosaggio da somministrare durante le prime sperimentazioni cliniche, permettono di valutare l'efficacia clinica del trattamento e di simulare *in silico* gli effetti che si potrebbero ottenere con protocolli di somministrazione differenti.

Esistono diversi strumenti di modellizzazione con caratteristiche diverse e specifici campi di applicazione. Da un lato si sono modelli con una forte componente meccanicistica, come i modelli di farmacocinetica basati sulla fisiologia, detti modelli Physiologically Based Pharmacokinetic (PBPK). Questi modelli integrano le informazioni sull'anatomia e la fisiologia dell'organismo con le proprietà fisico-chimiche della molecola in questione. Dall'altro ci sono modelli caratterizzati da una scarsa componente meccanicistica come i modelli classici di

farmacocinetica/ farmacodinamica (PK/PD). Infine esisitono modelli in cui la componente di farmacocinetica non è esplicitamente modellizzata (K/PD).

Il quesito scientifico alla base di questo lavoro di tesi è se esiste un approccio modellistico "ottimo" per affrontare un dato problema. In quest'ottica infatti deve essere sempre tenuta in considerazione la frase di George Box: "Tutti i modelli sono sbagliati, ma alcuni sono utili". Lo scopo di questo lavoro di tesi è stato investigare in alcuni casi di studio: i) l'adeguatezza di un particolare approccio modellistico allo specifico problema in termini di struttura del modello, dati necessari e/o disponibili, ipotesi di lavoro e robustezza dei risultati alle ipotesi fatte; ii) la dipendenza delle conclusioni dall'approccio adottato.

Nel Capitolo 1 dopo una breve introduzione sul processo di sviluppo di un nuovo farmaco e sul ruolo ricoperto dalla modellizzazione matematica, sono state illustrate nel dettaglio le caratteristiche delle tipologie di modelli qui considerati per descrivere la farmacocinetica e la farmacodinamica. Successivamente è stato formulato il quesito scientifico alla base di questo lavoro di tesi ed è stata illustrata la metodologia seguita per fornire una risposta.

Nel Capitolo 2 sono state valuate le capacità predittive dei modelli Whole-Body (WB) PBPK. Per questo scopo sono stati simulati sei scenari caratterizzati da un livello crescente di informazione e dati disponibili per lo sviluppo del modello, partendo dai dati dei soli esperimenti *in vitro*, fino ad arrivare ai dati di sperimentazioni cliniche. Questi scenari sono poi stati utilizzati per vedere l'accuratezza delle predizioni dell'esposizione sistemica in funzione dai dati disponibili. L'Etambutolo (EMB), uno degli antibiotici usati per il trattamento di prima linea della tubercolosi polmonare, è stato usato come caso di studio.

Quando la caratterizzazione fisiologica del soggetto malato non è disponibile, come nel caso di malattie oncologiche, è necessario ricorrere ad approcci meno meccanicistici, come i modelli PK/PD e K/PD, per trarre importanti conclusioni sull'efficacia dei candidati farmaci.

Nel Capitolo 3 sono stati analizzati e discussi i modelli matematici attualmente utilizzati in campo oncologico nella fase preclinica e traslazio-nale.

Nel Capitolo 4 è stata analizzata la dipendenza dei risultati dalla particolare strategia modellistica utilizzata, prendendo come caso di studio la predizione dell'effetto della somministrazione combinata di due farmaci oncologici (Sunitinib e Irinotecan) in topi xenograft.

Nel Capitolo 5, nel tentativo di aggiungere una componente meccanicistica ai modelli PK/PD, è stata misurata la concentrazione di farmaco nel tessuto tumorale di ratti xenograft. La crescita del tumore e l'effetto del farmaco citotossico Etoposide sono stati modellizzati con opportuno modello di PK/PD. La potenza del farmaco è stata quindi valutata considerando sia la sua concentrazione nel plasma -come negli approcci tradizionali- sia la concentrazione nel tumore, per discutere la bontà dell'uso della concentrazione plasmatica come surrogato di quella nei sito di azione.

Nel Capitolo 6 sono riportate le conclusioni generali.

Abstract (English)

The use of mathematical models to describe and predict the pharmacokinetics (PK), i.e., what the body does to the drug, and the pharmacodynamics (PD), i.e., what the drug does to the body, is fundamental across all the phases of the drug development process. Among the other things, these models allow to identify the most promising candidates during the preclinical studies, lead the dose selection for the First-In-Human (FIH) clinical trials, and enable to evaluate the effectiveness of a treatment and to simulate *in silico* different administration protocols.

Nowadays, there are several modeling tools, each of which characterized by different features and specific applicability fields. There are models with a strong mechanistic base, such as the Physiologically Based Pharmacokinetic (PBPK) models, which integrate the information on organism anatomy and physiology with the physicochemical drug properties. There are also models with a poor mechanistic base, such as the standard pharmacokinetics/pharmacodynamics (PK/PD) models. Finally, there are models in which the pharmacokinetics is not explicitely modeled (K/PD).

The scientific question of this thesis is whether an "optimal" modeling strategy exists for a given problem. In this perspective, the sentence of George Box: "All models are wrong, some are useful" should be kept in mind. *Via* some case studies, this thesis aimed to investigate two aspects: i) the suitability of a certain modeling strategy for a given problem in terms of model structure, available/required data, working hypotheses and the robustness of the results with respect to the assumptions made; ii) the dependency of conclusions from the adopted modeling approach.

In Chapter 1, to set the scene, a brief introduction on both the drug discovery and development process and the importance of mathematical modeling throughout all the phases of this process was given. The features of the modeling strategies considered in this work to describe the pharmacokinetics and the pharmacodynamics were outlined in details. Subsequently, the scientific question underlying this work of thesis was discussed together with the methodology used to address it.

In Chapter 2, the predictive performance of the Whole-Body (WB) PBPK models were investigated. To this aim, six *what-if* scenarios, in which data were added progressively into model development, starting from *in vitro* and animal experiments, up to human clinical trials, were created. Via these scenarios, the accuracy of the exposure predictions in dependence of the available data was evaluated. Ethambutol (EMB), one of the first-line antibiotics used for the treatment of pulmonary tuberculosis, was used as paradigm drug.

When the physiological characterization of the subject with the disease is not sufficient or not available, as in the oncology fields, less mechanistic approaches, i.e., the PK/PD and the K/PD models, were used to draw conclusions on the effectiveness of candidates.

In Chapter 3 the most important models currently used for cancer drug discovery were surveyed.

In Chapter 4 the dependency on the results from the specific modeling strategy was investigated using as a case study the predicted effect of two anticancer drug combination (Sunitinib and Irinotecan) in xenograft mice.

In Chapter 5 in the attempt to be more mechanistic, additional details on drug behavior were added by considering drug concentration profiles not only in plasma but also into tumor tissue.

In Chapter 6 overall conclusions were reported.

Contents

List of Figures

List of Tables

Chapter 1

Introduction

Drug discovery and development is a long, complex, expensive and full of risk process. Drugs typically take 12 years from the initial discovery stage to reach the market, with an estimated cost of £1.15bn per drug [1]. A lot of techniques have been adopted to improve the efficiency of this process and to reduce the attrition rate, i.e., the percentage of candidates which have been discarded throughout the entire process. Mathematical modeling, aiming to characterize the safety and efficacy of a new drug, has been recognized as an essential instrument during all the stages of the discovery and development process, and the so-called **Model Informed Drug Development (MIDD)** has become a fundamental process in pharmaceutical companies [2].

However, an accurate and adequate choice of modeling strategy is of paramount importance: the modeling approach to be adopted is directly related not only to the scientific question to address, but also to i) the available data, ii) the particular stages of drug discovery and development process, iii) the level of knowledge at the beginning of the modeling exercise. In this chapter, the entire phase of the drug

discovery and development will be illustrated. Then, the MIDD will be introduced and some modeling techniques will be presented. Pro and cons of each modeling strategy, as well as their field of application, will be discussed. Finally, the scientific questions underlying the work presented in this thesis were discussed together with methodological approaches used to address them.

1.1 Drug discovery and development

The drug discovery process can be divided into four sequential steps: "target identification", "hit identification", "hit to lead" and "lead optimization". In the target identification, an easy-to-reach molecular target (protein, enzyme, receptor or hormone) associated with a potential therapeutic response is selected. Subsequently, in the hit identification phase, the molecules interacting with the target are identified ("hits"). Hits are required to be easy-to-edited to act both on toxicity and formulations. In the next stage (hit to lead), lead compounds are identified starting from the selected hits and optimized during the lead optimization step generating candidates. If one or more candidates are considered promising, i.e, effective and safe, new investigations will be performed. The drug discovery process has therefore terminated, and the drug development process has just started.

In the preclinical phase *in vitro* and *in vivo* assays are performed to assess if the candidates have the required properties. *In vitro* experiments are usually used to assess physicochemical drug properties, such as molecular weight, solubility, permeability, plasma protein bindings, acid/basic nature, pKa, etc. In some cases, also the pharmacodynamics (PD), i.e., the effect of the candidates under study on a certain population of cells/bacteria can be evaluated. When *in vivo* experi-

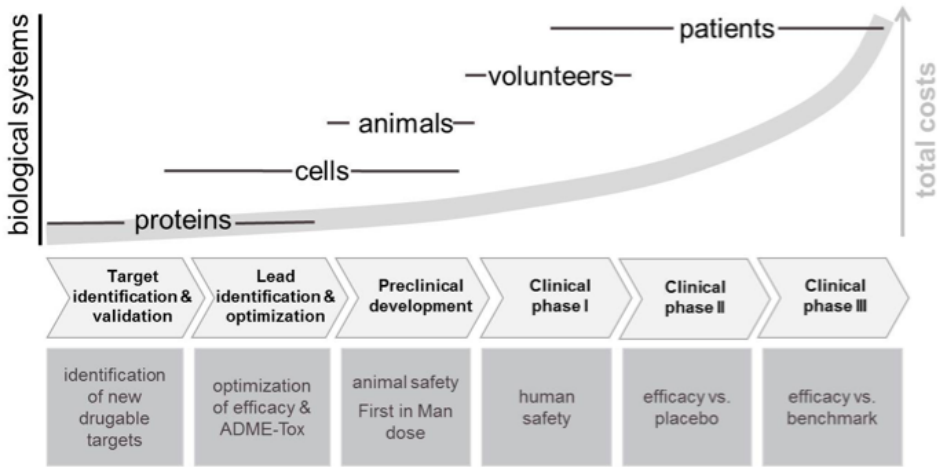

Figure 1.1: **Drug development process.** Figure taken from [3].

ments are performed, candidates are administered to a small number of animals, usually mice, rats or monkeys, to investigate their toxicity, pharmacokinetic (PK[1]) and pharmacodynamics (PD). Different doses, reflecting in different drug exposures, are usually tested to understand which is the compromise in terms of safety and efficacy. The information collected in this phase are integrated and used to predict the behavior of the drug in men and to select the dose(s) to be administered in First-In-Human (FIH) studies.

Phase I studies involves 20 to 100 people (healthy volunteers or patient for anticancer drugs) and lasts several months. The purpose of these studies is to assess drug safety, i.e., starting and maximum tolerated doses (MTD), and candidates PK to allow the definition of

[1]usually indicated with the acronym ADME: Absorption, Distribution, Metabolization, Elimination.

the safe dose range in human. Approximately 70% of the candidates move to the next phase [4].

In phase II studies up to several hundred of patients are enrolled. In this phase, lasting at least 3 years, both efficacy and short to medium term side effects are evaluated. The optimal doses and schedules at which drug elicits its action are identified. Approximately 33% of the candidates examined in this phase move to the next phase [4].

Phase III studies aim to confirm drug efficacy and to monitor adverse reactions on a larger scale. Thanks to the large number of patients enrolled (from 300 to 3000), results are more likely to show the equivalence, non-inferiority or superiority of the new therapy with respect to a comparator (standard-of-care or, more rarely, placebo). The long duration of this phase (1-4 years) allow to detect long-term or rare side effects undetected in Phase II. It has been estimated that the 25-30% of the candidates examined in this phase move to the next phase [4].

If evidences have shown that the drug is safe and effective for the intended use, regulatory agencies -the The Food and Drug Administration (FDA) in the USA and the European Medicine Agency (EMA) in the Europe- make a decision to approve the drug. Even following the launch of the new drug on the market, phase IV (pharmacovigilance) studies are conducted to monitor drug safety and efficacy. A general overview of the entire drug discovery and development process was reported in Figure 1.1.

As just discussed, the bottleneck is not in the discovery but in the development phase. Rising costs, mainly due to the required clinical trials and the complexity to interpret key findings, are not counterbalanced by the number of the drugs achieving the market. Among

the other measures proposed to improve the efficiency of the process, a smarter use of the modeling approach has been advocated.

1.2 Model informed drug development

In Lalonde et al., MIDD was defined as the "development and application of pharmaco-statistical models of drug efficacy and safety from preclinical and clinical data to improve drug development knowledge management and decision-making" [5].
The rationale underlining this strategy is the integration of six key components (PK/PD and disease models, competitor information and meta-analysis, design and trial execution models, data analysis models, quantitative decision criteria, and trial performance metrics) in a quantitative framework to be used throughout the drug discovery and development process.

MIDD was adopted by pharma companies to reduce the failure probability in drug development. Five highly interdependent features (for selected pathway, target, molecule, dose regimen, and patients) which determines the overall likelihood that a compound will be commercialized were identified (Figure 1.2). For each feature a specific tool is suggested: system biology helps in identifying the right pathway to act on, system pharmacology allows to identify the appropriate modality to engage the target, etc.

Nowadays it is believed that the MIDD helps in preventing and overcoming the most common causes of failure in drug development [6]: i) the insufficient characterization of the exposure-response relationship before the implementation of confirmatory studies in late-stage clinical development; ii) the poor knowledge of the treatment effect in the target population (difference from placebo or active comparator and/or variance); iii) an inadequate knowledge of the drug and of

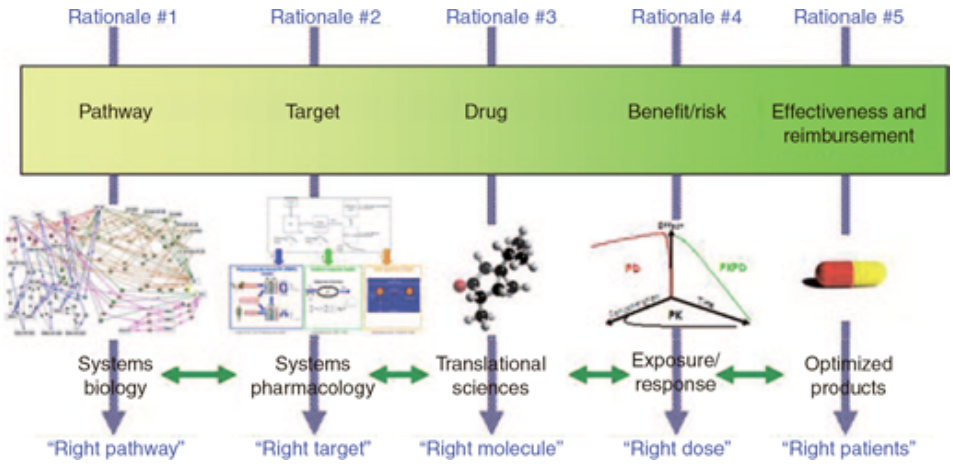

Figure 1.2: **The evolution of MIDD.** In this figure five inter-independent rationales leading the drug development and the preferred tools to achieve the goals (bottom of the figure) were illustrated. Figure taken from [6].

mechanistically related drugs because relevant data were not systematically collated, stored, and utilized; iv) the lack of team experience with the primary end point (often due to "enhancements" of the historically established end point). This assumption is corroborated by an estimation of a reduced the overall cost of drug development by as much as 50% [7] thanks to an extensive use of *in silico* technologies. There is hope that greater predictive power both in term of toxicity and efficacy can be achieved by using mathematical modeling. As a confirmation, the use of this tool to improve the drug development process was encouraged also by EMA [8] and FDA [9, 10, 11].

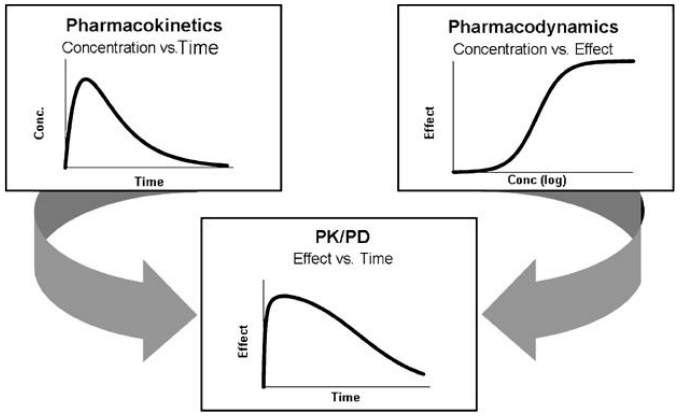

Figure 1.3: **PK/PD modeling relationship.** Schematics of the relationship between the PK and the PD.

1.3 Different modeling tools and different application fields

As mentioned in Chapter 1.2, a specific scientific question should be addressed with a specific modeling strategy (Figure 1.2). In this thesis three different modeling strategy, i.e., PK/PD, K/PD and PBPK models, have been examined. In the next paragraphs, the main features and appropriate fields of application will be discussed for each of them. In the next chapters, a case study for each modeling strategy will be presented.

1.3.1 PK/PD models

PK/PD models are one of the most widespread and used tool in drug development. PK describes the concentration of a drug in a body fluid, usually blood and/or plasma, over time [12]. PD describes the intensity of the drug effect in dependence of the drug concentration in

the body fluid. Through the combination of the PK and the PD part, PK/PD modeling tries to describe directly the time course of effect (Figure 1.3).

The process of drug disposition consists of drug absorption, distribution, metabolization and elimination (ADME) and determines the concentration-time curve. Briefly, the drug was absorbed from the site of administration (gut, muscle, epidermis), transferred to the systemic circulation (or administered directly there in case of intravenous IV administration) and distributed to the various tissues reaching in the biophase, where the drug elicits its therapeutical effect. Kidney and liver metabolize the drug by biotransforming it into other substances, usually to facilitate its elimination.

Classic PK models uses compartments, virtual space(s) in which the drug distributes homogeneously and instantaneously. These models consist of an interconnected compartments where the connections representing the material flows based on the ADME characteristics of the compound. A system of differential equations following the mass conservation law describes the variations of the quantity in the compartments over time.

PK/PD quantifies the concentration-effect relationship describing it for examples, in the form of as simple hyperbolic or sigmoidal relation.

Ideally, drug concentration(s) should be measured at the site of action where the interaction with the target occurs, but in most cases it is not possible. Thus, under the assumption that drug concentration in easy-to-access body fluids (blood or plasma) is a valid surrogate for the pharmacologically active unbound concentration at the site of action, drug blood or plasma concentrations are used to establish the

relationship.

1.3.2 K/PD models

When PK data or models are not available, a different strategy should be adopted. To establish the drug concentration-effect relationship, K/PD are used. As the lack of "P" in the name suggests, in these models PK data are missing. As it is explained in the work of Jacquim et al [13], who first approached these "concentration-free" models, the PD response is driven by a dose rate, as a function over time, rather than the standard drug concentration profile. In practice, the kinetics of the substance under study is inferred from the dynamics of the observed response [14]. However, uncertainty still exists in the assessed drug concentration-effect relationship estimated by this approach.

1.3.3 PBPK models

Physiologically-based pharmacokinetics (PBPK) models describe the PK of a substance by using both the substance-specific information and the prior knowledge of the body anatomy and physiology. The general idea of this modelization arose in 1942 [15]: the body is divided into physiologically relevant compartment, usually organs or tissues Figure 1.4. The fate of the substance within each compartment is described by a mass balance equation. By combining all the differential equations in a unique system, simulating the drug disposition in the entire body is possible and a Whole-Body (WB) PBPK model is built.

As can be seen in Figure 1.4, in PBPK models drug disposition was characterized by accounting for physicochemical drug properties as well as the vasculature interconnections of tissues and organs, the tissue composition, volume and blood perfusion, and its intrinsic clearance.

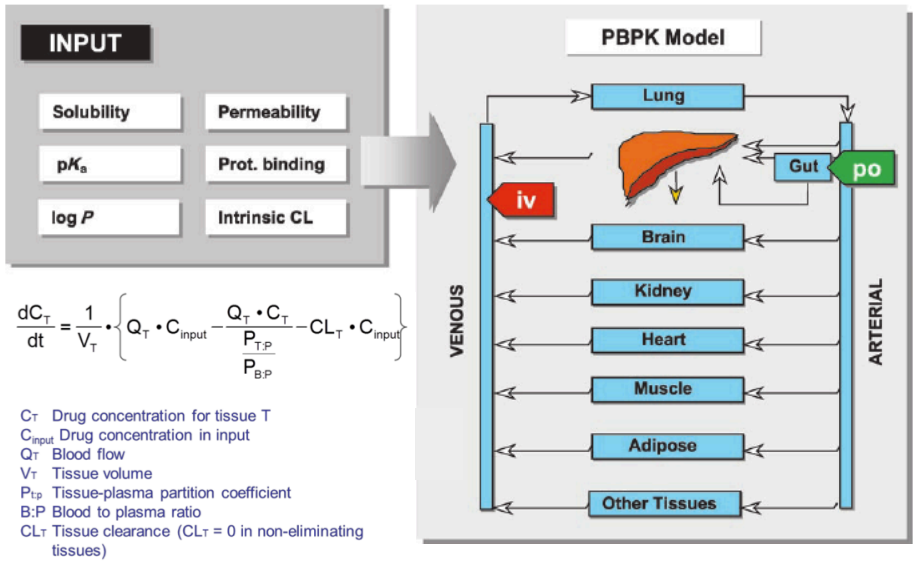

Figure 1.4: **PBPK models schematics.** The structure of a generic WB-PBPK model, together with the input necessary to predict drug disposition and the standar mass balance equation were reported.

1.4 The scientific question of the thesis

This thesis aimed to investigate two aspects: i) the suitability of a certain modeling strategy for a given problem in terms of model structure, available/required data, working hypotheses and the robustness of the results to the assumptions made; ii) the dependency of conclusions from the adopted modeling approach. Thus, it was evaluated in which cases findings were model-dependent, and if different (and, maybe opposite) conclusions would be drawn with different approaches. In other words, it was investigated whether an "optimal" modeling strategy exists to address a specific problem. *Via* some case studies dealing with different therapeutical areas, such as the oncology

and the infectious diseases, the modeling approach commonly thought to be the best to cope with the specific ultimate goal was tested.

Here, a general overview of this thesis was reported.

One of the most critical points in early drug development, is the prediction of the exposure in early clinical development. In fact, at this stage no clinical data were available, and the dose-exposure relationship is unknown. Thanks to the ability to integrate the *a priori* information on organism anatomy and physiology with the physicochemical drug properties, PBPK framework is one of the most promising tools to lead the dose selection in First In Human (FIH) studies. The contribution in terms of exposure prediction given by the WB-PBPK model was investigated in Chapter 2. The predictive performance of the PBPK models were assessed by six *what-if* scenarios, in which data were added progressively into model development, starting from *in vitro* and animal experiments, up to human clinical trials. Via these scenarios, the accuracy of the exposure predictions in dependence of the available data was evaluated. Ethambutol (EMB), one of the first line antibiotics used for the treatment of pulmonary tuberculosis, was used as paradigm drug.

In different contexts, as in the case of cancer patients, the PBPK modeling strategy could not be adopted, because of the insufficient physiological characterization of the patients. Thus, different and less mechanistic modeling strategies, such as PK/PD and K/PD models, are used to reach important conclusion on drugs effect. A survey of the available strategies in oncology have been deeply analyzed and presented in Chapter 3.

The dependence of results on the specific model used was investigated in Chapter 4, where a case study regarding the predicted effect

of the combination of two anticancer drugs was illustrated.

Finally, in an attempt to provide additional details on drug behavior, drug concentration into tumor tissue was measured in a xenograft rats study. In Chapter 5, drug potency was estimated considering both the drug concentration in plasma and active free drug concentration in tumor tissue.

Chapter 2

Evaluation of PBPK models predictive performances in early drug development: a case study using Ethambutol[1]

Whole-Body Physiologically–Based Pharmacokinetic (WB-PBPK) models enable to characterize the exposure profiles in the different organs through combining *a priori* information on both organism anatomy and physiology with physicochemical drug specific properties. However, it is unclear which data are needed for accurate predictions. In this work we investigated the predictive performances of the WB-

[1]The contents of this chapter are confidential. This is a work by *L. Carrara, P. Magni, D. Teutonico,O. Della Pasqua & F. Kloprogge*, and will be submitted on cpt:psp

PBPK models both for prospective evaluation of the molecules (prior to human clinical trials) as well as from a retrospective point of view (when human data were partially or totally available). Six *what-if* scenarios, in which data were added progressively for model development, were simulated. Ethambutol (EMB), one of the first line antibiotics used for pulmonary tuberculosis treatment, was used as paradigm drug. Key data and parameters were identified. A PBPK model, able to describe drug plasma concentration following EMB administration and to predict drug levels in the lung, was built.

2.1 Background

Physiologically Based Pharmacokinetic (PBPK) models are a class of mathematical models used to describe and predict the absorption, distribution, metabolism and excretion (ADME) of chemical substances, including small and large molecules. In contrast with the compartmental (PK) models, which provide a rather phenomenological description of the drug concentration profiles in plasma by means of relatively simple model structure, PBPK models yield a more detailed and mechanistic representation of the ADME processes.
In whole-body PBPK (WB-PBPK) models, the body is divided into physiologically-relevant compartments, usually tissue and organs [16]. For each organ a mass balance equation is written. These equations form an unique differential equation system that describes the fate of the substance in every compartment of the body [17].

One of the main features of the PBPK models is the possibility to integrate the information on the organism's anatomy and physiology with the physico-chemical drug properties derived from *in vitro* experiments. This feature is of primary interest in early drug development, during which one aims to predict drug disposition in human

before progressing with a candidate compound into the clinic, when the model is used prospectively as a screening tool. Another important aspect worth mentioning is the possibility of using WB-PBPK models to predict drug levels not only in plasma, but also in the biophase, which provides a stronger rationale for dose selection, enhancing the probability of positive results and success of the treatment [18, 19]. This is expecially relevant when considering target organs for which sampling in clinical trials requires invasive procedures or in cases where sampling is simply not possible [20].

However, which data are necessary to achieve accurate predictions is still unclear.

To explore the predictive performances of the WB-PBPK modelling, we chose a high impact and relevant cases, pulmonary tuberculosis (TB). Tuberculosis is one of the most widespread infection diseases in the world. Data from the Global Tuberculosis report show that in 2015 Tuberculosis killed 1.4 million of people, and 10.4 million of new cases were estimated in the same year [21]. Tuberculosis is an infection caused by *Mycobacterium tuberculosis*, which mainly affects the lung [22]. EMB, one of the first line antibiotics administered for pulmonary tuberculosis treatment [23], was used as paradigm drug.

Here, we investigated the predictive performances of the WB-PBPK modelling both for prospective evaluation of the molecules, prior to human clinical trials, and from a retrospective perspective, when human clinical data were available. To this aim, 6 *what-if* scenarios, which mimicked different degrees of prior information or data availability were simulated. Scenarios range from the poorest to the richest data situation. In the latter one, a PBPK model for EMB was fully parameterized, and plasma EMB concentration profiles in a population of TB patients, as well as drug concentration level in the lung, were predicted.

2.2 Materials and methods

The contents of this section are confidential.

2.3 Results

In scenario 1 the predicted AUC following IV EMB administration varied from 0.5 to 3.5 fold the nominal value because of the uncertainty on microsomal activity. The AUC predicted following oral administration varied 0.1-4.3 fold the nominal value when a default value of IPT computed *via* the empirical formula (Eq. **??**) was used (IPT=2.55×10^{-8} [dm/min] when LogP=-0.4 and IPT=8.45×10^{-8} [dm/min] when LogP=0.12), whilst it varied 0.2-3.75 fold when the "true" IPT (6.67×10^{-8} [dm/min]) estimated in scenario 5 was used.

Despite the uncertainty on hepatic clearance was not solved in scenario 2, animal clearance data improved the predictive performance of the PBPK model, and a predicted AUC of 0.5-2 fold was obtained following IV administration (Figure 2.1 B). For oral drug administration, when IPT was automatically calculated (Eq. **??**) AUC predictions of 0.1-1 fold the nominal value were obtained, compared to 0.25-2.2 fold when the "true" value was used. These results applied for both the lipophilicity values considered (predictions made using LogP=0.12 and following oral administrations were not shown).

Human plasma IV data (scenario 3) enabled to estimate some of the model parameters, such as clearance and lipophilicity. In scenario 3.C an identifiability problem in estimating two clearance processes by only plasma data arose. In the other sub-scenarios, IV plasma data were well described regardless of the specific EMB clearance hypotheses, which did however affect the prediction of the amount excreted

in the urine: this amount was underestimated in scenarios 3.A and 3.D, and overestimated in 3.B. AUC prediction following oral EMB administration varied from 0.2 to 0.96 fold (depending on clearance hypotheses) when automatically calculated IPT was used (Eq. **??**). A more narrow AUC variation was obtained (0.732-1.14 fold) when the estimated value was considered. For scenario 3.D IV plasma data fitting and urinary excretion predictions were shown in Figure 2.1 C, oral plasma predictions were reported in Figure 2.2 A. Results not shown for scenarios 3.A and 3.B

When also urinary data were used for model building (scenario 4), clearance processes were correctly identified and a PBPK model with hepatic clearance and both passive and active renal elimination was built. Rowland and Rodgers distribution model resulted to be the most adequate partition coefficient calculation method. Mean plasma concentration profile up to 12 hours (Figure 2.4 A) and the fraction of the drug excreted unchanged in the urine up to 72 hours (Figure Figure 2.4 B) after an hour infusion of 15 mg/kg of EMB to healthy volunteers were successfully described.
Testing different lipophilicity values (from -0.64 to 0.12), resulting in different IPT values, the predicted plasma EMB concentration following the first oral dose varies 0.3-1.2 fold the nominal value, while when the "true" IPT was used very accurate prediction (fold change 1) was obtained independently from the LogP considered.
Predicted plasma EMB concentration following the first oral dose and at steady state were reported in Figure 2.2 A and Figure 2.3 B, respectively.

In scenario 5 Weibull distribution parameters and IPT were estimated. Besides describing IV plasma and urinary data (Figure 2.4 A and B), the model successfully described mean plasma concentration profiles up to 15 hours after the first oral administration of 800, 1000

and 1200 mg of EMB to a simulated population of TB patients (Figure 2.4 C). Model parameters were reported in Table 2.1.

Furthermore, the model well predicted mean EMB plasma concentration profiles following the administration of different EMB formulations at different doses (Figure 2.6).

Good prediction of the inter-individual variability (IIV) of the plasma concentration profiles of the population under study following oral drug administrations were obtained by using the developed WB-PBPK model. The comparison between empirical and theoretical percentiles showed good agreement between 800 mg oral EMB data and population plasma concentrations profiles simulated via the PBPK model following the first dose (Figure 2.5 A). Good agreement between the percentiles was also observed at steady state (Figure 2.5 B), even if the 95^{th} percentile is under predicted by the PBPK model. Prediction for 1000 and 1200 mg of EMB were reported in App. A. A mismatch between the model predicted percentiles and the percentiles computed from the observed data [27] of the pharmacokinetic studies was noticed (App. A).

Steady state drug levels in plasma and AC of an independent dataset [31] were well predicted by the identified model both for male (Figure 2.5 C) and female patients (not shown).

Table 2.1: **EMB WB-PBPK model parameter estimates** EMB WB-PBPK model parameter estimates after completing the model building procedure (scenario 5).

Parameter	Value [unit]	Parameter meaning
Lipophilicity	-0.64 [LogP]	
Specific clearance	0.07 [1/min]	Drug hepatic clearance rate
TSspec	1.46 [1/min]	Drug active tubular secretion rate
GFR efficiency	1 [-] (fixed)	Efficiency of the passive renal elimination, i.e, glomerular filtration
Distribution model	Rowland and Rodgers [40, 41]	
Weibull dissolution time	16.41 [min]	Time at which 50% of the compound has dissolved
Weibull dissolution shape	0.53 [-]	Shape parameter of the Weibull distribution
IPT	6.67×10^{-8} [dm/min]	Intestinal permeability transcellular

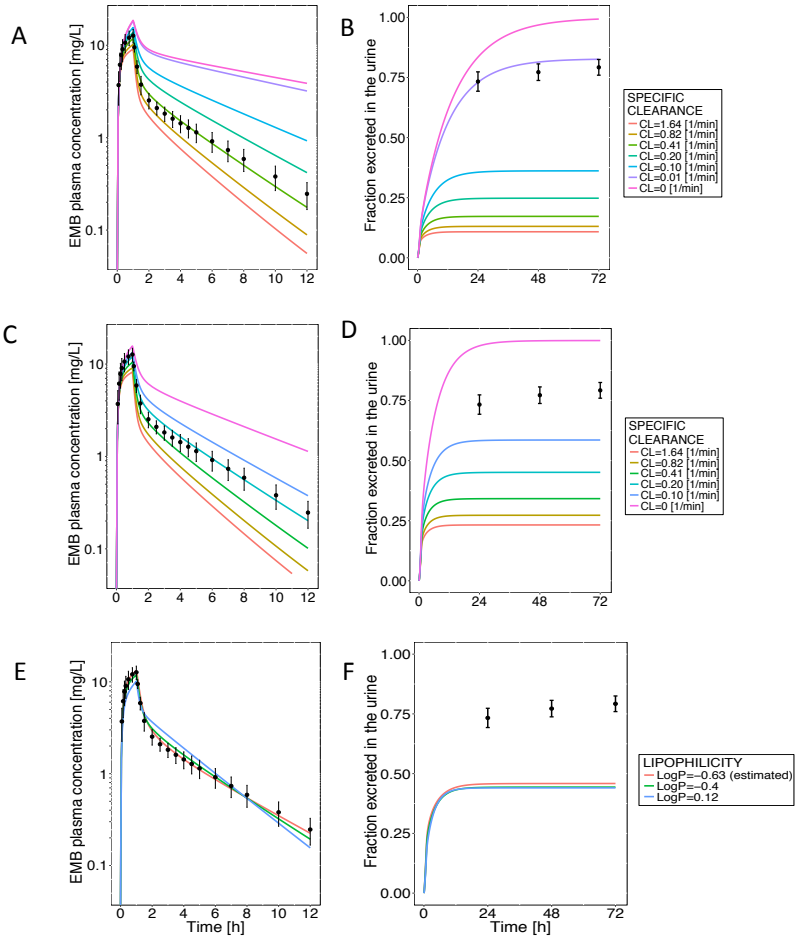

Figure 2.1: **Model predictions following IV administration.** Plasma concentration profiles (Figure A and C) and fraction of drug excreted unchanged in urine (Figure B and D) predicted following IV infusion (15mg/kg) in scenario 1 and in scenario 2, respectively. Each model-predicted curve corresponds to a different hepatic clearance value. Fits of plasma IV data (Figure E) and the prediction of the fraction excreted in the urine (Figure F) in scenario 3.D. Each curve corresponds to a different lipophilicity value. Data (black dots) were reported together with their standard deviation (black vertical bars).

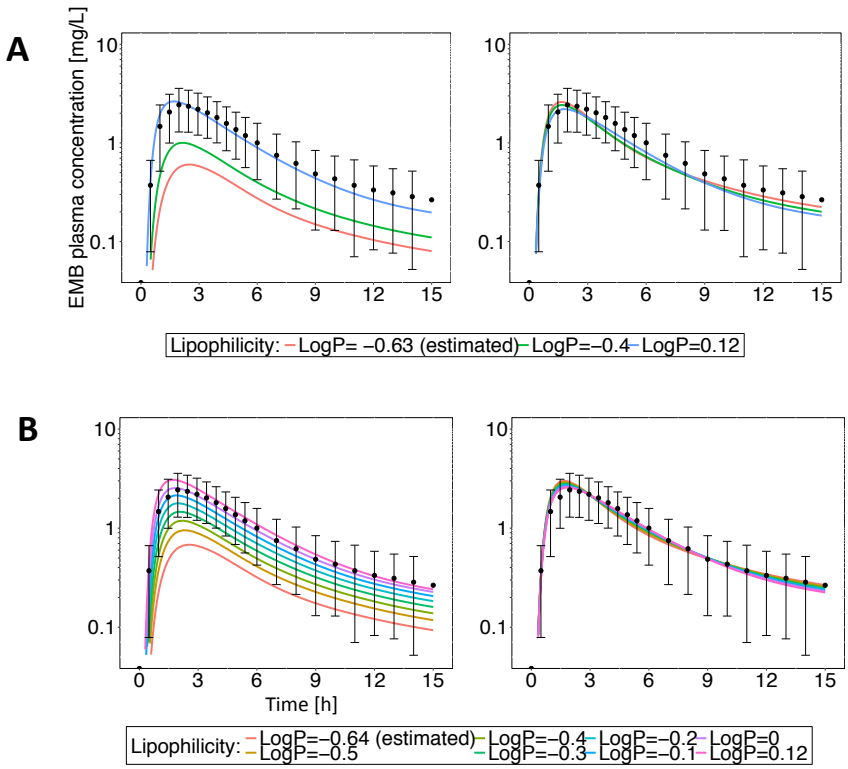

Figure 2.2: **Model prediction following the first oral administration.** A) Model predicted plasma concentration following the first oral dose (800 mg) in scenario 3.D. B) Model predicted plasma concentration following the first oral dose (800 mg) in scenario 4. Left: model-predicted curves using the IPT value computed on the basis of the molecular weight and the lipophilicity of the molecule (Eq. **??**). Right: model predicted curves when the "true" IPT but different LogP, corresponding to different colors of the curves, were used. Data (black dots) together with their standard deviation (black vertical bars).

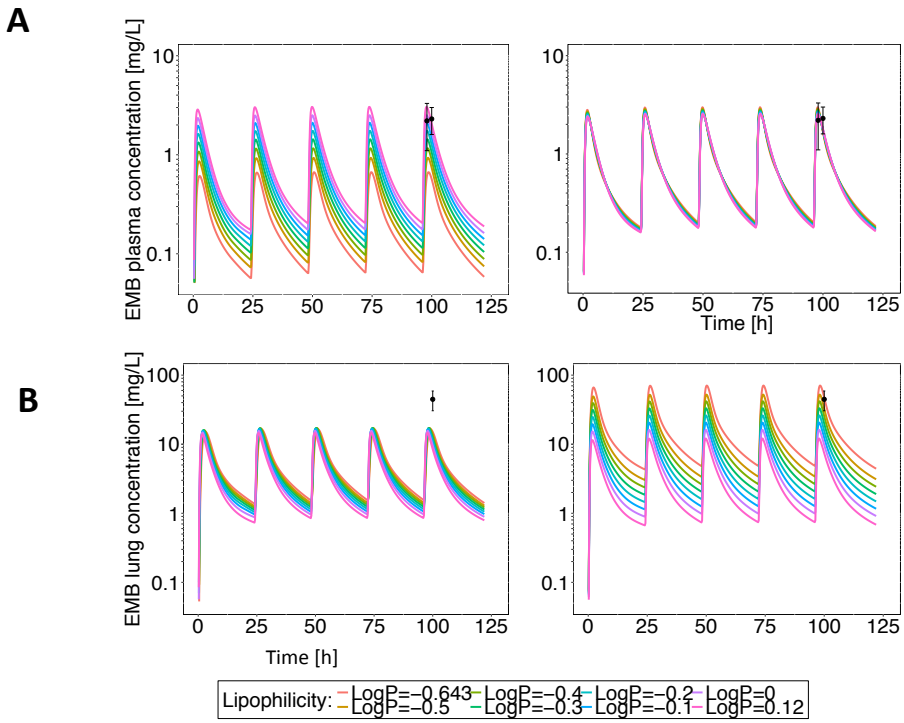

Figure 2.3: **Model prediction at steady state following oral administration.** Model predicted curves at steady state following 800 mg orally administered in scenario 4. A) Model predicted plasma concentration. 4. B) Model predicted lung concentration. Left: model-predicted curves using the IPT value computed on the basis of the molecular weight and the lipophilicity of the molecule (Eq. **??**). Right: model predicted curves when the "true" IPT but different LogP, corresponding to different colors of the curves, were used. Data (black dots) together with their standard deviation (black vertical bars).

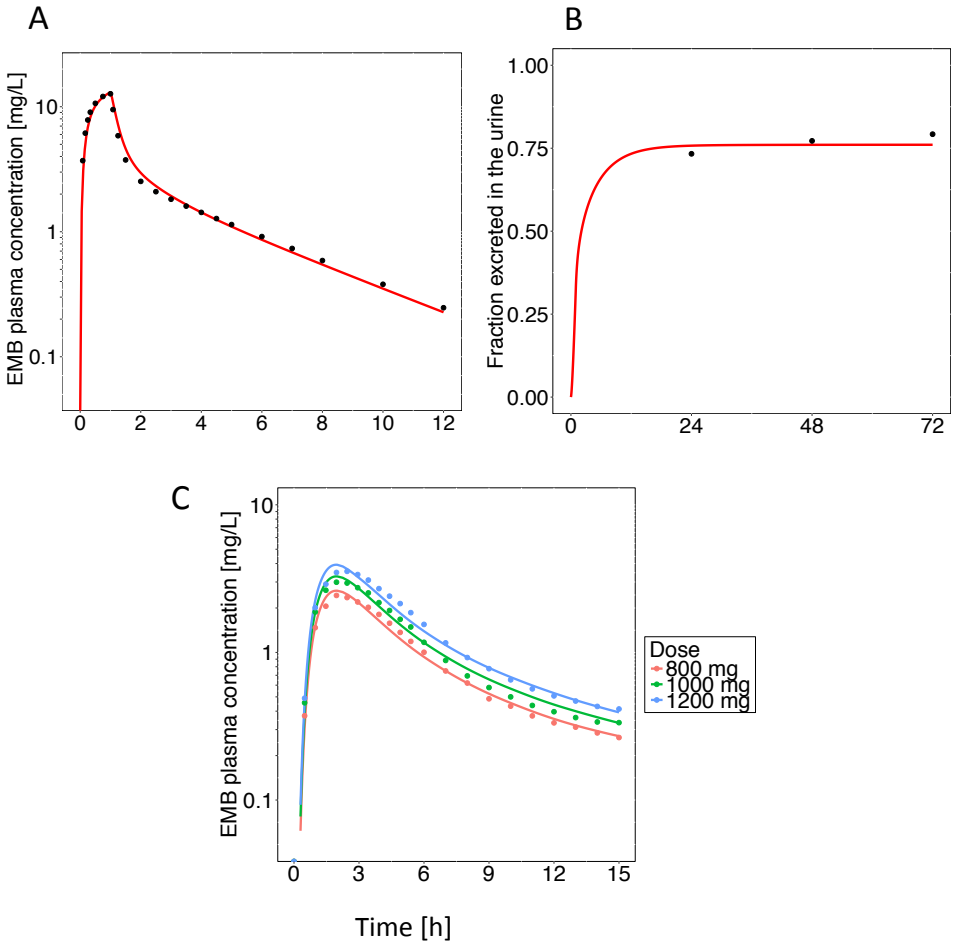

Figure 2.4: **Model-building results in rich data scenario.** A) and B): simultaneous model fit of plasma and urinary data following IV EMB infusion (scenario 4 and 5). C): simultaneous plasma data fit following oral EMB administration (scenario 5). Model-fitted curves were represented by continuous colored lines and data by dots.

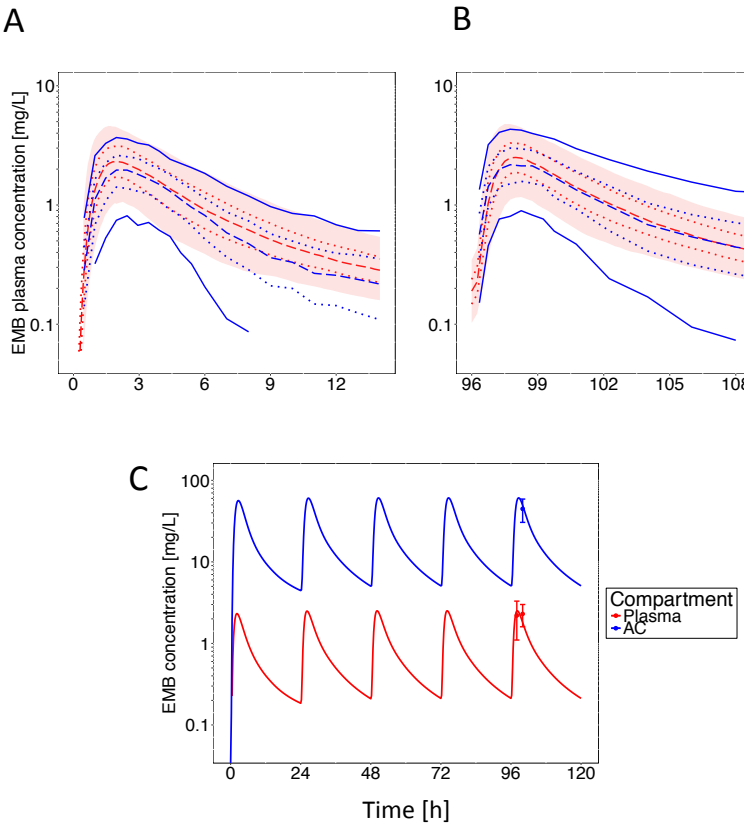

Figure 2.5: **WB-PBPK model plasma and lung predictions.** A) and B): predictions of population plasma EMB concentration profiles (scenario 6) following the first oral dose (800 mg) and at steady state, respectively. In both panels A) and B) the red shaded area represents the $5^{th} - 95^{th}$ percentiles of the PK-Sim population predicted plasma concentration profiles, the red dashed line and the red dotted lines represent the 50^{th}, 25^{th} and the 75^{th} percentiles. The blue continuous lines represent the $5^{th} - 95^{th}$ percentiles of the data, the blue dashed line and the blue dotted lines represent the 50^{th}, 25^{th} and the 75^{th} percentiles. C) model evaluation using data of an independent dataset [31]: prediction of mean male plasma (red line) and AC (blue line) drug levels at steady state.

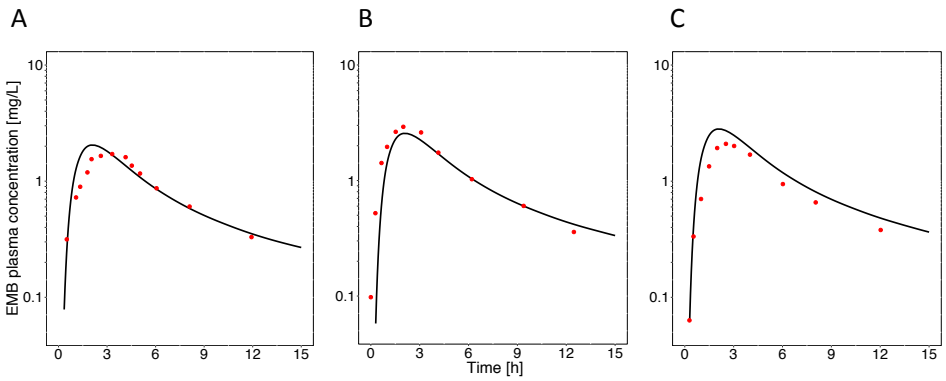

Figure 2.6: **Different EMB formulation predictions.** Model predicted plasma curve (black lines) compared with observed mean data (red dots) of studies in which different EMB formulations were administered: A) 800 mg of ETB-91-400A [28], in B) 1000 mg of EMB obtained from Hong Qi Pharmaceutical CO, Ltd, China [29] and in C) 1100 mg of Myrin-P Forte (Pfizer)[30] were administered.

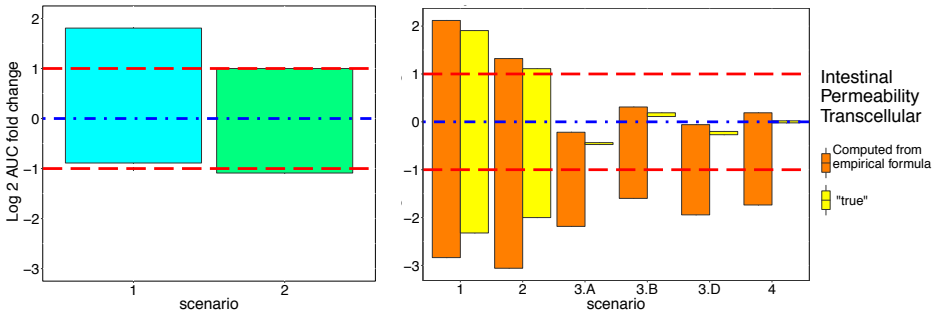

Figure 2.7: **WB-PBPK model predictive performances: exposure predictions for the scenarios under investigation** WB-PBPK model predictive performances expressed in terms of AUC fold change between the model-predicted and the observed exposure. Left: AUC prediction range following IV administrations (scenario 1 and 2). Right: AUC prediction range following oral EMB administration. In orange the AUC range of variation when IPT computed in the basis on molecular weight and lipophilicity was used (Eq. **??**), in yellow the AUC range of variation when predictions were made using the "true" IPT. The red dashed lines represent the 2 fold change of variations within which predictions are considered reasonably accurate; the blue dash-dotted lines indicate a AUC fold change of 1 in predicting drug exposure. A logarithmic scale on y axes was adopted to prevent visual representation bias.

2.4 Discussion

In this work the predictive performances of PBPK models were investigated using an high impact case, such as pulmonary tuberculosis. EMB was used as paradigm drug. We evaluated three different cases: i) when the WB-PBPK framework is used for prospective evaluation of molecules in absence of clinical data; ii) in *poor data* scenarios in human; iii) in a *rich data* context, when the model building phase can be competed.

Our step-by-step investigation proved that the accuracy in drug exposure predictions is directly related to the amount of the available data that, in turn, depends on the stage of the drug development process (Figure 2.7). Thus, the prediction accuracy is expected to increase throughout the process, as occurred in our case. It should be also noticed that the required level of accuracy varies among the different stages of drug development. For example, when extrapolating to humans making very precise prediction is really hard since a lot of information is still missing; while when human data are available the extrapolation to children is easier, because more information on the drug under study and more precise models are given.
Our case study could be used to assess more quantitatively the compromise between the data given and the level of accuracy in drug exposure prediction. Moreover, our results confirmed the importance of the model building phase, which provided important information on drug disposition not only in *rich data* situations, but also in *poor data* contexts. In addition, our analysis highlighted the crucial parameters and data for developing a WB-PBPK model for a renally cleared drug such as EMB.

For EMB, one of the main problem resulted to be the lack of information on clearance processes. The uncertainty on pre-clinical hepatic

clearance and the lack of active tubular secretion data prevented us from achieving accurate prediction of the drug exposure when *in vitro* experiments were the sole data source. The misprediction in AUC following IV administration reflected on a greater variation in AUC prediction following oral administration.

The introduction animal experiment data allowed not only to obtain relatively accurate exposure prediction following IV administration, but also indicated that, since the 20–60% of the drug was predicted to be excreted via the kidneys (except when the drug was supposed to be totally renally cleared (Figure 2.1 B, pink line), urinary samples should be collected in a EMB *first-in-human* study.

In the absence of clinical data, due to the huge clearance uncertainty it was not possible to distinguish the impact of lipophilicity on drug disposition predictions and the results listed above did not depend on the lipophilicity value used (LogP=0.12 [32] and LogP=-0.4 [37], results not shown).

In *poor data scenarios*, which mimicked the early development stages, a partial model building procedure was possible. The PBPK model described plasma IV data well, fact of the utmost importance at this stage of drug development with respect to the properly identification of the clearance processes (in our case renal elimination was not well predicted).

When also human urinary data are available, drug distribution and elimination can be adequately estimated.

For both scenarios 3 and 4, drug exposure following oral administration was poorly predicted when IPT value computed *via* an empirical formula is used (Eq. **??**). More accurate predictions were ob-

tained when the "true" IPT value was used, as displayed in Figure 2.7. This finding confirmed the authors' opinion that IPT is one of the most sensitive parameter of the WB-PBPK model, and the accuracy of exposure prediction dramatically depends on its value. Moreover, our results also demonstrated that in predicting plasma concentration, lipophilicity does not play a role "per se" but only for computing IPT (Figure 2.3 A), whilst it strongly impacts when tissue drug concentration should be predicted (Figure 2.3 B): when the "true" IPT value was used, AC drug concentration variations are bigger than the ones observed when IPT depends on lipophilicity itself (Figure 2.3 B).

In *rich data scenario*, mimicking the late development stages, the presence of both IV and oral data enabled to fully parameterized the PBPK model following the standard 2-step procedure, according to Kuepfer et al. [54]. Firstly, drug distribution and elimination were estimated using IV data (as in scenario 4). Subsequently, drug absorption was evaluated from oral plasma profiles. The model adequately described experimental data. Estimates are in agreement with literature and were reported in Table 2.1.

The estimated lipophilicity of -0.64 is consistent with the values reported in literature (LogP=-0.4 [37] and LogP=0.12 [32]).

In agreement with the physico-chemical properties of the drug, which is a strong base, Rowland and Rodgers distribution model [40, 41] explicitly accounting for the electrostatic interactions between ionized compounds, resulted to be the best partition coefficient calculation method.

Kidney passive excretion did not suffice to describe the amount of EMB excreted via the kidneys alone, as demonstrated in scenarios 1-3. In agreement with Lee and coworkers [24] who noticed that

EMB was actively eliminated *via* the kidneys, a first order tubular secretion was modeled and tubular secretion rate TS_{spec} of 1.46 min^{-1} was estimated. We found that, 72 hours after the IV infusion, the 43% of the total amount excreted *via* the kidneys was excreted actively, proving that tubular secretion is crucial in drug elimination. In accordance with the fact that EMB is a renally cleared drug, a low liver plasma clearance rate (0.07 min^{-1}) was estimated, below the maximum clearance value of 1.64 min^{-1} measured *in vitro* [32]. Following IV infusion a total plasma clearance of 0.45 L/h/kg was found, conforming to what stated in [24], where a value of 0.51 L/h/kg was reported. Following oral drug administration a total plasma clearance of 0.74 L/h/kg (mean) was found, in agreement with [27] where a value of 0.80 L/h/kg was reported.

The estimated IPT value of 6.67×10^{-8} dm/min is greater than the default value of 1.46×10^{-8} dm/min calculated using Eq. **??** and the estimated LogP=-0.64. Despite the difference between these two parameters was small, IPT needs to be estimated to well describe the data, confirming our hypothesis on the sensitivity of this parameter. Sensitivity analysis results were reported in App. A. A Weibull dissolution time of 16.41 min, similar to the value of 10.3 min estimated from *in vitro* dissolution curve [35], and a Weibull dissolution shape of 0.53, lower than the corresponding value of 1.42 from the *in vitro* experiment, were estimated. A fixed small intestine transit time of 260.5 min [48] is consistent with the value of 4 hours adopted in [54]. Formulation solubility in the GIT is a cutoff value for the intestinal absorption. According with biopharmaceutics classification system (BCS) EMB is a class III (high solubility and low permeability) compound or borderline class III/I (high solubility and high permeability) [55], [56], [29]. Thus an high drug formulation solubility value not limiting the absorption was chosen (formulation solubility=7.58 mg/mL). A constant bioavailability of 60-61% was obtained for the

three dose levels, indicating EMB linear pharmacokinetic. The drug fraction absorbed in the GIT is 65-66%, in agreement with previous findings reporting values of 75% to 80% [50].

When the WB-PBPK model is fully developed, good predictive performances are achieved. Although model parameters were identified on mean data, the variability of the biometrics of the populations included in the PK-Sim internal database well captures observed IIV of the plasma concentration profiles of the population under study after oral drug administrations. The variability in organ volumes, blood flow rates, etc., resulting in a different PBPK model parameterization, reflects the observed differences in plasma levels within the population in a similar manner to the IIV in nonlinear mixed effect models. No additional variability was necessary to capture the population PK profiles. By comparing the empirical and the theoretical percentiles, a good agreement between the data and the population plasma concentrations profiles simulated *via* the PBPK model was achieved both when the first EMB oral doses (Fig. Figure 2.5 A and App. A) and steady state were simulated (Figure 2.5 B and App. A).

Due to the difference in body weight distribution between the observed TB patients [27] and the PK-Sim simulated population (see the histogram in Figure **??**), it was impossible to use the PBPK model to simulate the EMB plasma concentration profiles of the observed population of patients. The PBPK model can be used to predict the variability in plasma concentration level in standard populations, but at the moment limitations still exist in simulating some "special" populations, whose biometric distributions are not the standard ones. In our case, severely underweight population such as the TB patients, could not be simulated.

Testing our PBPK model on data of other studies [31], [28], [29]

and [30], adequate predictive performance were showed. Mean EMB plasma concentration profiles following the administration of different formulations can be adequaletly predicted, proving that formulation do play a role in drug dissolution and absorption. Mean EMB level in plasma and in the lung at steady state are well predicted. The latter result, i.e, adequate EMB lung concentration predictions, has been achieved by means of the default WB-PBPK model, without customization by adding further compartments or creating a multi-compartment lung model as did by Gaohua et al. [49], who built a 28-compartment lung model.

In conclusion, in this work the predictive performance of the WB-PBPK modeling framework were investigated using EMB as paradigm drug. Despite emphasis is given to the mechanistic nature of WB-PBPK models, challenges still exist for prospective use of the approach with novel molecules, i.e., when full details of drug disposition properties are unknown or differ between species. Our case study illustrates the bias in WB-PBPK model predictions when supporting data on drug disposition are missing, a very common situation during lead optimization and candidate selection. However, when the WB-PBPK framework is used retrospectively, adequate descriptions of drug disposition were obtained and good predictions of the drug distribution in tissues were made. This confirms that an adequate model building phase is fundamental: WB-PBPK models provide a generic structure comprehending only passive processes; and active processes, related to the specific drug under study, must be included. It should be also stressed that thanks to the model building phase it is possible to better understand the drug behaviour and test hypotheses on drug distribution, metabolization and elimination. It should be clear, however, that the complexity level of these models is not a limitation: since the information on organism anatomy and physiology were already embedded, data can be accomodated by estimating few, but crucial, parameters.

2.5 Acknowledgement

The authors thank Siv Jönsson, Helen McIlleron and the Division of Clinical Pharmacology, University of Cape Town for kindly sharing the data of the two EMB pharmacokinetic studies.

Chapter 3

Current mathematical models for cancer drug discovery[1]

In some cases, PBPK modeling strategy cannot be applied. In oncology the insufficient physiological characterization of the patients and tumor tissues is the major obstacle for a properly (and successfully) use of the PBPK approach. Consequently, even at the early phases of oncology drug discovery, different and less mechanistic modeling strategies are used. Empirical methodologies may be enough for screening and ranking candidate drugs, but modeling approaches are needed for optimizing and making economically viable the learn-confirm cycles within an oncology research program and anticipating the dose regimens to be investigated in the subsequent clinical devel-

[1]The contents of this chapter are published in *L. Carrara, S.M. Lavezzi, E. Borella, G. De Nicolao, P. Magni & I. Poggesi* . Expert Opinion on Drug Discovery *2017, 12(8):785-799*

opment. The number of modeling approaches used in the discovery of anticancer drugs is consistently increasing and new models are developed based on the current directions of research of new candidate drugs. These approaches have contributed to a better understanding of new oncological targets and have allowed for the exploitation of the relatively sparse information generated by preclinical experiments. In addition, they are used in translational approaches for guiding and supporting the choice of dosing regimens in early clinical development.

In this Chapter, papers appearing in the literature of approximately the last decade reporting modeling approaches applicable to anticancer drug discovery have been listed and commented. Papers were selected based on the interest in the proposed methodology or in its application.

3.1 Introduction

Drug discovery and development in the oncology therapeutic area is a complex, expensive, and long process. Only approximately 5% of the new molecular entities evaluated in oncology first-in-human (FIH) studies are able to enter the market [57]. Whilst in the past the chemotherapeutic agents were chosen based on their generic cytotoxic activity, nowadays, with the advent of targeted therapies, preclinical experiments aim to test the hypothesis that the candidate drug is absorbed and distributed to the biophase, to assess its interaction with a predefined molecular target (activating, inhibiting, or modulating it), and to establish if this interaction leads to a significant antitumor effect without eliciting severe toxicity.

These aspects (adequate systemic and relevant drug biophase ex-

posure, target interaction and modulation, dowstream effects, tumor inhibition and toxicity) represent the building blocks of the so-called pharmacological audit trail [58, 59]. In an audit trail, *in vitro* and *in vivo* experiments are performed to (1) select promising compounds based on the availability of an adequate administration route and dosing regimen, a suitable antitumor activity and a manageable tolerability profile; and (2) determine a safe and efficacious starting dose for the FIH studies.

When *in vitro* experiments are performed, tumor cell cultures are exposed to drug candidates, usually at constant concentrations for a predefined time. The aim is to screen and rank a large number of test compounds, assessing if there is an inhibition of cell proliferation, which is typically assessed via the measurement of viable cell count over time. Other endpoints, such as target engagement and downstream effects, can also be assessed as part of these studies to provide information on the potency of the candidates and on the relevant mode of action. These experiments are high throughput, relatively simple, and do not include the complexity of the whole organism.

In *in vivo* experiments, the selected compounds are administered to animal models to investigate the antitumor efficacy [60, 61]. Ectopic xenografts are the most widely used animal models [62]. They consist in immunosuppressed animals, usually mice or rats, where human cancer cells are inoculated subcutaneously in the flank. The time course of tumor dimension is measured following the application of different dosing protocols. In order to overcome some limitations of ectopic xenograft models (e.g. in these conditions tumors never metastasize [60]), alternative experimental models have been proposed. For instance, orthotopic xenografts, in which human cancer cells are implanted in the same tissue where the tumor originally develops are used [63]. In the perspective of personalized medicine, the use of patient-

derived xenografts (PDX) has also been recently introduced [64]. In the same experiments, pharmacokinetic (PK) and pharmacodynamic (PD) data (e.g. marker of target engagement and modulation) data may be collected; safety and tolerability are also assessed to establish if the antitumor activity is obtained without eliciting overt or intolerable toxicity.

Mathematical models represent the most comprehensive tools for synthesizing and integrating the results of *in vitro* and *in vivo* experiments. They are able to accommodate the relative sparsity of the data and lack of design optimality, to facilitate the comparisons across different candidates, and, most importantly, to allow the translation of preclinical results into the clinical setting.

This chapter reviews some of the mathematical approaches published in the recent literature. Due to the increasing number of original contributions dealing with modeling in oncology (see Figure 3.1), this work is not intended to be a comprehensive review: the approaches mentioned here are of particular interest either for the proposed methodologies or for their application. They are summarized in Table 3.1 and Table 3.2 for the *in vitro* and *in vivo* experiments, respectively. The reader should note that not all the models reported in Table 3.1 and Table 3.2 will be described in details in the next sections of this review. Other reviews can be consulted for a more comprehensive picture on this topic [65, 66, 67, 68].

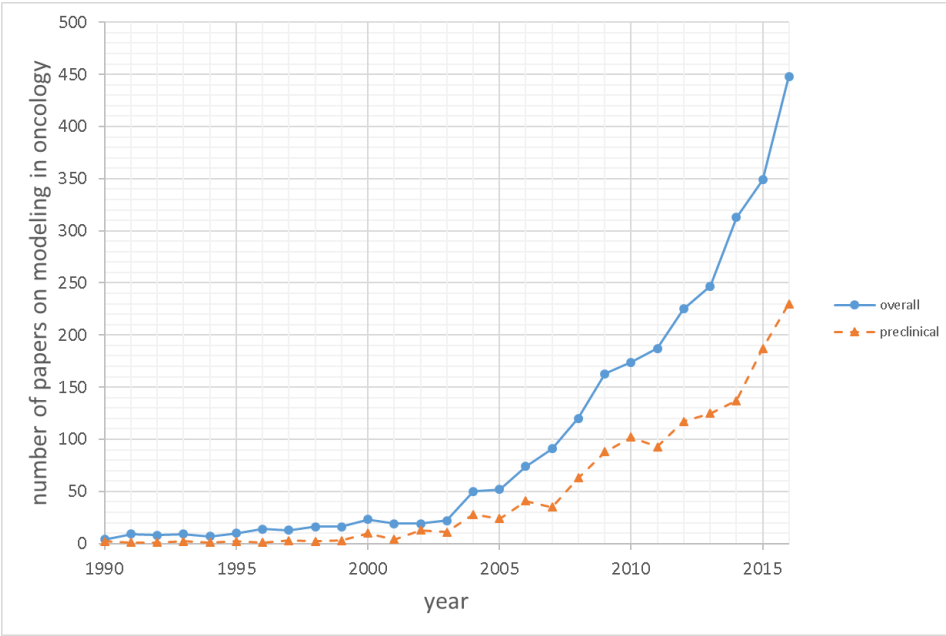

Figure 3.1: **The trend in papers on modeling in oncology.** The overall trend, based on a Google Scholar search meeting the terms "Pharmacometrics" OR "model-based drug development" OR "PK-PD models" AND "oncology", is represented as solid line and filled circles. Adding to the research terms previously listed AND "preclinical", the pattern represented by the dashed line and filled triangles is obtained. Despite the research bias, due to the presence of true/false negatives and to the fact that the overall trend of scientific production is not discounted for, a strongly exponential growth can be observed. Only in the last year, 230 papers on preclinical modeling were published.

3.2 Modeling the results of in vitro experiments

In vitro data are typically modeled using empirical Hill model [69] (Eq. 3.1):

$$Effect = \frac{E_{max} \cdot C^{\gamma}}{EC_{50}^{\gamma} + C^{\gamma}} \tag{3.1}$$

where E_{max} is the maximal effect (e.g. the inhibition of either the activity of the molecular target or of cell growth in culture), C is the candidate drug concentration, EC_{50} is the concentration eliciting 50% of the maximal effect, and γ is the shape factor, representing the steepness of the Hill curve.

The Hill model is convenient to describe a global endpoint, such as the number of surviving cells at fixed time points following drug exposure. However, it was observed that this static representation may be too simplistic, especially when different protocols of drug exposure are applied to cells in culture, as the parameters of empirical models are dependent on the experimental protocols. In this case, other empirical approaches have been proposed including the dependency of the antiproliferative effect on both concentration and time of exposure [70, 71, 72]. These approaches were further refined incorporating mechanistic elements, such as cell cycle time, cell cycle phase specificity, and the potential of drug resistance [73]. More recently, other longitudinal approaches describing the system behavior (i.e. cell count) over time were proposed. Different dynamic semi-mechanistic and mechanistic models are summarized in Table 3.1.

Del Bene et al. [74] developed a semi-mechanistic model consisting of a system of differential equations in which the unperturbed growth

of proliferating cells in culture, the perturbed growth due to drug action, and a cell mortality chain are described. The unperturbed growth of proliferating cells is represented by a first-order process (Eq. 3.2):

$$\frac{dN_p(t)}{dt} = \lambda \cdot N_p(t) \qquad N_p(t=0) = N_0 \tag{3.2}$$

where $N_p(t)$ is the number of proliferating cells at time t, λ is the time constant of the exponential growth, and N_0 is the initial number of cells in culture. The candidate drug makes some of the cells nonproliferating: the perturbed growth is dependent on both the number of proliferating cells and the drug concentration via a proportionality constant k_2, representing the antitumor potency of the compound, as in Eq. 3.3:

$$\frac{dN_p(t)}{dt} = \lambda \cdot N_p(t) - k_2 \cdot C \cdot N_p(t) \qquad N_p(t=0) = N_0 \tag{3.3}$$

where C is the concentration of the candidate drug, considered constant. The nonproliferating cells enter a mortality chain described by a three-compartmental system N_1, N_2, N_3 (Eq. 3.4):

$$\begin{aligned}
\frac{dN_1(t)}{dt} &= k_2 \cdot C \cdot N_p(t) - k_1 \cdot N_1(t) \qquad N_1(t=0) = 0 \\
\frac{dN_2(t)}{dt} &= k_1 \cdot N_1(t) - k_1 \cdot N_2(t) \qquad N_2(t=0) = 0 \\
\frac{dN_3(t)}{dt} &= k_1 \cdot N_2(t) - k_1 \cdot N_3(t) \qquad N_3(t=0) = 0 \\
N_{total}(t) &= N_p(t) + N_1(t) + N_2(t) + N_3(t)
\end{aligned} \tag{3.4}$$

and eventually undergo cell death. This approach was successfully used to model simultaneously data from experiments where A2780 ovarian tumor cells were exposed to numerous antitumor agents (both

chemotherapeutic agents and target-mediated compounds) at different exposure times and concentrations. In addition, using this mathematical model, it was possible to derive a closed form expression of EC_{50} as a function of the exposure times. Based on the similarity with the structure of the Simeoni model (described in the next section) [75], Del Bene and coworkers suggested that the parameters obtained from in vitro studies may be used in a translational approach to predict the in vivo effects in xenograft models and, thus, in human subjects.

In another model, proposed by Moreno and coworkers [76], a Gompertz function was used to describe the unperturbed cell proliferation. For camptothecin and topotecan, the drug action was incorporated in the model as inhibition of the proliferation while for cisplatin cell death induction was considered. In the latter case, a delay, introduced as a signal transduction process, significantly improved the fitting of the time course of cell count following drug administration. Cisplatin is reported to induce apoptosis, which was found to be correlated with the activation of caspase-3 [77]. Interestingly, Moreno et al. reported that their model was consistent with the observed levels of activated caspase-3 [76], suggesting that their model has mechanistic grounds.

Lin and coworkers [78], after setting up a perfusion cell culture system to assess the effect of anticancer compounds, developed a mathematical model to describe the experimental observations. The approach was inspired by a model characterizing the antimicrobial effect of ceftazidime [79]. In [78], the cells consisted of two subpopulations, the nonreplicating cells (whose number is described by $N_{non-rep}$) and the replicating ones (N_{rep}). Nonreplicating cells become replicating via a first-order process governed by the rate constant $k_{non-rep \to rep}$ (transition process). Replicating cells revert to nonreplicating cells via the rate constant $k_{rep \to non-rep}$ (replication process). When the total number of cells ($N = N_{rep} + N_{non-rep}$) is far from the carrying capac-

ity ($N \ll Nmax$), replicating cells generate two nonreplicating cells. When the system approaches the carrying capacity ($N \sim N_{max}$), only one non-replicating cell is generated. This phenomenon is called replication efficiency (Rep) and can be expressed by the following equation:

$$Rep = 2\left(1 - \frac{N(t)}{N_{max} + N(t)}\right) \tag{3.5}$$

Overall, the anticancer drug activity was implemented via generic inhibitory functions on the transition ($Inh_{transition}$) and/or the replication ($Inh_{replication}$) processes (Eq. 3.6):

$$Inh = 1 - \frac{I_{max} \cdot C}{IC_{50} + C} \tag{3.6}$$

where I_{max} is the maximal effect, C is the (constant) concentration, and IC_{50} is the concentration leading to 50% of the maximal effect. In some cases, tolerance had to be included as a decreasing exponential with time on the I_{max} parameter. The overall model is therefore represented by the following system of differential equations (Eq. 3.7):

$$\begin{aligned}
\frac{dN_{non-rep}(t)}{dt} &= Rep \cdot Inh_{replication} \cdot k_{rep \to non-rep} \cdot N_{rep}(t) \\
&\quad - Inh_{transition} \cdot k_{non-rep \to rep} \cdot N_{non-rep}(t) \\
\frac{dN_{rep}(t)}{dt} &= Inh_{transition} \cdot k_{non-rep \to rep} \cdot N_{non-rep}(t) \\
&\quad - k_{rep \to non-rep} \cdot N_{rep}(t)
\end{aligned} \tag{3.7}$$

$$\begin{aligned}
N(t) &= N_{non-rep}(t) + N_{rep}(t) \\
N(t=0) &= N_0(t)
\end{aligned}$$

This model accurately described the time course of cancer cells count following the treatment with different formulations of tetraiodothy-

roacetic acid, resveratrol, and cetuximab given as single agents or in combination. The outcome of the modeling of the combination experiments suggested a nearly additive effect of these agents. The authors stated that this approach was useful for translating the *in vitro* effects into the *in vivo* setting in both animals and human subjects.

Table 3.1: **Summary of recent modeling approaches used to describe in vitro experiment results in oncology drug discovery.** Cell count in culture was always the observed variable. The papers are reported by year of publication. NLME: nonlinear mixed effect; NSCLC: non-small cell lung cancer.

Tumor type	Drug(s)	Model type	Notes	Reference
DHD/K12-PROb rat colon adenocarcinoma	Single agents: camptothecin, topotecan, cisplatin	Gompertz growth (with or without delay); drug effect via cell kill; NLME	Constant concentration	[76]
A2780 human ovarian carcinoma	Single agents: 5-fluorouracil, cisplatin, docetaxel, etoposide, gemcitabine, SN38 (irinotecan), paclitaxel, vinblastine and four compounds in early discovery phase	Exponential growth; drug effect via cell kill; nonlinear regression on average data	Constant concentration	[74]

(Continued overleaf)

(Continued from the preceding page)

Tumor type	Drug(s)	Model type	Notes	Reference
U-87MG human glioblastoma, Colo-205 human colon cancer, MDA-MB-231 human breast adenocarcinoma	Single agents and combination: tetraiodothyroacetic acid, resveratrol and cetuximab	Two subpopulations of cells (nonproliferating/proliferating) with transition and replication efficiency term; drug effect via inhibition of transition and/ or proliferation; NLME	Constant concentration	[78]
H1299 human NSCLC	Single agents and combination: gemcitabine and erlotinib	Empirical models	Constant concentration. Drug sequencing also examined in *in vivo* experiments	[80]
MIA-PaCa-2 human pancreatic carcinoma, BxPC-3 human pancreatic adenocarcinoma	Single agents and combination: gemcitabine and trabectedin	Logistic growth; interaction term as proposed by Koch [81]; tumoristatic concentration; nonlinear regression	Constant concentration	[82]

3.3 Modeling the results of in vivo experiments

After the assessment of the antitumor effect of drug candidates in *in vitro* systems, *in vivo* experiments are typically performed in xenografted rodents. Although in preclinical species chemically or physically induced experimental tumor models are also often used, no mathematical modeling efforts have been reported in the recent literature for modeling the tumor size changes in this kind of experiments. Some of the available mathematical approaches describing in vivo preclinical antitumor effect directly relate the candidate drug plasma concentrations to the stasis or reduction of tumor size [75, 83]. Other models describe the catenary of events from target engagement and activation to the downstream changes (e.g. the phosphorylation of specific substrates) leading to tumor stasis or shrinkage [84]. The use of mechanistic elements facilitates the translation from preclinical to clinical situation. In the literature of the last few years, many examples of preclinical and translational modeling are reported and some of them are summarized in Table 3.2.

3.3.1 PK-PD models directly describing tumor growth inhibition

Single-agent therapy

The more recent models in this area are indebted with the seminal works of Anne Laird [85, 86] and William Jusko [87, 88], who proposed mathematical models to describe tumor growth and the anticancer drug candidate effect in animals. One of the currently most popular PK–PD models of tumor growth inhibition (TGI) is the model proposed by Simeoni et al. (Figure 3.2 a), also called cell distribution model [75, 89]. The unperturbed growth in the control group is de-

scribed by an exponential phase followed by a linear one (Figure 3.2 b). In the perturbed growth model (treated animals), it is assumed that following drug administration only a fraction of cancer cells keeps proliferating. The cells damaged by the drug stop proliferating and enter a transit compartmental system that leads to cell death (Figure 3.2 c). The rate of tumor growth is reduced by a factor proportional to both drug concentration and weight of proliferating cells, via a proportionality constant that represents the drug antitumor potency. The separation between tumor and drug-related parameters is a key factor for translational purposes, and it is one of the likely reasons of the popularity of this model. The translatability of the parameter describing the antitumor potency was further demonstrated by an outstanding correlation with the drug systemic exposure obtained at the dose(s) at which 10 drugs (5-fluorouracil, cisplatin, docetaxel, doxorubicin, etoposide, gemcitabine, irinotecan, paclitaxel, vinblastine, vincristine) are administered in the clinical practice [90].

Bonate, in a review paper [91], suggested that a more traditional Gompertzian growth may be more suited for describing the unperturbed growth as it includes also the plateau that is sometimes observed in xenograft models. Whilst Gompertzian growth has been extensively used [85], in case the plateau is not observed, this growth is definitely less flexible with respect to the growth function proposed by Simeoni et al. [75].

Another popular model is the signal distribution model proposed by Lobo and Bathasar [83]. Here, the delayed time course of the drug induced cell kill is modeled using four transit compartments. The last compartment induces cell death on a population of cells that is proliferating following a first-order growth. In a more recent work [89], it has been shown that both cell distribution and signal distribution models could describe accurately the antitumor effect observed

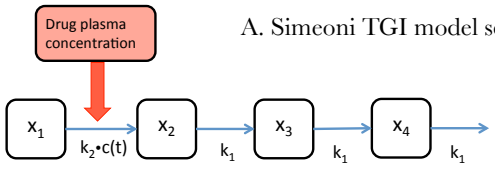

B. Unperturbed growth model

$$\frac{dw(t)}{dt} = \frac{\lambda_0 \cdot w(t)}{\left[1+\left(\frac{\lambda_0}{\lambda_1}\cdot w(t)\right)^{\varphi}\right]^{\frac{1}{\varphi}}}$$

$$w(0) = w_0$$

C. Perturbed growth model

$$\frac{dx_1(t)}{dt} = \frac{\lambda_0 \cdot x_1(t)}{\left[1+\left(\frac{\lambda_0}{\lambda_1}\cdot w(t)\right)^{\varphi}\right]^{\frac{1}{\varphi}}} - k_2 \cdot c(t) \cdot x_1(t)$$

$$\frac{dx_2(t)}{dt} = k_2 \cdot c(t) \cdot x_1(t) - k_1 \cdot x_2(t)$$

$$\frac{dx_3(t)}{dt} = k_1 \cdot x_2(t) - k_1 \cdot x_3(t)$$

$$\frac{dx_4(t)}{dt} = k_1 \cdot x_3(t) - k_1 \cdot x_4(t)$$

$$x_1(0) = w_0 \quad x_{2,3,4}(0) = 0$$

$$w(t) = x_1(t) + x_2(t) + x_3(t) + x_4(t)$$

Figure 3.2: **Schematics of Simeoni TGI model.** A) Schematics of Simeoni TGI model. B) The equations of the unperturbed growth model. C) The equations of perturbed growth model. λ_0 and λ_1 are the tumor growth rates in exponential and linear phase, respectively, w_0 is the tumor weight at inoculation time, k_1 is the first order rate of transit in the three- compartmental mortality chain, k_2 is the drug potency, and $c(t)$ is the drug concentration over time. $W(t)$ is the total tumor weight, measured during the experiments. Reproduced from [65] with permission of the American Association for Cancer Research.

following administration of liposomal paclitaxel to mice xenografted with Colon-26 tumors, despite these models were demonstrated to be mathematically distinct.

Additional complexities were added to the basic cell or signal distribution models on an ad hoc basis. Stuyckens et al. [92] proposed a modification of the Simeoni model to account for the development of resistance to antitumor therapy using an exponential decline function to modulate the potency parameter k_2. Another modification was proposed by Pigatto et al. [93] to account for the schedule-dependent effect of etoposide on TGI in rats. The saturable killing effect at higher drug candidate concentration was modeled via an E_{max} function, resulting in a variable potency parameter (Eq. 3.8):

$$k_{2variable} = k_{2max} \cdot \left(1 - \frac{c(t)}{IC_{50} + c(t)}\right) \tag{3.8}$$

where k_{2max} is the maximal cytotoxic drug potency and IC_{50} is the concentration providing half of k_{2max}. It is interesting to notice that this model was applied in a nonlinear mixed effect (NLME) context considering interindividual variability on tumor-related parameters.

Another popular model was developed by Hahnfeldt and coworkers for antiangiogenic compounds [94]: the authors formulated a mathematical model to describe the effect of endostatin, angiostatin, and TNP-470 on Lewis lung xenografts, using a bidirectional control of the tumor on its vasculature. The authors modeled the tumor growth via a Gompertz function (Eq. 3.9),

$$\frac{dV(t)}{dt} = -\lambda \log\left(\frac{V(t)}{K(t)}\right) V(t) \tag{3.9}$$

in which a variable called carrying capacity $K(t)$ is the limit for tumor growth (here $K(t)$ is defined as the maximal sustainable tumor

size due to the input of oxygen and nutrients), $V(t)$ is the tumor volume, and λ is a constant related to tumor growth. $K(t)$ was assumed to be related to the balance of four different processes: (1) the natural exponential growth of the tumor in absence of limitations, (2) the inhibitory and (3) the inducing processes contributing to tumor growth due to the availability of energy and nutrient input via the vasculature, and (4) the inhibitory action of the antiangiogenic agent. Thus, the effect of these factors on $K(t)$ was expressed using four distinct terms in the following differential equation:

$$\frac{dK(t)}{dt} = -\lambda_2 K(t) + bV(t) - dK(t)V(t)^{\frac{2}{3}} - eK(t)g(t) \qquad (3.10)$$

where λ_2, b, d, and e are coefficients (to be estimated) and $g(t)$ is a function describing the exposure to the antiangiogenic agent. The authors claimed that this modeling approach was also applicable to the clinics: simulations suggested that the investigated compounds should be given using continuous dosing. The concept of carrying capacity was adopted and modified in many recent papers [95, 96, 97].

Ribba et al. [97], for instance, studied the unperturbed tumor growth in mice xenografted with HT29 and HCT116 colorectal cancer cell lines. The authors considered the simultaneous presence in the tumor of proliferating nonhypoxic tissue (P) and hypoxic tissue (Q), and nonproliferating necrotic tissue (N), and described the dynamics of these cell subpopulations. Nonhypoxic and hypoxic tissues proliferate following similar dynamics (generalized-logistic equations), in which the maximal tumor size is given by the carrying capacity (K). Whilst the tumor grows, the carrying capacity also increases. At the same time, a fraction of the proliferating nonhypoxic cells is transformed into hypoxic cells, and, in turn, a portion of the hypoxic cells is converted into necrotic cells. Both the growth of P and Q and

the transition between them are ruled by the hypoxic stress s, defined as the ratio between P^* and K, where $P^* = P+Q+N$. The equations are as follows:

$$\begin{aligned}
&\frac{dP(t)}{dt} = \lambda_P \cdot P(t) \cdot (1 - s(t)^\alpha) - k_{P\to Q} \cdot P(t) \cdot s(t)^\alpha \\
&\frac{dQ(t)}{dt} = k_{P\to Q} \cdot P(t) \cdot s(t)^\alpha + \lambda_Q \cdot Q(t) \cdot (1 - s(t)^\alpha) - k_{Q\to N} \cdot Q(t) \\
&\frac{dN(t)}{dt} = k_{Q\to N} \cdot Q(t) \\
&\frac{dK(t)}{dt} = b \cdot P^* \\
&P(t=0) = P_0 \qquad Q(t=0) = 0 \qquad N(t=0) = 0 \qquad K(t=0) = K_0 \\
&P^* = P(t) + Q(t) + N(t) \\
&s(t) = \frac{P^*}{K(t)}
\end{aligned} \tag{3.11}$$

where λ_P and λ_Q are the proliferation rates of the nonhypoxic and hypoxic tissues, respectively, $k_{P\to Q}$ and $k_{Q\to N}$ are the rate constants for the transitions from nonhypoxic to hypoxic cells and from hypoxic to necrotic cells, respectively, and α is a parameter to be estimated. One of the main features of this model is that it allowed the incorporation of biomarker data related to tumor tissue hypoxia status with good accuracy, indicating its strong mechanistic base. The model was parameterized based on the linear dimension of the tumor as in the field of clinical oncology tumor dimensions are often described by the sum of the major dimensions of the measurable lesions.

The effect of vaccines on tumor growth was also modeled. Parra-Guillen et al. [14], for instance, developed a semi- mechanistic K-PD model to describe the TGI caused by a vaccine administration in

C57BL/6 mice developing tumors following the inoculation of human papillomavirus E7 protein. The model is schematically summarized in Figure 3.3.

Combination therapy

Combination therapy, which involves the administration of two or more drugs, is very common in anticancer treatments. Investigating the effect of multiple drug administration is therefore necessary.

Koch et al. [81] described the antitumor effect of anticancer compounds given alone or in combination in in vivo xenograft models. The starting point was the Simeoni TGI model [75] with minor modifications. The combined administration of two anticancer compounds was described through the interaction term $TI(t)$ (Eq. 3.12):

$$TI(t) = k_2^A c^A(t) + k_2^B c^B(t)\psi \tag{3.12}$$

where $k_2^A, k_2^B, c^A(t)$ and $c^B(t)$ are the potency parameters and the plasma concentrations of the compounds A and B, respectively. The empirical parameter ψ indicates the nature of the drug–drug interaction: values of ψ less than, equal to, or greater than 1 correspond to antagonistic, additive, or synergistic effects, respectively. This approach was also used by Li et al. [80] to model the schedule-dependent effect of the combined administration of erlotinib and gemcitabine.

Terranova et al. [98] described the effect of the combined administration of anticancer drugs starting from a previous approach proposed by Rocchetti et al. [99]. When drugs A and B are given in combination, it is assumed that cells hit by one agent can also be hit by the other one as well. As a consequence, 16 possible states of tumor cells are represented by a 4×4 mortality matrix, modeling the chance that the potency of a compound can change because of the interaction

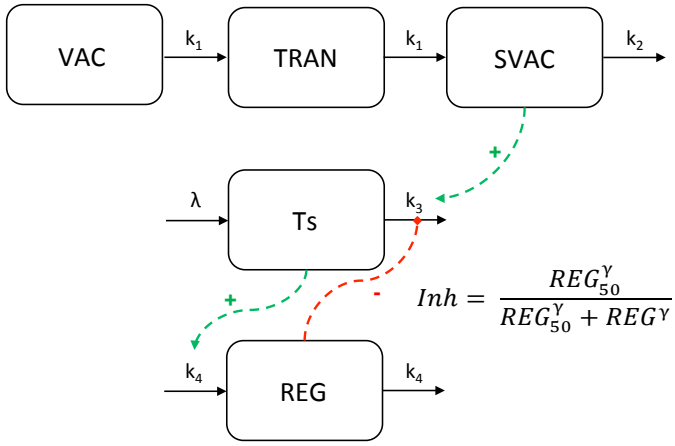

Figure 3.3: **Model for vaccine action on tumor growth.** The pharmacokinetics of the vaccine (VAC) is described by an exponential decline (K-PD model). After a delay, described by a transit compartment model (TRAN), the vaccine produces a signal (SVAC) responsible for decreasing the size of the tumor via a second order process (Ts). A push-and-pull model is included to describe a feedback resistance mechanism (REG) to the action of the vaccine. Reproduced from [14] with permission of Springer.

with the other drug. Drugs interplay was modeled as proportional both to the weight of proliferating cells and drugs concentrations via an interaction term γ. When γ is equal to, less than, or greater than 1, an additive, antagonistic, or synergistic interaction is modeled, respectively. The remaining model parameters are in agreement with the Simeoni model [75]. Differently from [81], in which only k_2^A and k_2^B are estimated from single agent experiments and $\lambda_0, \lambda_1, w_0, k_1$ and ψ are estimated from the combination data, in this approach all the model parameters are estimated from single agent data, and only the interaction parameter γ is estimated from combination experiments.

When dealing with antiangiogenic therapies, the Simeoni TGI model [75] can be used to accommodate their tumoristatic effect. Nevertheless, the effect of these compounds could be better described by the Hahnfeldt model [94]. Another potential alternative is to include an inhibitory function on the unperturbed growth, rather than using the cell kill mortality chain adopted in the Simeoni model. This approach was used by Rocchetti and coworkers [100] for tumor inhibition data in which bevacizumab was administered as single agent. Data from combination experiments in which bevacizumab was given with a Polo-like kinase 1 (PLK1) inhibitor were also analyzed. In this case, the cytotoxic effect of the PLK1 inhibitor was described using the Simeoni model. The observed weak antagonistic effect between the two compounds was modeled via an inhibitory function, parameterized with bevacizumab concentration ($c_b(t)$), applied on the potency parameter $k_{2,PLK1}$ of the PLK1 inhibitor, as reported in Eq. 3.13:

$$k_{2,PLK1,inh} = k_{2,PLK1} \frac{c_b(t)}{IC_{50,b} + c_b(t)}. \tag{3.13}$$

The model was used to propose sequencing and timing of the two components of the combination to be explored in the next phases of development. Wilson and coworkers [96] used a model based on the

carrying capacity [94] to describe tumor diameters data following the combined administration of the cytotoxic agent irinotecan and the antiangiogenic compound sunitinib. The authors concluded that a weak synergism was present between the two drugs.

3.3.2 PK–PD tumor growth models incorporating the interaction with the target

PK–PD tumor growth models incorporating the interaction with the target

In the approaches described in the previous section, tumor dimensions alone were modeled, and only incidentally biomarker data were included for increasing the mechanistic base of the model. In the models presented in this section, events leading to the antitumor response (target engagement and downstream events, such as the inhibition of the phosphorylation of certain proteins) are instead explicitly considered. These events are integrated as root cause of the eventual inhibitory effect on the tumor growth, in agreement with the biomarker definition of Danhof and coworkers [101]. This integration can facilitate the translation from animals to humans [102] (see Section 3.3.2). In many published papers, biomarker dynamics are therefore linked to tumor growth by combining PK–PD models (see Table 3.2). For instance, standard indirect effect models [103] may be used to describe markers of target engagement, considered in turn as drivers of the effect on tumor growth.

Bueno and coworkers [84] proposed a model to link the plasma concentrations of a receptor $TGF - \beta$ kinase antagonist to the percentage of phosphorylated Smad2 and Smad3 (pSmad) in tumors. It was reported that pSmad interacts with Smad4 and forms a complex that, after entering the nucleus, regulates the transcription of several

genes responsible for tumor proliferation [104]. The authors therefore assumed a standard indirect response model (type I, inhibition of the production of the response, Eq. 3.14) [105] to describe the rate of change of pSmad concentration in tumors:

$$\frac{dpSmad(t)}{dt} = k_{in} \cdot \left(1 - \frac{I_{max} \cdot c_{inhibitor}(t)}{IC_{50} + c_{inhibitor}(t)}\right) - k_{out} \cdot pSmad(t), \quad (3.14)$$

where k_{in} is the zero-order rate of pSmad production, I_{max} is the maximal inhibitory activity, IC_{50} is the concentration of inhibitor leading to half of the maximum effect, $c_{inhibitor}(t)$ is the plasma concentration of the inhibitor, and kout is the first-order rate describing the disappearance of pSmad. Tumor data in Calu-6 non-small cell lung cancer and MX1 breast cancer xenografts were modeled using two alternative approaches, including a Simeoni-like model. It was assumed that the extent of pSmad inhibition (expressed by $\frac{[pSmad_{baseline} - pSmad(t)]}{pSmad_{baseline}}$) reverts tumor proliferation via a two-compartment transit system [106]. The model was able to accommodate both pSmad concentrations and tumor volumes data with good accuracy. Alternative dosing regimens (one day on/one day off and one week on/one week off) were compared and resulted in similar tumor growth profiles. The authors concluded that this model was also able to provide information on the $TGF - \beta$ kinase transduction processes.

Salphati and coworkers [107] developed a PK–PD model for the effects of a phosphatidylinositol 3-kinase (PI3K) inhibitor in MCF-7 breast cancer xenografts. PI3K catalyzes the phosphorylation of substrates that leads to the activation of the protein kinase Akt and other downstream effectors, such as PRAS40 [108]. The authors firstly proposed two separate indirect response models: the first one links PI3K plasma concentration to TGI, and the second one relates drug plasma concentration to the inhibition of Akt and PRAS40 phosphorylation.

An integrated drug-to-biomarker and biomarker-to-tumor model was finally proposed, and comparable results in terms of IC_{50} were obtained between the two approaches.

Sardu et al. [109] derived the conditions under which the antitumor effect is equivalent when the drug-induced tumor growth modulation is expressed directly, considering drug plasma concentration, and indirectly, by means of biomarker inhibition. For instance, when an integrated model consisting of a type I indirect response model (inhibition of production) linked to the Simeoni TGI model [75] was considered, it was demonstrated that, in steady state conditions, the following does hold (Eq. 3.15):

$$\overline{c} = IC_{50} \cdot \frac{\overline{I}}{I_{max} - \overline{I}} \tag{3.15}$$

where $\overline{c}$ is the concentration at steady state providing the inhibition $\overline{I}$, and I_{max}, and IC_{50} are the maximal inhibition and the concentration leading to 50% of the maximal effect on the biomarker. In these conditions, for a marker causally related to the antitumor activity, the antitumor potency (k_2) and the IC_{50} for two candidates A and B with the same mode of action are linked via a direct proportionality relationship, as in Eq. 3.16:

$$\frac{k_2^B}{k_2^A} = \frac{IC_{50}^A}{IC_{50}^B} \tag{3.16}$$

As a consequence, antitumor potency of new candidates can be characterized via biomarker experiments, without the more resource-demanding experiments in xenografted animals.

Additional complexities were included in some recent papers dealing with tumor growth models incorporating the interaction with the

target. Ji et al. [110] described the effect of an epidermal growth factor receptor (EGFR) tyrosine kinase inhibitor on the phosphorylation of EGFR (pEGFR), and the subsequent TGI in MCF-7 breast cancer xenografts. The authors adopted an indirect response model for pEGFR inhibition; a time-dependent term was included for the development of tolerance. Tumor growth was modeled with a logistic equation and modulated by an inhibition index computed from the biomarker model. Delays in candidate drug effects were accommodated using a transit compartment system. In the opinion of the authors [110] , this model provided a deeper understanding of the potential relationships between the tolerance of the pharmacological action on pEGFR and the development of tumor resistance. Titze et al. [111], besides using an integrated biomarker-TGI model, considered also an in-target biomarker of toxicity (hyperglycemia) following the administration of an insulin growth factor receptor inhibitor.

Combination therapy

Systems pharmacology-type models were also reported in the literature; they included more complex networks of events leading to the tumor response. Harrold et al. [112], for instance, developed a multiscale model based on a target-mediated drug disposition (TMDD [113]) model for rituximab given in combination. The interaction with the target CD20 was considered, and several downstream additional events were quantified (modulation of RKIP and downstream changes of NFkB, Bcl-xL, and Fas expression). Dependent on the CD20 interaction, rituximab was assumed to both inhibit the tumor growth and induce a cell kill process. The model was used to establish the effects of rituximab alone and in combination with cytotoxic agents (fenretinide or rhApo2L) in Ramos lymphoma xenografts, and a synergistic interaction was demonstrated. The authors claimed that this model could provide a mechanistic framework for optimizing the antitumor

effect of CD20 antagonists given in combination.

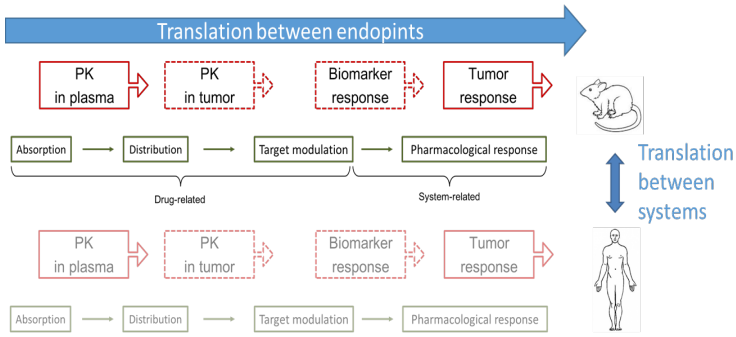

Figure 3.4: **Schematics depicting the conceptual translational approaches.**

Translational capabilities of PK-PD models

In some cases, impressive correlations have been found between model-based parameters obtained from PK–PD models directly describing TGI data in xenograft models and the doses used in clinical settings [90]. The use of these parameters, especially when they are obtained from models with some mechanistic grounds, allows a much more efficient translation between preclinical and clinical settings compared to experiment-dependent metrics of antitumor efficacy [114]. Examples of translational modeling in agreement with this concept appeared in the recent literature and some of them are reported in Table 3.2. It has to be noticed that the various audit trail steps [58] that lead from target interaction to clinical response represent a translational process in itself (translation between endpoints, see Figure 3.4) that strengthen the mechanistic base of the modeling approach. Therefore, approaches incorporating the various levels of biomarkers should be considered as having the highest value in terms of their

translational capabilities across different systems. Some examples are detailed here below.

A group particularly active in this field is the one of Yamazaki and coworkers; in a series of papers [115, 116, 117, 118, 119, 120] the link between PK, PD markers, and TGI was explored for different agents with translational purposes. In [115], data of PF02341066 (crizotinib), a cMet inhibitor, were evaluated. Crizotinib PK, marker of target engagement (phosphorylated cMet, pcMet) and tumor size data were modeled following administration of the compound in GTL16 gastric carcinoma or U87MG glioblastoma xenografts. An indirect response model [102] for pcMet was linked to a one-compartment PK model via an effect compartment [121, 122], which was interpreted as a distributive delay from the systemic circulation to the tumor biophase. An exponential growth, saturable at higher tumor sizes, described tumor size dynamics, while an inhibitory function was adopted for compound effect. The authors concluded that, in order to have more than 50% TGI, a strong (>90%) cMet phosphorylation inhibition was needed. Additional considerations were done in subsequent papers [116, 119], where phosphorylation of the anaplastic lymphoma kinase (ALK) was used as an additional marker of target engagement. In this case, PK–PD–TGI models suggested that 50% ALK phosphorylation inhibition was sufficient to obtain a 50% TGI. Overall, this led to indications that a 75% pALK and a 95% pcMet inhibition are needed to achieve a positive outcome in the clinics. Analogous approaches were applied to other ALK inhibitors [117], in which, similarly to previous papers [116, 119], a 50% ALK phosphorylation inhibition led to a 50% inhibition of tumor growth. The fact that this was observed with compounds with significantly different PK profiles demonstrates that the relationships between PD target modulation and antitumor efficacy were similar between compounds with the same mechanism of action. This confirms that the events downstream to target inhibition

are essentially system-related. This can provide a third dimension in the translational processes: quantitative knowledge can be translated from a candidate compound to the following back-up compounds. It is important to underline that this can cover for the relative sparsity of the information generated in the early discovery phases.

A model similar to [117] was developed by Wang and coworkers [123] to evaluate the effect of gefitinib on LN229 wild- type or mutant-bearing mice. PK, phosphorylated-extracellular signal-regulated kinase 12 (pERK) and tumor size were assessed. A standard compartmental model, a precursor pool indirect response model [106], and a signal distribution TGI model [83] were used. This approach was applied to both wild-type and mutant tumors to establish the condition to obtain the same pERK profile (PK/PD equivalence condition): this was achieved when a 1.83 higher dose was given to the xenografts bearing the wild-type tumor with respect to the ones bearing the mutant tumor. Human PK data, brain tumor to blood ratio from literature and the preclinical pERK model were used as the basis of a simulation exercise, which revealed that a double dose should be used in patients with the wild- type tumor. Also Tanaka et al. [124] combined data obtained in rats bearing CA20948 pancreatic tumors (PK in plasma, S6K1 inhibition in tumor and peripheral blood mononuclear cells (PBMCs) and tumor inhibition) and in human subjects (PK in plasma, and S6K1 inhibition in PBMC). A model was developed in rats linking S6K1 inhibition in tumors or PBMC and antitumor effect. The PD model was then applied to the data available in humans, only correcting for the PK differences between species. Simulations indicated that to obtain similar PD profiles providing antitumor effect in the animal model, weekly doses of 20–30 mg or daily doses of 5 mg should be used in humans.

Table 3.2: **Summary of recent modeling approaches used to describe in vivo experiment results in oncology drug discovery.** Two categories were considered: in vivo direct models (where tumor size was modeled) and in vivo models with biomarkers (where target engagement and downstream events were considered). For each category, the papers are reported by year of publication.

AUC: area under the plasma concentration-time curve; CpG: CpG 1826, CpG1826: 5-TCCATGACGTTCCTGACGTT-3, a TLR9 ligand; CTX: cyclophosphamide; EGFR: epidermal growth factor receptor; NLME: nonlinear mixed effect; pALK: phosphorylation of the anaplastic lymphoma kinase; PBMC: peripheral blood mononuclear cell: pcMet, phosphorylated cMet; PD: pharmacodynamic; pEGFR: phosphorylation of EGFR; pERK: phosphorylated-extracellular signal- regulated kinase 1/2; PK: pharmacokinetic; pMEK: phosphorilated MEK; pSmad: phosphorylated Smad; TD: tumor diameters; TGF: tumor growth factor; TGI: tumor growth inhibition; TMDD: target-mediated drug disposition; TV: tumor volumes.

Tumor type	Drug(s)	Marker endpoints	Observation	Model type	Notes
In vivo direct PK-tumor growth inhibition					
PC3 human prostate cancer, HCT116 human colon carcinoma [81]	Single agents and combination: various drug candidates	-	TV	Simeoni model [75] with interaction term; nonlinear regression	

(Continued overleaf)

(Continued from the preceding page)

Tumor type	Drug(s)	Marker endpoints	Observation	Model type	Notes
COLO-205 human colon cancer [125]	Single agents: GDC-0973, mitogen-activated protein kinaseextracellular signal-regulated kinase (ERK)1/2 inhibitor	-	TV	Exponential growth; drug effect via saturable E_{max} cell kill; tumoristatic concentration; nonlinear regression	PK predictions in human via allometry and clinical dose based on tumoristatic concentrations
L540cy human Hodgkin's Lymphoma, Karpas299 human anaplastic large cell lymphoma [126]	Antibody–drug conjugate: brentuximab-vedotin	-	TV [2]	Multiscale model; modified Simeoni model [75] with saturable E_{max} cell kill; nonlinear regression	PK predictions in human by incorporating patient data to simulate tumor response and progression-free survival

(Continued overleaf)

[2]connected to the other clinical endpoints based on literature data

(Continued from the preceding page)

Tumor type	Drug(s)	Marker endpoints	Observation	Model type	Notes
Various xenograft and allograft models [127]	Single agents: vismodegib (GDC-0449), erlotinib, trastuzumab, sunitinib, dasatinib, 5-FU, carboplatin, docetaxel	-	TV	Modified Simeoni model [75] with saturable Hill cell kill; simulated TGI in humans	Simulated TGI in humans correlated significantly with overall clinical response
MDA-MB-361/DYT2 human breast adenocarcinoma, MDA-MB-435/5T4 transfected human breast adenocarcinoma, N87 human gastric cancer, H1975 human NSCLC, 37622A (PDX)	Antibody–drug conjugate: trastuzumab-DM1 [128]	-	TV	Logistic growth; Modified Simeoni model [75] with saturable E_{max} cell kill; tumoristatic concentration; NLME	Paramter form xengraft together with predicted PK in humans to simulate clinical data

(Continued overleaf)

(Continued from the preceding page)

Tumor type	Drug(s)	Marker endpoints	Observation	Model type	Notes
H1299 human NSCLC [80]	Single agents and combination: gemcitabine and erlotinib	-	TV	Simeoni model [75] with interaction term as proposed by Koch [81]; nonlinear regression	
HT29 human colon adenocarcinoma, A549 human pulmonary adenocarcinoma, DU145 human prostate cancer, MX-1 human breast carcinoma [100]	Single agents and combination: bevacizumab and NMS-P937	-	TV	Simeoni model [75] with interaction term; nonlinear regression	Simulations of different regimen to optimize the antitumor effect
A2780 human ovarian carcinoma, HT29 human colon adenocarcinoma, BxPC-3 human pancreatic adenocarcinoma [98]	Single agents and combination: 5-fluorouracil, cisplatin, gemcitabine, irinotecan, and four other drug candidates	-	TV	Simeoni model [75] with interaction term; nonlinear regression	

(Continued overleaf)

(Continued from the preceding page)

Tumor type	Drug(s)	Marker endpoints	Observation	Model type	Notes
Human papillomavirus E7 protein, MC38 mouse colon carcinoma [14]	Vaccine: CyaA-E7	-	TD	PK signal modeled with a declinining exponential; tumor size dynamics and tumor interaction with immune system	No PK, only doses
Human papillomavirus E7 protein [129]	Single agents and combination: CyaA-E7 (vaccine), CpG and CTX	-	TD	Expansion of Parra-Guillen [14] to account for PD effect triggered by CpG and CTX	No PK, only doses

(Continued overleaf)

(Continued from the preceding page)

Tumor type	Drug(s)	Marker endpoints	Observation	Model type	Notes
MMTV-HER2 Fo5 transgenic mice mammary tumor derived from MMTV HER2 transgenic FVB mouse, Founder Number 5 (Fo5), BT474EEI derived from human breast tumor line [130]	Antibody–drug conjugate: trastuzumab-DM1	-	TV	Various models compared; tumoristatic concentration; NLME	
RCC CAKI-2 human renal cell carcinoma [95]	Pazopanib	-	Preclinical: TV; clinical: TD	Hahnfeldt model [94]; drug effect on both growth and carrying capacity (parameterized on AUC); NLME	Same model with an empirical correction working for both preclinical and clinical data

(Continued overleaf)

(Continued from the preceding page)

Tumor type	Drug(s)	Marker endpoints	Observation	Model type	Notes
HT29 human colon adenocarcinoma [96]	Single agents and combination: sunitinib and irinotecan	-	TD	PK signal modeled with a declining exponential; Hahnfeldt model [94] with carrying capacity	No PK, only doses
Ramos human Burkitt lymphoma, RL human non-Hodgkin's lymphoma, REH human acute lymphoblastic leukemia [131]	Antibody–drug conjugate: inotuzumab ozogamicin	-	TV	Plasma and cellular PK of antibody and cytotoxic, including data on CD-22 from *in vitro* data; modified Simeoni [75] (with saturable growth and saturable E_{max} cell kill); nonlinear regression	Parameters from xenograft together with predicted PK in humans (allometry) to simulate clinical data

(Continued overleaf)

(Continued from the preceding page)

Tumor type	Drug(s)	Marker endpoints	Observation	Model type	Notes
W256 rat Walker carcinosarcoma [93]	Etoposide	-	TV	Nonlinear regression; modified Simeoni [75] (with saturable E_{max} cell kill); NLME	
		Integrated PK-markers-TGI			
CA20948 rat pancreatic cancer [124]	RAD001 (everolimus)	S6K1 activity in PBMC and tumor	TV [3]	Target S6K1 activity was defined at the dose providing significant antitumor activity; nonlinear regression	Clinical dose anticipation. Use of S6K1 in PBMC as pharmacological biomarker in clinical studies.
GTL16 human gastric carcinoma, U-87MG human glioblastoma [115]	PF02341066 (crizotinib)	pcMet in tumors	TV	Nonlinear regression; effect compartment and indirect response model for pcMet	Near complete pcMet inhibition required to elicit significant TGI

(Continued overleaf)

[3] no modelling

(Continued from the preceding page)

Tumor type	Drug(s)	Marker endpoints	Observation	Model type	Notes
Calu-6 human NSCLC, MX-1 human breast carcinoma [84]	LY2157299	pSmad in tumors	TV	Indirect response model; tumor growth (exponential or Simeoni [75]) inhibition linked to pSmad using a two-compartment transduction system	Simulation of alternative dosing regimens (intermittent) Information on TGF transduction provided
LN229 human glioblastoma wild type/EGFR mutant [123]	Gefitinib	pERK in tumors	TV	Precursor pool model; integrated growth (saturable) model; nonlinear regression	
A375 human melanoma, COLO-205 human colon cancer [132]	GDC-0879	pMEK in tumors	TV	Indirect response model; integrated TGI (exponential growth); nonlinear regression	60% pMEK inhibition required for tumor stasis

(Continued overleaf)

(Continued from the preceding page)

Tumor type	Drug(s)	Marker endpoints	Observation	Model type	Notes
MCF-7 human breast carcinoma [107]	GDC-0941	pAkt and PRAS40 in tumors	TV	Two separate indirect response models to relate PK to tumor volumes (exponential growth) and inhibition of Akt and PRAS40 phosphorylation; integrated PK-biomarker-tumor growth model; nonlinear regression on average data	

(Continued overleaf)

(Continued from the preceding page)

Tumor type	Drug(s)	Marker endpoints	Observation	Model type	Notes
HCT116 human colon carcinoma, HT29 human colon adenocarcinoma [97]	-	Hypoxia/ necrosis markers	TD	Hahnfeldt model [94] with carrying capacity and distinction between non-hypoxic, hypoxic and necrotic tumor cells; NLME	Modeling generic tumor growth with angiogenesis process
Ramos human Burkitt lymphoma [112]	Single agents and combination: rituximab, fenretinide and rhApo2L	Fraction of bound receptor, NFkB, Bcl-xL and Fas induced by CD20	TV	TMDD, receptor occupancy, network of markers, different modes of action; nonlinear regression	Synergy concluded

(Continued overleaf)

(Continued from the preceding page)

Tumor type	Drug(s)	Marker endpoints	Observation	Model type	Notes
H3122 human NSCLC, Karpas299 human anaplastic large cell lymphoma [116]	PF02341066 (crizotinib)	pALK in tumors	TV	Effect compartment and indirect response model for pcMet; separated TGI; NLME	50% pALK inhibition required for significant antitumor efficacy 70% pALK inhibition projected in patients given the 500 mg/day clinical dose
MDA-MB-231 human breast adenocarcinoma [127]	GDC-0917	cIAP1 degradation in PBMC	TV	Inhibitory E_{max}; separated TGI (exponential growth, saturable cell kill); non-linear regression	Simulation of human behavior in agreement with observations
H3122 human NSCLC [133]	PF06463922	pALK	TV	Precursor pool model for biomarker; separated TGI; NLME	60% pALK inhibition to be targeted in the clinics

(Continued overleaf)

(Continued from the preceding page)

Tumor type	Drug(s)	Marker endpoints	Observation	Model type	Notes
H3122 human NSCLC [117]	Single agents: PF06463922, PF06471402	pALK	TV	Precursor pool model for biomarker; separated TGI; NLME	Consistent PD modulation was found to be active for compounds with the same mode of action
GEO human colon carcinoma[111]	BI 893923	pIGF1R, blood glucose level	TV	Effect compartment and indirect response model; transit compartment system; Simeoni growth [75] drug effect via pIGF1R; separated indirect response model for glucose (tolerability); NLME	Modeling of in-target safety marker (blood glucose)

(Continued overleaf)

(Continued from the preceding page)

Tumor type	Drug(s)	Marker endpoints	Observation	Model type	Notes
MCF-7 human breast carcinoma [110]	TM208	pEGFR	TV	Combined tolerance/ indirect response model; logistic growth; drug effect via pEGFR inhibition; NLME	

3.4 Discussion

An increasing number of modeling approaches is continuously proposed in the literature to support the drug discovery in the oncology therapeutic area. The examples examined in this review provide a relatively comprehensive range of applications, from the high throughput *in vitro* screen to the more laborious assessment of antitumor efficacy in *in vivo* models with all the satellite PK and PD evaluations. Diverse types of anticancer drugs were considered in the reviewed modeling exercises: "classic" cytotoxic agents, antiangiogenic compounds, vaccines, and targeted therapies. As far as *in vitro* experiments are concerned, the modeling approaches transitioned from simple Hill equations to models able to deal with the time course of cell growth, both in control and treated cells. This allowed exploiting the possibility to translate *in vitro* results to the *in vivo* context. In all cases, the candidate drugs with new modes of action boosted the development of new modeling approaches. For instance, the carrying capacity concept was used for antiangiogenic compounds and the quantitative modeling of the pharmacological audit trail was started when there was the need of supporting the new targeted therapies. Furthermore, some of the modeling approaches also allowed the exploration of the effect of combination therapies, a situation that is very common in cancer treatment. Complex models, aiming to provide a more detailed explanation of the tumor growth and TGI processes, should be adopted with caution due to potential a posteriori identifiability problems. Large uncertainty of the estimates may lead to unreliable results; this could be particularly critical when these models are used for simulating untested conditions.

Optimizing the experimental design is of paramount importance. Recent papers indicated in a rigorous manner the importance of measuring the tumor volumes in xenografted animals also in the regrowth

phase, and not only in the tumor inhibition phase [134]. This approach provides more stable parameter estimates and thus may lead to a lower number of experiments and the minimization of the use of experimental animals. The adoption of appropriate statistical analysis tools is equally important: for instance, the selected methods should allow to properly handle the missing or censored data of the experiments [135, 136]. In addition, also the modeling strategy should be carefully evaluated and adapted to the experimental design. Although simple nonlinear regression can provide important conclusions for the development of oncology candidates, the use of NLME should be preferred, especially in case of large interindividual variability or experimental designs that imply additional intergroup variabilities. Indeed, NLME allows estimating appropriate random effects (for instance, intergroup, interindividual, interoccasion, intercompound), reducing the bias and decreasing the parameter uncertainties. A further improvement in drug discovery may be given by the use of more mechanistic models, such as system pharmacology or physiologically based (PB) PK–PD models [137]. In particular, due to the advent of commercial tools, enabling an easier model building procedure, and the translational capabilities of the PBPK models, this approach is increasingly used. However, the expensive model validation and the incomplete physiologically characterization of the subjects with tumors [138] represent the major obstacles to the more general and effective use of these approaches.

In many instances, drug plasma concentration is used as a surrogate for drug concentration in tumor. When complexities do exist in the link between plasma and tumor time courses, plasma concentration–time data may not be a good surrogate for the tumor exposure, hence preventing a full understanding both of PK in tumor tissue and, therefore, of the overall drug effect. A potential solution is the direct measurement of drug concentration in tumors [93].

PK information is of great importance to set up the target values of systemic exposure to be explored in the clinical investigations. Besides drug plasma concentrations, biomarkers are also widely used as drivers of anticancer treatment effect. Predefined levels of biomarker modulation can be used as target to guide the choice of the dosing regimen to be explored in the first clinical trials.

Sometimes, the extrapolation from preclinical to human subjects may be unsuccessful; in particular, this may be due to the use of models (animal species, cell lines, etc.) that are not fully representative of the disease in human patients and/ or of the actual patient situation. It should be stressed, however that, with some level of mathematical sophistication, it may be possible to disentangle and integrate all the factors that lead to tumor stasis or shrinkage in experimental models and human patients. Simple metrics of activity (e.g. *in vivo* percentage of TGI) are too much linked to the specific experimental conditions to be extended and translated directly to the clinics. Only experiment-invariant parameters, derived from models characterized by some mechanistic grounds (that allow the definition of drug-related and system-related parameters) and able to describe in quantitative manner uncertainty and intersubject variability, have the best chances to be applicable in a translational exercise. A smart use of mathematical and statistical modeling not only is essential for summarizing and integrating data (that in many instances are sparse and obtained in different experiments), but represents the only efficient way to extract the information from the studies performed in the drug discovery phase.

Chapter 4

Combination therapy in oncology: does the assessment depend on model choice?[1]

The simultaneous administration of several anticancer drugs is very common in cancer treatment. Especially when drugs are characterized by different ways of action, these protocols allow to hit cancer cells from multiple sides, and thus, to increase the probability to achieve a therapeutical result. Several models were proposed to describe the effect the combination therapies and to quantify whether drugs interact in a synergistic or antagonist way. However, different models drew opposite conclusions on the nature of the interaction between antiangiogenic and cytotoxic drugs (see Sec. 3.3.1).
The scientific question addressed in this chapter is whether the inferred

[1]The contents of this chapter are confidential

nature of the anticancer drug combination depends on the specific modeling strategy or not. To this aim, the combination of Sunitinib and Irinotecan in xenograft mice was used as case study. The impact of the three factors supposed to play a role in determining the nature of the interaction between the two drug, the pharmacokinetics model, the preprocessing of data (mean vs median) and the pharmacodynamic model, were studies.

4.1 Background

As discussed in Chapter 3, combination therapy is very common in anticancer treatment. The rationale underpinning the simultaneous administration of two (or more that two) drugs is to attack tumor cells from different sides, in order to increase the potency of the treatment and to achieve a faster and long-lasting tumor eradication.To this purpose, different class of drugs, with different ways of action, are given. One of the most commonly given combination therapy is the combined administration of cytotoxic and antiangiogenic agents. Antiangiogenic agents act by inhibiting the Vascular Endothelial Growth Factor (VEGF) signal generated by cancer cells to build new blood vessels [139]. Via these vessels, oxygen and nutrients needed for tumor growth are delivered. Consequently, by turning off the VEGF signal, tumor is deprived of the essential elements for growth. Instead, standard cytotoxic drugs act exerting a toxic action on tumor cells. They damage tumor cells DNA, and consequently trigger apoptosis processes leading to a tumor reduction [140].
However, the results of this combination therapy are currently under investigation, since the nature of the interaction of these anticancer drug is not completely clear. In some works, a synergistic interactions between antiangiogenic and cytotoxic agents was reported [96], whilst in some others a negative interaction was found [100].

The aim of this chapter was to investigate if different modeling strategies lead to different results in terms of effectiveness of combination therapy, and consequently, to determine whether the conclusions on the drug-drug-interaction are model-dependent or not.

An adapted version of Rocchetti TGI model (PK/PD model) and an adapted version of Ouerdani model (K/PD model) were applied to the same dataset comprehending both single agent (vehicle, antiangiogenic agent and cytotoxic agent) and combination treatment arms (antiangiogenic + cytotoxic drugs). Three factors were supposed to play a role in determining the nature of the interaction between the two drugs: the pharmacokinetics model, the data analyzed (mean vs median of measurements in different animals) and the pharmacodynamic model, as can be seen in Figure 4.1. As better explained in the Sec. 4.2.5, a combination of all these three factors was created.To distinguish the impact of each factor on the conclusions, results were summarized based on the factor under investigation (Figure 4.1).

4.2 Materials and methods

4.2.1 Animal data

Athymic nu/nu mice were xenografted with HT-29 colorectal cancer cells. The three orthogonal tumor dimensions (length, width and height) were collected using a caliper. When tumor volume reached 200-300 mm^3 treatment(s) started. A placebo arm, 2 single agent arms and 2 combination treatment arms were considered. Each arm was formed by 15 rodents. Placebo group animals received only placebo. One single agent arm was administered with 40 mg/kg of Sunitinib, an antiangiogenic drug, *via* oral gavage. The other was administered

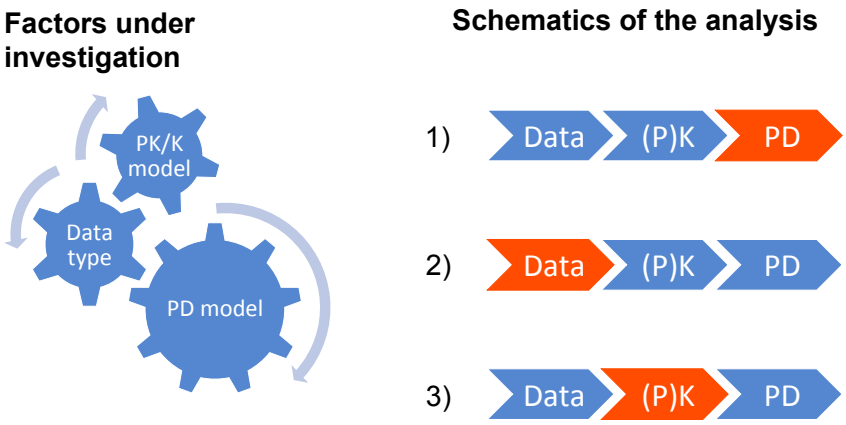

Figure 4.1: **Schematics of the analysis.** On the left: the three factors under investigation were reported: The PD model (adapted Rocchetti model vs adapted Ouerdani TGI model); the data analyzed (mean vs median) and the models describing the time course of the drugs in plasma (PK vs K model). On the right: the way in which the results of this analysis were summarized. Each factor was examined separately to better distinguish and indentify its impact.

with 90 mg/kg of Irinotecan, a cytotoxic compound, *via* 5-minutes IV infusion. The combination treatment arms were administered both with Sunitinib and Irinotecan, given at the same doses than the single agent arms.

Sunitinib was always administered once a day for 12 days starting from day 33. Irinotecan was always given only once: in the single agent arm it was administered at day 33; in one combination therapy arm (combination therapy protocol 1) at day 35 and in the second combination therapy arm at day 48 after injection (combination therapy

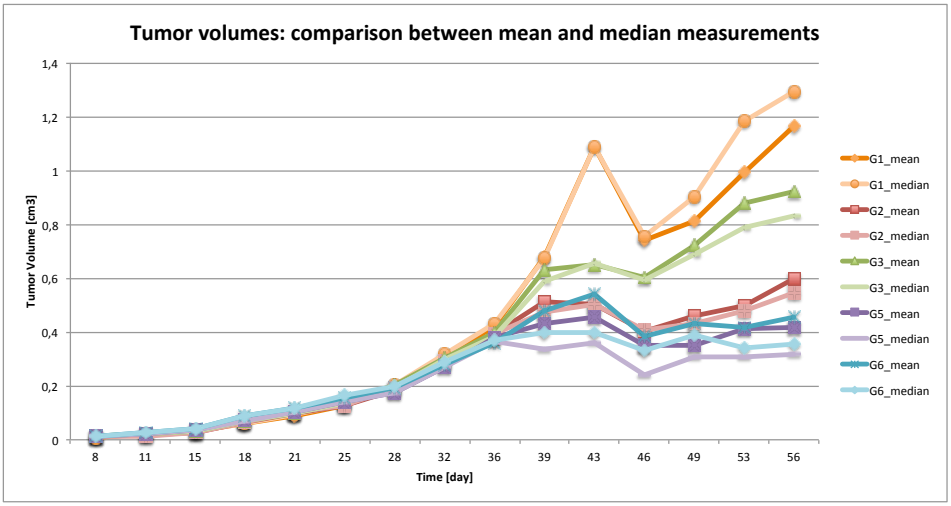

Figure 4.2: **Mean and median tumor volumes data time course.** Mean and median tumor volumes xenograft data. All the different treated arms analyzed in this work were reported. The group G1 is the control group, G2 is the single agent Sunitinib-treated group, G3 is the single agent Irinotecan-treated group, G5 is the "combination therapy protocol 1" arm, G6 is the "combination therapy protocol 2" arm.

protocol 2).

4.2.2 An adapted version of Rocchetti TGI model

The adapted version of the Rocchetti TGI model used to perform the analyses reported in this chapter was presented here. As in the original work of Rocchetti and coworkers [100], the tumor growth in vehicle-treated animals was modeled as an exponential growth followed by a linear one by using the Simeoni model [75] (Figure 3.2 b). The TGI observed in single agent cytotoxic-treated animals was described by using the Simeoni TGI model [75] (Figure 3.2 c). The effect of the

antiagiogenic compound was described starting from [100], where an inhibitory E_{max} function to model the Sunitinib tumoristatic effect was used. An effect compartment was added to accomodate the Sunitinib delayed effect [141]. The final model describing the TGI caused by the antiangiogenic drug is the following one (Eq. 4.1)

$$\begin{aligned}
&\frac{dC_{eff}(t)}{dt} = k_{eff} \cdot c_A(t) - k_{eff} \cdot C_{eff}(t) \\
&\frac{dW(t)}{dt} = \frac{\lambda_0 W(t)}{\left[1 + \left(\frac{\lambda_0}{\lambda_1} \cdot W(t)\right)^{\psi}\right]^{\frac{1}{\psi}}} \cdot \left(1 - \frac{E_{max} \cdot C_{eff}(t)}{IC_{eff,50} + C_{eff}(t)}\right) \\
&C_{eff}(t=0) = 0 \\
&W(t=0) = w_0
\end{aligned} \tag{4.1}$$

$c_A(t)$ is the Sunitinib plasma concentration over time and the state $C_{eff}(t)$ is the time course of the "effective" drug concentration, i.e., the one driving the therapeutical effect. The delay observed between the Sunitinib administration and its effect was expressed *via* the time constant k_{eff} [day^{-1}]. From now on, this model was indicated as *adapted Rocchetti TGI model*.

In **combination therapy**, the null-interaction hypothesis between the antiangiogenic and the cytotoxic drugs was tested. This hypothesis consists in postulating an additive behaviour of the two drugs, each of which acts as the other drug was not been administered. From a mathematical perspective, it is described by a join model (Eq. 4.2) which integrates the tumoristatic effect of Sunitinib (Eq. 4.1) and the TGI action of Irinotecan (Figure 3.2). The subscript A and B are referred to Sunitinib and Irinotecan, respectively.

$$
\begin{aligned}
&\frac{dC_{eff}(t)}{dt} = k_{eff} \cdot c_A(t) - k_{eff} \cdot C_{eff}(t) \\
&\frac{dX_1(t)}{dt} = \frac{\lambda_0 X_1(t)}{\left[1 + \left(\frac{\lambda_0}{\lambda_1} \cdot W(t)\right)^{\psi}\right]^{\frac{1}{\psi}}} \cdot \left(1 - \frac{E_{max} \cdot C_{eff}(t)}{IC_{eff,50} + C_{eff}(t)}\right) - k_2 \cdot c_B(t) \cdot Z_1(t) \\
&\frac{dX_2(t)}{dt} = k_2 \cdot c_B(t) \cdot X_1(t) - k_1 \cdot X_2(t) \\
&\frac{dX_3(t)}{dt} = k_1 \cdot X_2(t) - k_1 \cdot X_3(t) \\
&\frac{dX_4(t)}{dt} = k_1 \cdot X_3(t) - k_1 \cdot X_4(t) \\
&W(t) = X_1(t) + X_2(t) + X_3(t) + X_4(t) \\
&C_{eff}(t=0) = 0 \qquad X_1(t=0) = w_0 \qquad X_{2,3,4}(t=0) = 0
\end{aligned}
\tag{4.2}
$$

4.2.3 An adapted version of Ouerdani model

An adapted version of the model proposed by Ouerdani and coworkers [95] was adopted. The tumor growth was described following the spirit of the Hahnfeldt model [94]. In vehicle-treated animals, the tumor growth over time was modeled *via* the following ODE system Eq. 4.3:

$$
\begin{aligned}
&\frac{dV(t)}{dt} = \lambda \cdot V(t) \cdot \left(1 - \frac{V(t)}{K(t)}\right), \qquad V(t=0) = V_0 \\
&\frac{dK(t)}{dt} = b \cdot V(t)^{2/3}, \qquad K(t=0) = K_0
\end{aligned}
\tag{4.3}
$$

where P is the tumor volumes cm^3, λ its growth rate constant [day^{-1}], K the carrying capacity and b the capacity rate constant

[day^{-1}], which regulates how quickly the carrying capacity growth. Similarly to what proposed by Wilson and coworkers [96], here it was assumed that the antiangiogenic drug acts only on tumor vasculature variable K, which, in turns, controls the tumor growth Eq. 4.4.

$$\begin{aligned} \frac{dV(t)}{dt} &= \lambda \cdot V(t) \cdot \left(1 - \frac{V(t)}{K(t)}\right), && V(t=0) = V_0 \\ \frac{dK(t)}{dt} &= b \cdot V(t)^{2/3} - \beta_S \cdot p_S \cdot S(t) \cdot K(t), && K(t=0) = K_0 \end{aligned} \tag{4.4}$$

The state variable S represents the total amount of Sunitinib in the system, and the K-parameter p_S is the Sunitinib elimination constant (further details on this model parameterization were given in Sec. 4.2.4). Sunitinib effect is proportional to its dosing rate $p_S \cdot S$; whilst drug effectiveness is represented by the term β_S (Eq. 4.4).

A Simeoni-like mortality chain [75] was used to model the Irinotecan effect, resulting in the following model Eq. 4.5

$$\begin{aligned} \frac{dV_1(t)}{dt} &= \lambda \cdot V(t) \cdot \left(1 - \frac{V(t)}{K(t)}\right) - \beta_C \cdot p_C \cdot C(t) \cdot V_1(t), && V_1(t=0) = V_0 \\ \frac{dV_2(t)}{dt} &= \beta_C \cdot p_C \cdot C(t) \cdot V_1(t) - k_c \cdot V_2(t), && V_2(t=0) = 0 \\ \frac{dV_3(t)}{dt} &= k_c \cdot V_2(t) - k_c \cdot V_3(t), && V_3(t=0) = 0 \\ \frac{dV_4(t)}{dt} &= k_c \cdot V_3(t) - k_c \cdot V_4(t), && V_4(t=0) = 0 \\ \frac{dK(t)}{dt} &= b \cdot V_1(t)^{2/3}, && K(t=0) = K_0 \\ V(t) &= V_1(t) + V_2(t) + V_3(t) + V_4(t) \end{aligned} \tag{4.5}$$

where, similarly to the Sunitinib effect model parameterization: i) C is the amount of Irinotecan in the system (details in Sec. 4.2.4); ii) drug effect is proportional to its dosing rate $\beta_C \cdot p_C$, and iii) β_C and p_C represent the Irinotecan effectiveness and elimination rate, respectively.

To analyze combination therapy data the null-interaction between the antiangiogenic and the cytotoxic drugs was described by a join model (Eq. 4.6) integrating the Sunitinib effect of vasculature (Eq. 4.4) and the TGI action of Irinotecan (Eq. 4.5). The letters S and C are referred to Sunitinib and Irinotecan, respectively. From now on, this model was indicated as *adapted Ouerdani TGI model*.

$$
\begin{aligned}
&\frac{dV_1(t)}{dt} = \lambda \cdot P \cdot \left(1 - \frac{V(t)}{K(t)}\right) - \beta_C \cdot p_C \cdot C(t) \cdot V_1(t), \qquad V_1(t=0) = V_0 \\
&\frac{dV_2(t)}{dt} = \beta_C \cdot p_C \cdot C(t) \cdot V_1(t) - k_c \cdot V_2(t), \qquad V_2(t=0) = 0 \\
&\frac{dV_3(t)}{dt} = k_c \cdot V_2(t) - k_c \cdot V_3(t), \qquad V_3(t=0) = 0 \\
&\frac{dV_4(t)}{dt} = k_c \cdot V_3(t) - k_c \cdot V_4, (t) \qquad V_4(t=0) = 0 \\
&\frac{dK(t)}{dt} = b \cdot V_1(t)^{2/3} - \beta_S \cdot p_S \cdot S(t) \cdot K(t), \qquad K(t=0) = K_0 \\
&V(t) = V_1(t) + V_2(t) + V_3(t) + V_4(t)
\end{aligned}
\tag{4.6}
$$

Parameter	Value	Unit
V_d	7.6	[L/Kg]
F	60%	-
k_a	5.3663	[day^{-1}]
k_{10}	12.8842	[day^{-1}]
MW	398	[g/mol]

Table 4.1: **Sunitinib PK model parameters.** V_d is the volume of distribution; F is the bioavailability; k_a is the absorption and constant of the one-compartment model with absorption; MW is the molecular weight.

4.2.4 PK and K models and parameters

In the adapted Rocchetti model (Sec. 4.2.2), a standard compartmental approach for modeling the time course of the drugs under investigation was used. A one-compartment model with absorption described the time course of Sunitinib in plasma following oral administration [142]. Model parameters were reported in Table 4.1.
The time course of Irinotecan in plasma following IV administration was described by a two-compartment model [75], and the corresponding model parameters were reported in Table 4.2.

In the adapted Ouerdani TGI model (Sec. 4.2.3), the drug kinetics modelization typically used in the K/PD modeling [13] was adopted. In agreement with Wilson and coworkers [96], an exponential decay following each dose of Sunitinib and Irinotecan was supposed, as reported in Eq. 4.7. T_S and T_C stand for the Sunitinib and Irinotecan administration time. The K-parameters p_S and p_C were fixed to 2.12 and 0.085 day^{-1}, respectively [96].

Parameter	Value	Unit
V_1	4.85	[L/Kg]
k_{12}	0.276	[day^{-1}]
k_{21}	1.4784	[day^{-1}]
k_{10}	13.272	[day^{-1}]
MW	587	[g/mol]

Table 4.2: **Irinotecan PK model parameters.** V_1 is the volume of the central compartment; k_{12}, k_{21} and are the first order rate constant between compartments of the two-compartment model; k_{10} is the elimination constant; MW is the molecular weight.

$$\begin{aligned} \frac{dS(t)}{dt} &= -p_S \cdot S(t) \qquad S(t = T_S) = 1 \\ \frac{dC(t)}{dt} &= -p_C \cdot C(t) \qquad C(t = T_C) = 1 \end{aligned} \tag{4.7}$$

4.2.5 Analysis

To investigate how the conclusions of negative, null, or positive interaction between the antiangiogenic and the cytotoxic drug might change based on the i) data; ii) K or PK model; the PD model used; the following model combinations were examined.

- adapted Rocchetti TGI model with PK
- adapted Rocchetti TGI model with K (see App. B)
- adapted Ouerdani TGI model with K
- adapted Ouerdani TGI model with PK (see App. B)

All these modeling approaches were applied to perform pool analysis on both i) mean and ii) median data, resulting in 8 different models combinations.

Analyses were conducted using Monolix (version 4.4.0, Lixoft). Model parameters were estimated *via* a simultaneous fitting of the placebo and the two single agent arms. A proportional error model was adopted. Estimates were used to simulate the TGI effect exerted by the combination therapies under the hypothesis of null-interaction between compounds. To better distinguish the role of each factor, results were summarized based on the factor under investigation (Figure 4.1).

4.3 Results

4.3.1 PD models comparison

Data were described well by both PD models (adapted Rocchetti TGI model and adapted Ouerdani TGI model), as can be seen in Figure 4.3a. The adapted Ouerdani TGI model captured the "wave-shape" of the Sunitinib single agent arm data better than the adapted Rocchetti TGI model, which conversely better modeled the effect of the cytotoxic agent. When used to simulate the effect of the combination therapy under the null interaction hypothesis, both PD models showed that the bigger TGI effect was obtained by administering the combination therapy protocol 1 (Figure 4.3b in green), in agreement with observed data. In Figure 4.3 results obtained using median data were reported. Similar findings were obtained using mean data (not reported).

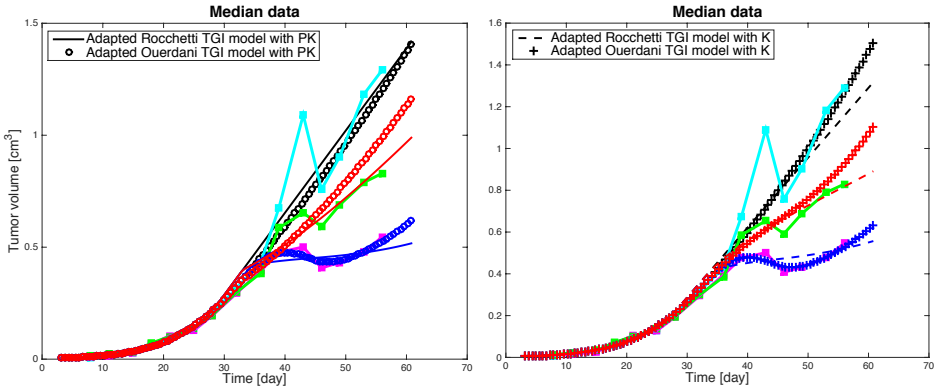

(a) PD models fits comparison.

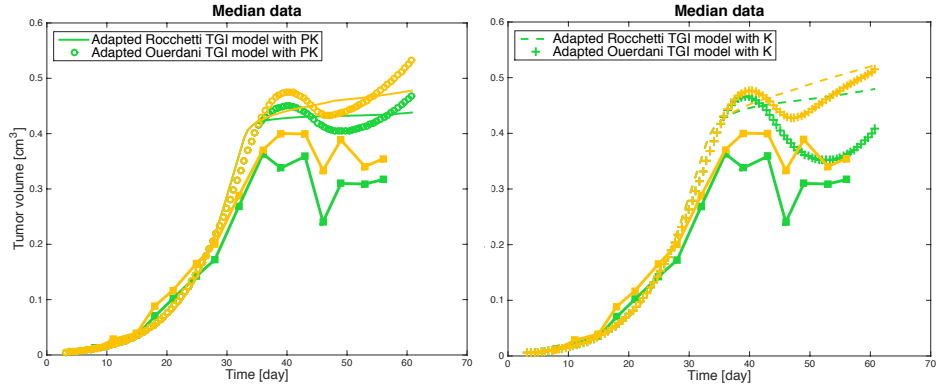

(b) PD models prediction comparison.

Figure 4.3: **PD models comparison.** The adapted Rocchetti TGI model and adapted Ouerdani TGI model were compared. The contribution of the PK part was reset. In Figure 4.3a the simultaneous fittings of the control and the two single agent arms. In black the control arm, in blue the antiangiogenic arm and in red the cytotoxic arm fits. The corresponding observed data were reported in cyan, pink and green. In Figure 4.3b predictions of the combination therapy protocol 1 (green) and 2 (yellow). Squares with solids line indicated experimental data. On the left of Figure 4.3a and Figure 4.3b the PD models with PK, on the right the PD models with K.

4.3.2 Mean/median data comparison

In describing tumor growth in vehicle-treated animals, a small difference in modeling the final phase of tumor growth was observed when the adapted Ouerdani TGI model (both with K and PK) was used to describe mean rather than median data (Figure 4.4); whilst the same fits were obtained when the adapted Rocchetti TGI model was used to accommodate mean and median data. A bigger difference between the use of mean and median data was observed when tumor growth profiles following single-agent Sunitinib treatment were considered, expecially for the adapted Rocchetti TGI model with PK and the adapted Ouerdani TGI model with K (Figure 4.5). The use of mean or median tumor growth measurement was irrelevant when modeling the Irinotecan TGI effect (Figure 4.6).

When predicting the combination therapy protocols, the comparison between experimental data and the mean and median TGI curves simulated under the null-interaction hypothesis showed a weak synergism between Sunitinib and Irinotecan. However, when uncertainty on the estimates was considered and propagated, observed data are in the predictions bandwidths, and the null-interaction hypothesis between the antiangiogenic and the cytotoxic agent was difficult to be rejected (Figure 4.7). The adapted Ouerdani TGI model resulted to be more sensitive to the difference between mean and median data than the adapted Rocchetti TGI model (Figure 4.7).

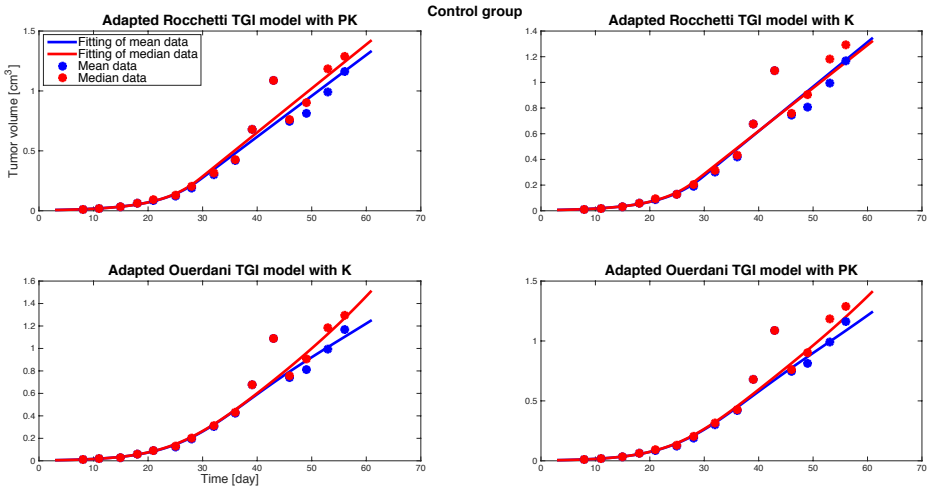

Figure 4.4: **Mean/median data control arm fits comparison**
Unperturbed tumor growth fits using the adapted Rocchetti TGI and the adapted Ouerdani TGI model (both with PK and K). The blue and the red lines are the curve-fitting obtained by using mean and median data, respectively. Blue and red dots represent the mean and the median data, respectively.

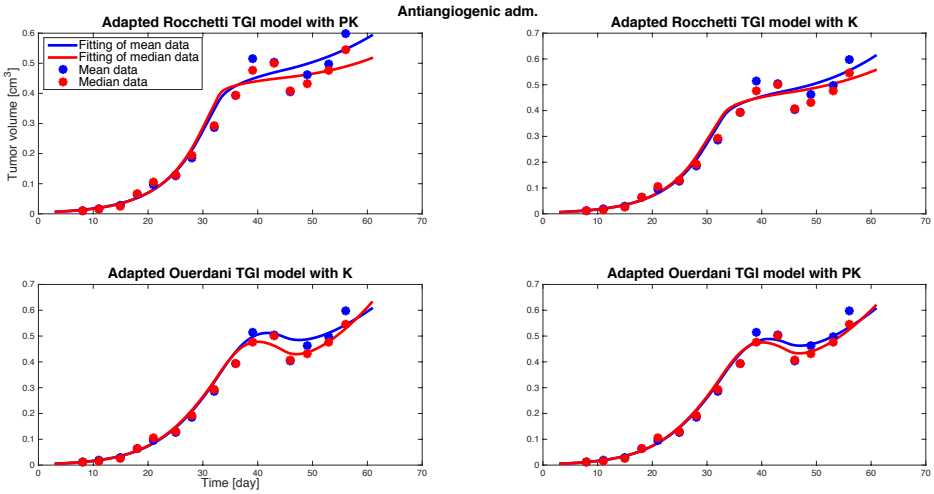

Figure 4.5: **Mean/median data antiangiogenic arm fits comparison** Tumor growth fits using the adapted Rocchetti TGI and the adapted Ouerdani TGI model (both with PK and K) following the Sunitinib administration. The blue and the red lines are the curve-fitting obtained by using mean and median data, respectively. Blue and red dots represent the mean and the median data, respectively.

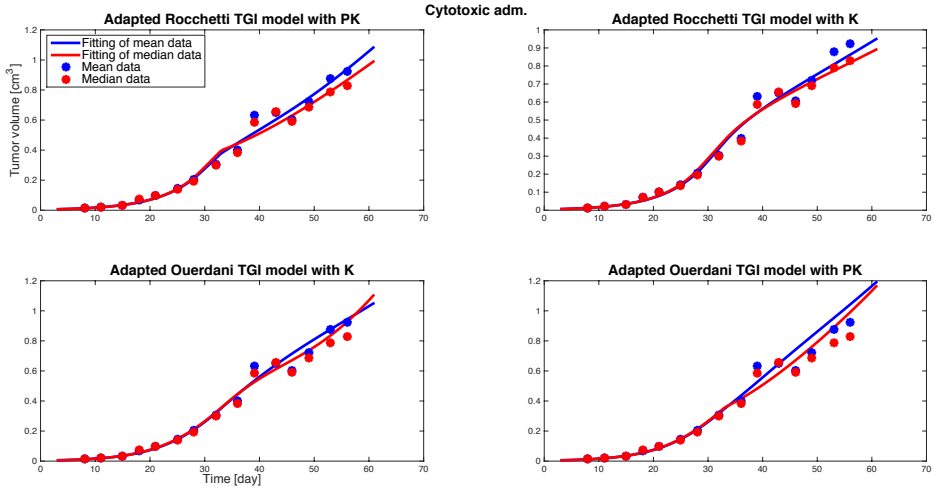

Figure 4.6: **Mean/median data cytotoxic arm fits comparison**
Tumor growth fits using the adapted Rocchetti TGI and the adapted Ouerdani TGI model (both with PK and K) following the Irinotecan administration. The blue and the red lines are the curve-fitting obtained by using mean and median data, respectively. Blue and red dots represent the mean and the median data, respectively.

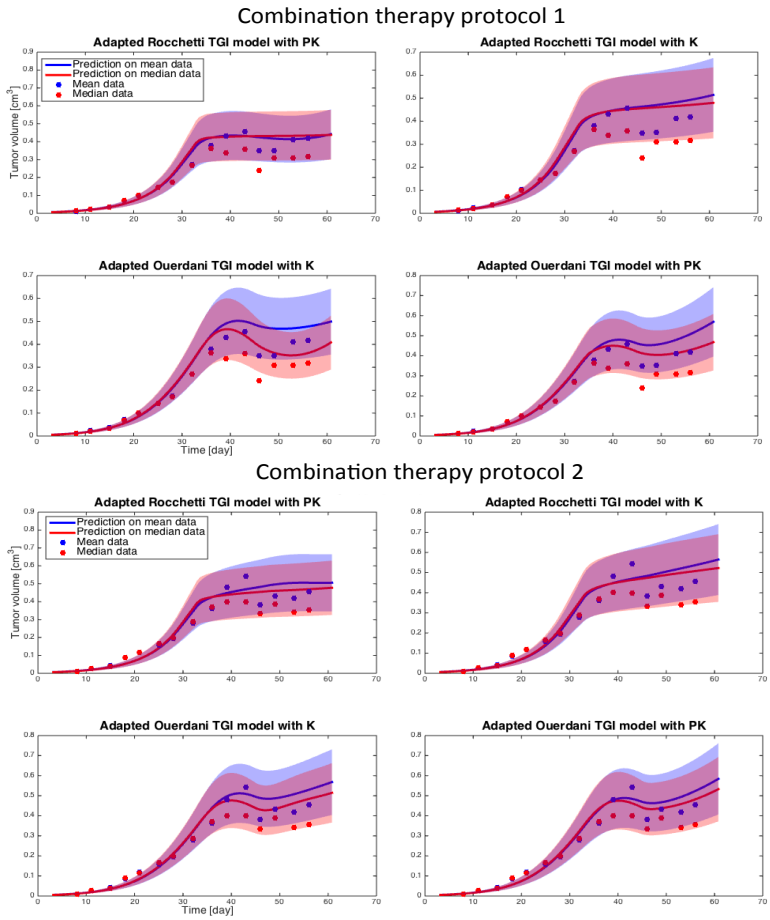

Figure 4.7: **Mean/median data combination therapy prediction comparison.** TGI prediction comparison when combination therapy is given under the null-interaction hypothesis. On the top: simulation of the combination therapy protocol 1. On the bottom: simulation of the combination therapy protocol 2. Blue and red lines are the prediction obtained by using mean and median data, respectively. The corresponding shaded areas are the prediction bandwidth when uncertainty on the estimates was considered. Blue and red dots represent the mean and the median data, respectively.

4.3.3 PK/K model comparison

No big difference between the use of PK or K models was found in modeling the unperturbed tumor growth, whilst a small difference between the adapted Rocchetti TGI with PK and the same model with K for the cytotoxic treatment was observed in the final part of the tumor growth curves. The adapted Ouerdani TGI model maintained its characteristic "wave-shape" describing the TGI effect of Sunitinib both when PK and K were used (Figure 4.8). When simulating combination treatments, the tumor growth curves predicted by the adapted Rocchetti TGI model with PK were lower than the ones obtained by using the same PD model with K; whilst the same pattern could not be seen when the adapted Ouerdani TGI model was used.

4.4 Discussion

In this chapter, the impact of different modeling strategies on the predicted effect of the combination of two anticancer drugs was investigated. Three factors were supposed to play a role: the (pharmaco)kinetic model, the pharmacodynamic model and the data used for the analysis. To better distinguish the impact of each factor, results were summarized as shown in the schematics of Figure 4.1. The K vs the PK model, the different PD models (adapted Rocchetti TGI model and adapted Ouerdani TGI model) and the implication of the use of mean or median data when a pool approach was adopted were examined *via* a case study in which an antiangiogenic and a cytotoxic agent were administered to xenograft mice.

The different mathematical structure of the two PD models determined a different modelization of the effect of the antiangiogenic agent. The adapted Rocchetti TGI model (Eq. 4.1) does not allow a

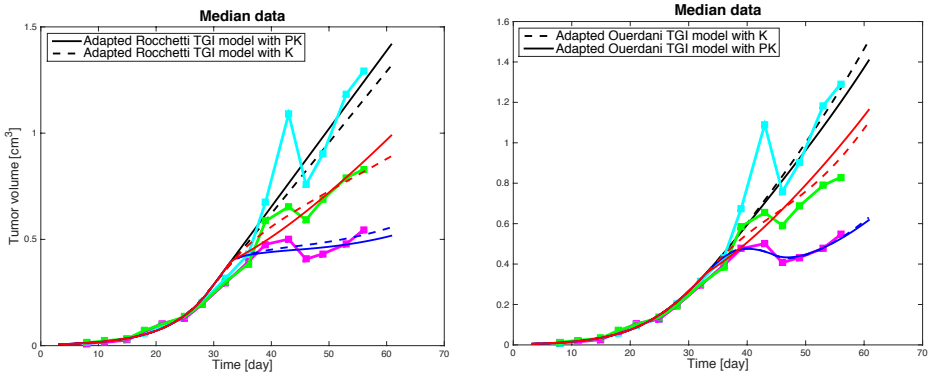

(a) PD models fits comparison.

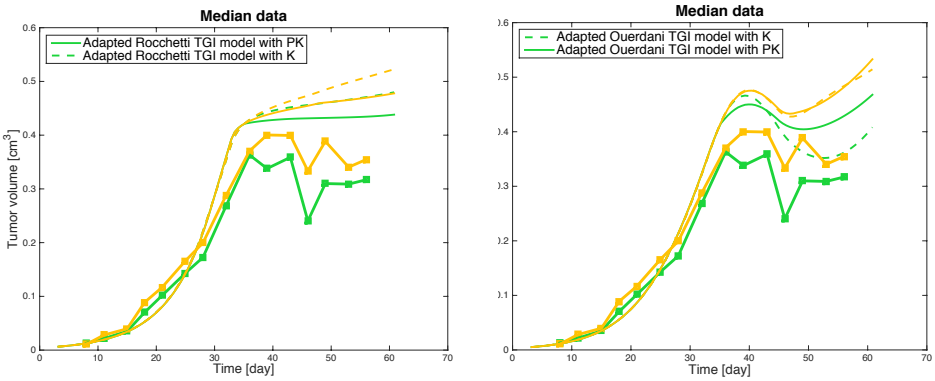

(b) PD models prediction comparison.

Figure 4.8: **PK/K models comparison.** The PK and the K models were compared by applying them to the same PD model. In Figure 4.8a the simultaneous fittings of the control and the two single agent arms. In black the control arm, in blue the antiangiogenic arm and in red the cytotoxic arm fits. The corresponding observed data were reported in cyan, pink and green. In Figure 4.8b the predictions of the combination therapy protocol 1 and 2. In green the combination therapy protocol 1, in yellow the combination therapy protocol 2. Squares with solids line indicated experimentals data. On the left the adapted Rocchetti TGI model, on the right the adapted Ouerdani TGI model.

decrease in tumor volume, since the inhibitory E_{max} function cannot be less than zero. Consequently, the time derivative cannot be negative, as in the original version without the effect compartment [100]. Only a tumoristatic effect can be modelled. Conversely, in the adapted Ouerdani TGI model the time derivative of the tumor volume can be negative and in doing so, the decrease of tumor dimensions following the antiangiogenic agent administration can be better accommodate, independently from (pharmaco)kinetic model used. However, it should be noticed that both the PK and the K strategy modeled a very fast kinetics of this drug, whose plasma concentration is close to zero one day after the administration.

The adapted Rocchetti TGI model better describes the (small) TGI effect exerted by the cytotoxic agent. This result is independent from the adoption of PK or the K model, even if the two approaches model a very different plasma concentration curves: a fast Irinotecan plasma elimination (around 2 days following the administration) is modeled by the PK model [75], whilst a very long elimination (more than one month following the administration) is described by the K model because of the very long elimination constant (p_C=0.085).

The adapted Ouerdani TGI model resulted to be more sensitive to the difference between mean and median data than the adapted Rocchetti TGI model which resulted to be more robust.

No differences in simulating the combination treatments were noticed due to the use of different PD and different K or PK models, as well as when different central tendency measurement were adopted. When predicted curves were compared with mean or median data, a weak synergism between the two drugs could be assumed, but when uncertainty was propagated, the null-interaction hypothesis could not be rejected.

As could be seen in Figure 4.2, the difference between mean and median data of the same experimental arm seems to be bigger than the difference among the experimental arms themselves. As already discussed in Chapter 3 (section 3.4), to face large inter-individual or intergroup variability a population approach might be a solution. Unfortunately, in our case, this strategy could not be used: two subpopulations seemed to be present both in the control and in the Sunitinib-treated arm, as can be seen in Figure 4.9a and Figure 4.9b. Our supposition was confirmed by the estimation of a a significant mixture on the model parameter λ_1 (λ_1=0.0105 [g $\cdot$ day^{-1}] and λ_1= 0.0431 [g $\cdot$ day^{-1}]; p-value $< 1 \times 10^{-10}$), but only one population was indentified in the Irinotecan-treated arm Figure 4.9c. As a consequence, the "slow" linear tumor growth rate for the cytotoxic agent could not be simulated under the null-interaction hypothesis. Even eliminating from the dataset used to identified model parameters mice characterized by a small linear tumor growth rate, it would not be possible to draw conclusions on the nature of the interaction between the two compounds with a population strategy. In fact, it was not possible to correctly classify the subject belonging to each group, resulting in an inability to disentangle the differences in tumor growth *per-se* from the ones due to the combined therapy.

In conclusion, the case study examined here seems to prove that results do not depend on the specific model used. However, general conclusions cannot be drawn, especially in a case like this, where a very noisy dataset (see Figure 4.10) and a non-optimal administration protocol with only one dose of cytotoxic agent were accounted.

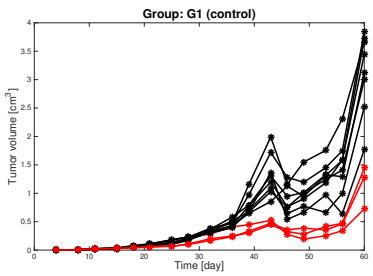

(a) Tumor growth in the control arm.

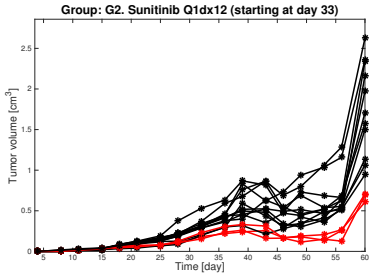

(b) Tumor growth in the antiangiogenic-treated arm.

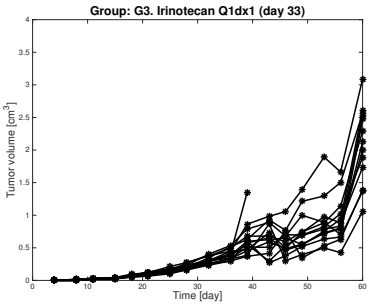

(c) Tumor growth in the cytotoxic-treated arm.

Figure 4.9: **Individual tumor growth profiles over time** Individual tumor growth profiles over time of mice belonging to the control arm (Figure 4.9a), Sunitinib (Figure 4.9b) and Irinotecan (Figure 4.9c) single agent treated arms. In red the tumor growth profiles of the mice characterized by a "slow" linear tumor growth rate, in black the ones with a"fast" linear tumor growth rate. This classification was made by means of a model mixture on model parameter λ_1. As can be noticed, in the control and in the Sunitinib-treated arms, two sub-populations of animals were present, whilst in the cytotoxic-treated arm only mice with a "fast" linear tumor growth rate were observed.

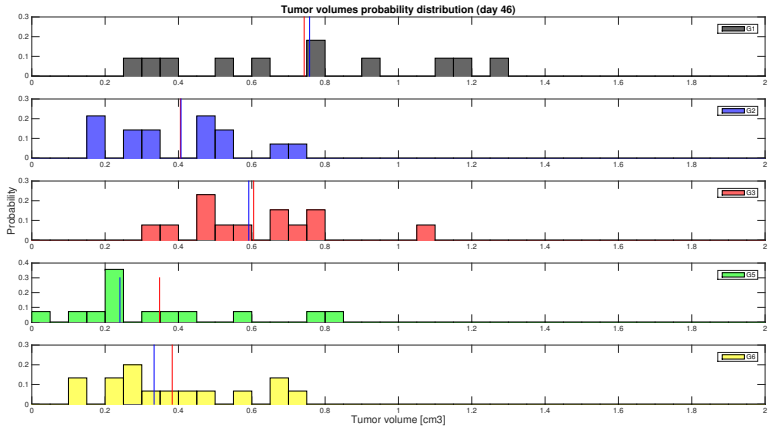

Figure 4.10: **Individual tumor volume probability distribution.**
The tumor volumes probability distribution for each group were reported. Tumor dimensions were collected at day 46 after inoculum. In black the tumor volumes distribution for the control group; in blue for the single agent Sunitinib arm; in red for the single agent Irinotecan arm; in green and in yellow for the "combination therapy 1" and the "combination therapy 2" group, respectively. Red and blue vertical lines represent the mean and the median of the tumor volumes in each group. The tumor volumes measured in the Irinotecan arm were entirely in the range of variation of the tumor volumes of the control animals; and a similar trend was observed also for the Sunitinb treated animals. On the contrary, tumor volumes collected in both the combination therapy arms were better separated from the ones belonging to the vehicle-treated animals.

Chapter 5

Pharmacokinetic/ pharmacodynamic modeling of etoposide tumor growth inhibitory effect in Walker-256 tumor-bearing rat model using free intratumoral drug concentrations[1]

[1]The contents of this chapter are published in *M.C. Pigatto, R.M. Roman, L. Carrara, P. Magni & T. Dalla Costa.* European journal of pharmaceutical science *2017, 97:70-78*

The purpose of this study was to establish a population PK/PD model linking etoposide free tumor and total plasma concentrations to the inhibition of solid tumor growth in rats. Walker-256 tumor cells were inoculated subcutaneously in the right flank of Wistar rats, which were randomly divided in control and two treated groups that received etoposide 5 or 10 mg/kg IV bolus every day for 8 and 4 days, respectively, and tumor volume was monitored daily for 30 days. The plasma and intratumoral concentrations-time profiles were obtained from a previous study and were modeled by a four-compartment population pharmacokinetic (popPK) model. PK/PD analysis was conducted using MONOLIX v.4.3.3 on average data and by mean of a nonlinear mixed-effect model. PK/PD data were analyzed using a modification of Simeoni TGI model by introduction of an E_{max} function to take into account the concentration dependency of $k_{2variable}$ parameter (variable potency). The Simeoni TGI-E_{max} model was capable to fit schedule-dependent antitumor effects using the tumor growth curves from the control and two different administered schedules. The PK/PD model was capable of describing the tumor growth inhibition using total plasma or free tumor concentrations, resulting in higher k_{2max} (maximal potency) for free concentrations (25.8 $mL{\cdot}\mu g^{-1}{\cdot}day^{-1}$-intratumoral vs. 12.6 $mL{\cdot}\mu g^{-1}{\cdot}day^{-1}$ total plasma). These findings indicate that the plasma concentration may not be a good surrogate for pharmacologically active free tumor concentrations, emphasizing the importance of knowing drug tumor penetration to choose the best antitumor therapy.

5.1 Background

In the past decades, the application of PK/PD modeling in the drug development process has increased substantially and has received more attention from the industry and regulatory agencies [143, 144,

145]. The PK/PD modeling using preclinical and clinical data has become a useful alternative for rational development of new drugs through early understanding of dose–response relationship and has enabled the optimization of dosing regimens for existing approved drugs, respectively [146, 147, 148].

Because anticancer agents usually have a narrow therapeutic window, PK/PD models can be extremely useful in oncology guiding the selection of adequate doses that improve treatment efficacy and reduce toxicity [149]. PK/PD models developed in oncology have been applied to describe the relation between drug plasma concentration and tumor growth [150, 75], biomarker response [151, 115], as well as adverse effects [152, 153], using data from animals or humans.

The most usual PD marker in oncology is the tumor growth, where the measurements of the tumor volume are used to construct the time course of growth after administration of anticancer agents [75, 107, 150, 154]. The most popular preclinical PK/PD model of tumor growth was developed by Simeoni et al [75]. This model was primarily developed for ranking competing preclinical candidates and was expanded to describe the tumor growth dynamics after administration of drug combinations [98] as well as to predict suitable doses in humans from animal studies [90].

The PK data most used to build the PK/PD model in preclinical and clinical oncology studies are the plasma concentrations assuming that these are a good surrogate for the drug concentrations reached in the tumor. Nevertheless, linking the effect to drug plasma concentrations can be misleading, since drug delivery into solid tumors is limited due to the heterogeneous microenvironment, with abnormal vascularization, hypoxic areas and high interstitial pressure characteristic of the tumor [155, 156, 157, 158]. Drug plasma concentrations

are commonly higher than those determined in the tumor as observed previously with epirubicin [159], methotrexate [160] an reviewed by Fuso Nerini et al. [161].

In this scenario, PK models that describe the concentrations in the tumor compartment can provide a better understanding of the drug distribution and drug efficacy helping to optimize dosing schedules. Up to date only a few PK/PD models have related anticancer tumor concentrations and effect, such as the model reported for temozolomide [158], gefitinib [123, 162, 123] and paclitaxel [163]. Furthermore, these studies only investigated drug penetration into brain tumors, demonstrating the need for studies that consider the anticancer distribution to other types of solid tumors.

The anticancer agent etoposide is a topoisomerase II inhibitor used for treating hematopoietic malignancies and different solid tumors, such as small cell lung cancer, breast cancer and Kaposi's sarcoma. Although the systemic PK and PD of etoposide are extensively studied [164, 165], little is known about its distribution in solid tumors and PK/PD modeling linking its intratumoral concentrations with antitumor effect has not been reported.

In this context, the present study aims to comparatively model the PK/PD relationship between total plasma and free interstitial tumor etoposide concentrations to the tumor growth kinetics observed in a Walker-256 (W256) tumor-bearing Wistar rat model.

5.2 Materials and Methods

5.2.1 Chemicals and reagents

Etoposide (purity $\geq$ 98%) and Trypan Blue solution 0.4% were purchased from Sigma-Aldrich (St. Louis, USA). Ethyl alcohol (anhydrous) and formic acid were purchased from Tedia (Fairfield, USA). Ultra- pure water was obtained in a Millipore Milli-Q system (Bedford, USA). Polyethylene glycol (PEG) 300, polysorbate 80 and citric acid were acquired from Labsynth (Sao Paulo, Brazil). Glucose sterile solution was purchased from Basa (Caxias do Sul, Brazil). All other chemicals and reagents used in this study were of pharmaceutical or analytical grade. Etoposide solution (5 mg/mL) was prepared for IV administration containing 3% citric acid 10%, 25% polyethylene glycol, 7.5% polysorbate 80, 10% ethanol (v/v) and the final volume was obtained with 5% glucose solution. This formulation is similar to the commercial injectable formulation used in humans [166, 165].

5.2.2 Animals and tumor model

Male Wistar rats (150–200 g) were supplied by the Center for Reproduction and Experimentation of Laboratory Animals (CREAL/ UFRGS - Porto Alegre, Brazil) and received food and water ad libitum. Animal procedures were approved by UFRGS Ethical Committee on Animal Use (CEUA/UFRGS, protocol number 22302) and were conducted under standard conditions according Brazilian law and the guideline on experimental animal care and use.

To obtain the tumor model, W256 carcinosarcoma cells were implanted intraperitoneally (IP) into Wistar rats (1×10^7 viable cells per animal). After 5–7 days of implantation, the ascitic tumor was harvested from the peritoneal cavity and the cell viability was evalu-

ated by Trypan blue exclusion test (Phillips, 1973) using a Neubauer's chamber (Brand, Wertheim, Germany). To produce a solid tumor, 2×10^7 viable cells in 1 mL of phosphate-buffered solution were inoculated subcutaneously into the right flank of the animal. During harvesting and inoculation procedures the animals were anesthetized with a ketamine-xylazine (100–10 mg/kg). After inoculation, the animals were kept on separated in cages (4 rats/cage) in standard conditions of temperature, humidity and 12-h light–dark cycle during the period of treatment.

5.2.3 Pharmacokinetic study

The pharmacokinetics of etoposide in W256 tumor-bearing Wistar rats was previously investigated in plasma and tumor [167]. A population PK model (popPK) was developed using MONOLIX v. 4.3.3 (Lixoft, Orsay, France). The popPK model simultaneously described total etoposide concentrations in plasma and free concentrations in two regions of the tumor – center and periphery consisting of four-compartments with a saturable distribution into the tumor compartments and first-order elimination. The system of differential equations for the popPK model is given in Eq. 5.1:

$$
\begin{aligned}
\frac{dA_1(t)}{dt} &= k_{21} \cdot A_2(t) + k_{31} \cdot A_3(t) + k_{41} \cdot A_4(t) - (k_{10} + k_{12}) \cdot A_1(t) - \\
&\quad - \frac{V_{max} \cdot A_1(1)}{A_1(t) + V_1 \cdot k_m} - \frac{V_{max} \cdot A_1(1)}{A_1(t) + V_1 \cdot k_m} \\
\frac{dA_2(t)}{dt} &= k_{12} \cdot A_1(t) - k_{21} \cdot A_2(t) \\
\frac{dA_3(t)}{dt} &= \frac{V_{max} \cdot A_1(1)}{A_1(t) + V_1 \cdot k_m} - k_{31} \cdot A_3(t) \\
\frac{dA_4(t)}{dt} &= \frac{V_{max} \cdot A_1(1)}{A_1(t) + V_1 \cdot k_m} - k_{41} \cdot A_4(t) \\
A_{1,2,3.4}(t = 0) &= 0 \\
C_{plasma}(t) &= \frac{A_1(t)}{V_1} \\
C_{T.peripheral}(t) &= \frac{A_3(t)}{V_3} \\
C_{T.center}(t) &= \frac{A_3(t)}{V_3} \cdot F_p + \frac{A_4(t)}{V_4} \cdot (1 - F_p)
\end{aligned}
\tag{5.1}
$$

A covariate model, in which the volume of plasma compartment V_1 is a function of the body weight, was used (Eq. 5.2):

$$
V_{1i} = 0.171 \cdot \left(\frac{BW_i}{0.290} \right)^{0.581} \tag{5.2}
$$

where V_{1i} is the volume of the central compartment for the i^{th} individual; 0.171 is the (population) volume of the central compartment estimated by the popPK model; 0.581 is the exponential scaling factor; BW is animal's individual body weight (kg); and 0.290 is the mean body weight (kg) in the PK group.

For the present PK/PD modeling, two sets of concentrations were used: total plasma concentration and free tissue concentration in the peripheral region of the tumor, because this region has a higher density of viable cancer cells that can be killed by the drug. Etoposide has a relatively short elimination half-life in tumor periphery ($\sim$2.39 h^{-1}) and in plasma ($\sim$ 1.83 h^{-1}), thus no accumulation was observed with the dose interval applied in the PD study. Total plasma and free peripheral tumor concentration-time profiles for the different treatments investigated in the PD experiments were simulated by fixing the following mean estimates values from the PK model previously described [167]: elimination rate micro-constant from the central compartment (k_{10}) was 1.27 h^{-1}; the distribution rate micro-constants between compartments k_{12}, k_{21}, k_{31} and k_{41} were 2.86 h^{-1}, 2.88 h^{-1}, 3.99 h^{-1}, and 0.216 h^{-1}, respectively; the volume of the tumor periphery compartment (V_3) was 0.112 L; volume of the tumor center compartment V_4 was 2.99 L; maximum transporter velocity from the plasma to tumor (V_{max}) was 0.907 $\mu g \cdot h^{-1}$; Michaelis-Menten constant (k_m) was 5.15 μg/mL and the drug fraction (F_p) was 0.155. In the model it was assumed that the concentrations measured by microdialysis in the center of the tumor represent a mixed concentration of the real central concentration (1-F_p) and the periphery concentration (F_p).

5.2.4 Pharmacodynamic study

Five days after the tumor inoculation of the W256 carcinosarcoma cells into the animal right flank, when tumors had reached a palpable volume of 1 cm^3 in average, rats were selected and randomized into control and two treated groups and treatments started. IV bolus doses of etoposide were administrated to the two treated groups as following: 10 mg/kg once daily for 4 days (n=10) or 5 mg/kg once daily for 8 days (n=11). In order to maintain ceteris paribus condition, vehicle was administrated to the control group (n = 10).

Rats were clinically evaluated and weighted daily until 30 days after the inoculation time. Dimensions of the tumors were measured daily using a caliper and tumor mass was calculated as defined by Eq. 5.3 [84, 75]:

$$Tumor \quad weight \quad [g] = \rho \cdot \frac{length \quad [cm] \cdot width^2 \quad [cm^2]}{2} \tag{5.3}$$

assuming density ρ= 1 g/cm^3. Rats with a tumor diameter higher than 4 cm, 20% weight loss and/or inability to eat and/or drink water were sacrificed before the end of the experiment according to the international guidelines for animal care and euthanasia [168].

5.2.5 Population Pharmacokinetic/Pharmacodynamic Model

To describe the tumor growth in response to etoposide dosing, the Simeoni TGI model [75] was used. Please refer to Chapter 3 section 3.3.1 for a detailed description of this model.

5.2.6 Data analysis

Total plasma and free peripheral tumor concentration-time profiles of etoposide were obtained using the PK model previously developed [167] as described in subsection 5.2.3. PD parameters were estimated performing a simultaneous fitting of the tumor growth curves observed both in control and treated animals.

PK/PD model was implemented using MONOLIX version 4.3.3. PD parameters were estimated using the stochastic approximation expectation maximization (SAEM) algorithm with log-likelihoods esti-

mated by linearization and standard errors estimated by stochastic approximation.

A limit of quantification of 3 mm diameter corresponding to a 0.01 g was the minimum value that can be appreciate with the caliper. For the analysis, tumor measurements below the limit of quantification were coded as left censored data.

In this work, two different approaches were adopted: a pool approach using a Naïve Average Data (NAD) and a population approach. NAD is a very simple method that focuses the attention only on the typical population response. Average value of the data was computed for each sample time. Model was fitted against mean data. Contrariwise, with the population technique data from all the individuals involved in the study were taken into account. In this way, through a suitable mathematical model, it is possible to describe both typical subject data and variability among subjects.

Individual parameters P_i were supposed to be log-normally distributed. Random effects η_i were used to model inter-individual variability. They represent the random variation of the individual parameters around the population value Θ (Eq. 5.4):

$$P_i = \Theta \cdot \exp(\eta_i) \tag{5.4}$$

Random effects were normally distributed with zero mean and variance Ω, as it can be seen in the formula $\eta_i \sim N(0, \Omega)$. Different error models were tested for the residual unknown variability.

Fitting of predicted tumor growth curves against experimental data and precision estimates were the first criteria used to evaluate the adequacy of the model. Furthermore, it is important to underline

that the first analysis was made using a NAD approach. Therefore, model was selected through the pool approach, and then implemented in a population context. The model evaluation was performed using goodness-of- fit plots (GOF) and visual predictive check (VPC), which is a common diagnostic tool that makes a comparison between statistics obtained from the simulated data using the estimated population parameters and the true observed data.

5.3 Results

The tumor growth inhibition and regrowth data from animals that received IV bolus administration of vehicle, etoposide 10 mg/kg-4 days and 5 mg/kg-8 days are shown in Figure 5.1, Figure 5.2 and Figure 5.3. The tumor growth curves showed a great difference between control and treated groups. Following international guidelines [168], the animals from the control group were sacrificed after 13.5 $\pm$ 2.5 days of tumor inoculation due to the size of the tumor. It was not possible to evaluate any animal until the end of experiment (30 days). The treated group that received etoposide 10 mg/kg-4 days presented higher variability in the tumor regrowth; in average the animals were sacrificed after 27.2 $\pm$ 2.0 days of tumor inoculation, however 3 animals (Figure 5.3 numbers 4, 5 and 9) showed a slower tumor regrowth followed by regression in the last days of the experiment (data not shown). On the other hand, only 3 out of 11 animals were sacrificed 29 days after inoculation in the 5 mg/kg-8 days group. The other animals were evaluated until the end of experiment.

The first modeling attempt employed the Simeoni TGI model described in 5.2.5 using a pool approach, as illustrated in Figure 5.3. One can observe that the model was not adequate to simultaneously describe the tumor growth in the control group and in the two treated groups, either considering etoposide plasma or tumor concentrations.

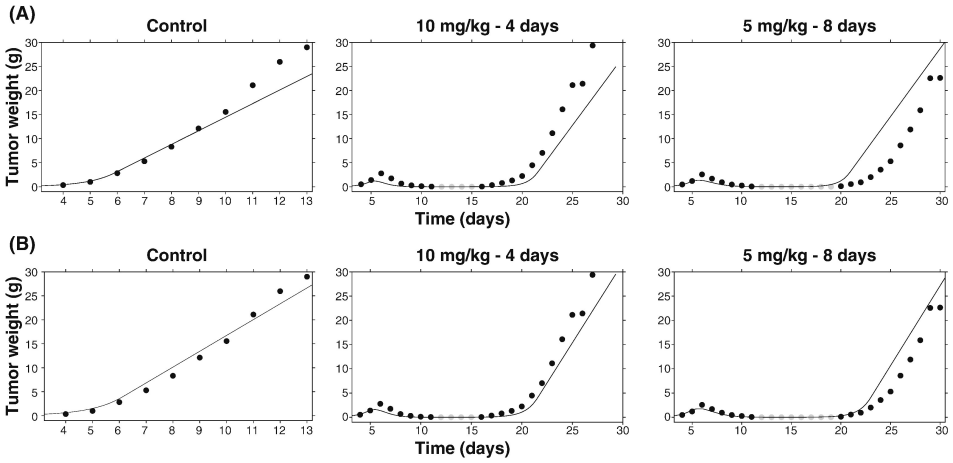

Figure 5.1: **Model fits using the Simeoni TGI model.** Plots with average observed (black dots), left censored data (grey dots) and model-fitted (line) tumor growth curves in rats given either the vehicle (control) or etoposide IV (10 mg/kg for 4 days or 5 mg/kg for 8 days). Model fits using the Simeoni TGI model considering total plasma (A–upper panels) and free tumor (B-lower panels) concentration.

The experimental regrowth curves showed that the 8-days treatment with 5 mg/kg/day presented greater tumor growth inhibition (regrowth observed after 21.4 ± 1.1 days) compared with 4-days treatment with 10 mg/kg/day (regrowth observed after 16.8 ± 0.8 days). These results indicate that etoposide has a schedule-dependent antitumor effect because the total drug dose used in each treatment (40 mg/kg) and the respective area under the curve (AUC) are the same for both regimens. When the PK/PD model uses tumor concentrations as the PK input (Figure 5.3B), a slightly better fit can be observed because etoposide free concentrations at the site of action correlates better with effect than total plasma concentrations.

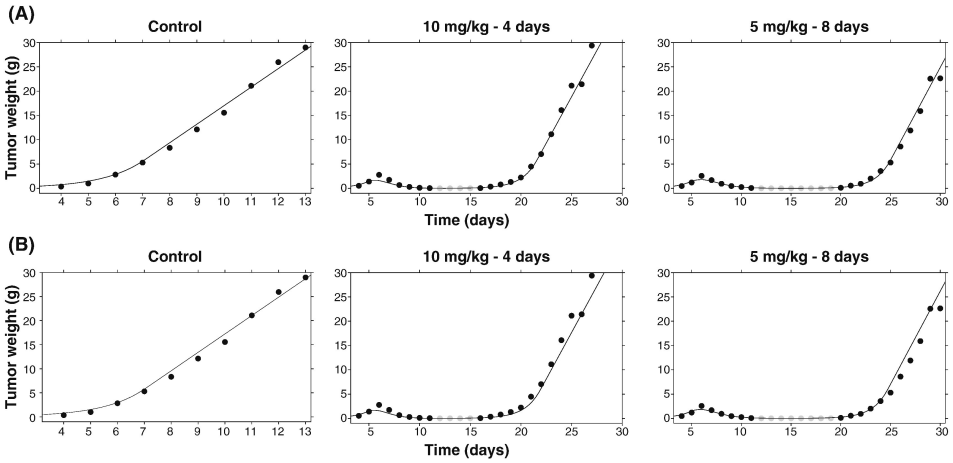

Figure 5.2: **Model fits using the Simeoni TGI-E$_{max}$ model.** Plots with average observed (black dots), left censored data (grey dots) and model-fitted (line) tumor growth curves in rats given either the vehicle (control) or etoposide IV (10 mg/kg for 4 days or 5 mg/kg for 8 days). Model fits using the Simeoni TGI-E$_{max}$ model considering total plasma (A-upper panels) or free tumor (B-lower panels) concentration

In fact, separate fitting of control and each treatment group (fitting not shown) estimated different values for the parameter k_2 using plasma concentrations (4.98 and 6.74 mL·μg^{-1}·day^{-1} for 10 mg/kg-4 days and 5 mg/kg-8 days, respectively) or tumor concentrations (17.7 and 20.9 mL·μg^{-1}·day^{-1} for 10 mg/kg-4 days and 5 mg/kg-8 days, respectively). These results indicate that etoposide potency differs between the two schedules, according to the terms definition of the model employed to fit the data. Either way, Simeoni TGI model was not adequate to simultaneously describe the effect of etoposide different schedules on the W256-tumor bearing rats.

Additionally, a total reduction of tumor volume (no measurable

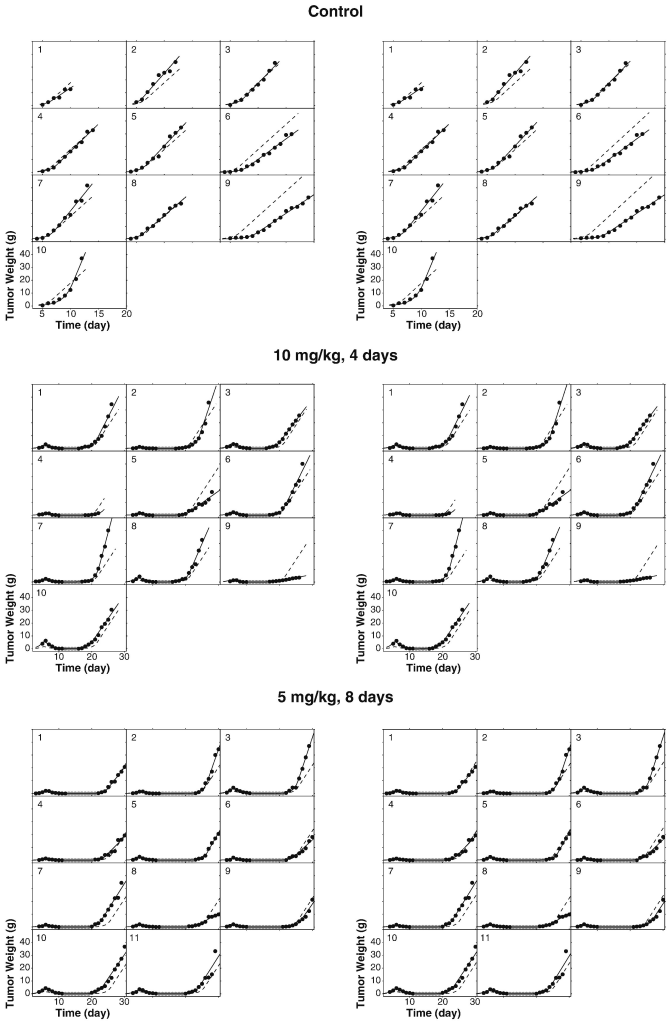

Figure 5.3: **Individual fits using the Simeoni TGI-E$_{max}$ model.** Plots with observed (black dots), left censored data (grey dots), individual predicted (solid lines) and population predicted (dashed lines) tumor growth curves obtained in rats given either the vehicle (control) or etoposide IV (10 mg/kg-4 days or 5 mg/kg-8 days). In left panels total plasma concentrations were used, while in right panels free tumor concentrations were considered.

tumor) was observed between 11.6 ± 0.5 day and 16.8 ± 0.8 day for the 10 mg/kg-4 days treatment and between 12.1 ± 0.7 day and 21.4 ± 1.1 day for the 5 mg/kg-8 day treatment.

In the attempo to improve data fitting it was assumed that k_2 in the Simeoni TGI model was variable and could be described by a inhibitory E_{max} function to takes into account its dependence on drug concentration (Eq. 5.5):

$$
\begin{aligned}
k_{2variable} &= k_{2max} \cdot \left(1 - \frac{c(t)}{IC_{50} + c(t)}\right) \\
\frac{dX_1(t)}{dt} &= \frac{\lambda_0 X_1(t)}{\left[1 + \left(\frac{\lambda_0}{\lambda_1} \cdot W(t)\right)^{\psi}\right]^{\frac{1}{\psi}}} - k_{2variable} \cdot c(t) \cdot Z_1(t) \\
\frac{dX_2(t)}{dt} &= k_{2variable} \cdot c(t) \cdot X_1(t) - k_1 \cdot X_2(t) \\
\frac{dX_3(t)}{dt} &= k_1 \cdot X_2(t) - k_1 \cdot X_3(t) \\
\frac{dX_4(t)}{dt} &= k_1 \cdot X_3(t) - k_1 \cdot X_4(t) \\
W(t) &= X_1(t) + X_2(t) + X_3(t) + X_4(t) \\
X_1(t=0) &= w_0 \qquad X_{2,3,4}(t=0) = 0
\end{aligned}
\tag{5.5}
$$

This function was parameterized (I_{max}, assumed equal to 1) with IC_{50} that is the concentration that represents 50% of k_{2max} (the maximum drug potency). The new parameter $k_{2variable}$ was inserted into the Simeoni TGI model in place of k_2. According to the equations above, when drug concentration is close to zero (smaller than IC_{50}): $k_{2variable}$ similar to k_{2max}. Instead, when concentration increases, the $k_{2variable}$ decreases. Note that, this modellization is equivalent to consider a saturable killing cell effect of the drug with the increases of its

concentration, but it focuses the attention on the drug potency, one of the most import parameter of the Simeoni model. The mathematical relationship adopted in this paper is closed to that used in [100] to describe the interaction between an antiangiogenic and a cytotoxic drug. Through this equation, it is possible to explain the lower anticancer effect obtained when 10 mg/kg-4 days was administered to the animals in comparison with 5 mg/kg-8 days. As observed in Figure 5.2 (average data) and Figure 5.3 (individual data), the Simeoni TGI-E_{max} model was able to simultaneously fit all control and the two treated groups. The model was able to provide a good description of the data both using total plasma (Figure 5.2A and Figure 5.3-left panels) and free tumor concentrations (Figure 5.2B and Figure 5.3-right panels).

The population parameter estimates are presented in Table 5.1, together with inter-individual and residual variability. Population parameters were identified with good precision (RSE $\leq$ 12%) and they were independent of the concentration used (plasma or tumor), except k_{2max}, which was of 12.6 mL·μg^{-1}·day^{-1} when total plasma concentrations were used and 25.8 mL·μg^{-1}·day^{-1} when free tumor concentrations were assumed. This difference is due to 82% lower tumor exposure to free etoposide than to total plasma concentrations. If free plasma concentrations were taken into account they would have been higher than the free concentrations determined in the tumor considering that etoposide plasma unbound fraction is about 30% and the tumor penetration factor in the periphery (AUC_{0-t}(tumor, free)/AUC_{0-t}(plasma,free) is about 60%. Furthermore, etoposide tumor penetration was shown to be saturable, with $AUC_{tumor,free}$ does not increasing proportionally with the dose increase [167]. Then, it makes no difference if free or total plasma concentrations are used, because both of them do not adequately reflect concentrations in target tissue. Accordingly to what previously was said, since the decrease in tumor cells growth rate is proportional to drug concentration via

the proportional constant $k_{2variable}$, the greater the concentration, the lower the potency of the compound.

Inter-individual variability was considered only for parameters related to the tumor growth w_0, λ_0 and λ_1 . The inter-individual variability was moderate, ranging from 7.3 to 60.5% and it can be attributed to the differences in the tumor progression among the animals. Moreover, the variability estimated for tumor-related parameters could also be caused by the loss of some cells during the inoculation, determining differences in the growth curve between the animals. The inter-individual variability for the drug-related parameters (k_1, k_{2max} and IC_{50}) was not considered because it did not improve the fitting. The error model chosen was a proportional plus power error model as follows (Eq. 5.6):

$$y = f + b \cdot f^c \cdot \varepsilon \tag{5.6}$$

where y is the data and f the model prediction. The coefficient of variation is expressed by b; c is fixed to 0.5; ε is the random variable to express the residual unknown variability, normally distributed with mean zero and variance 1. Residual variability was a bit high of 40% for both free tumor and total plasma concentrations.

GOF plots presented in Figure 5.4 illustrate that the proposal PK/PD model adequately characterized etoposide antitumor effect. The individual and population predicted values are in good agreement with the observed tumor weights, using total plasma (Figure 5.4A) or free tumor concentrations (Figure 5.4B) as PK input in the model. Overestimation in the population predictions at higher tumor weights is caused by animals that presented a tumor growth slower than the others. For these animals it was possible to measure the dimension of the tumor until 19 days post-inoculation. For the others animals, espe-

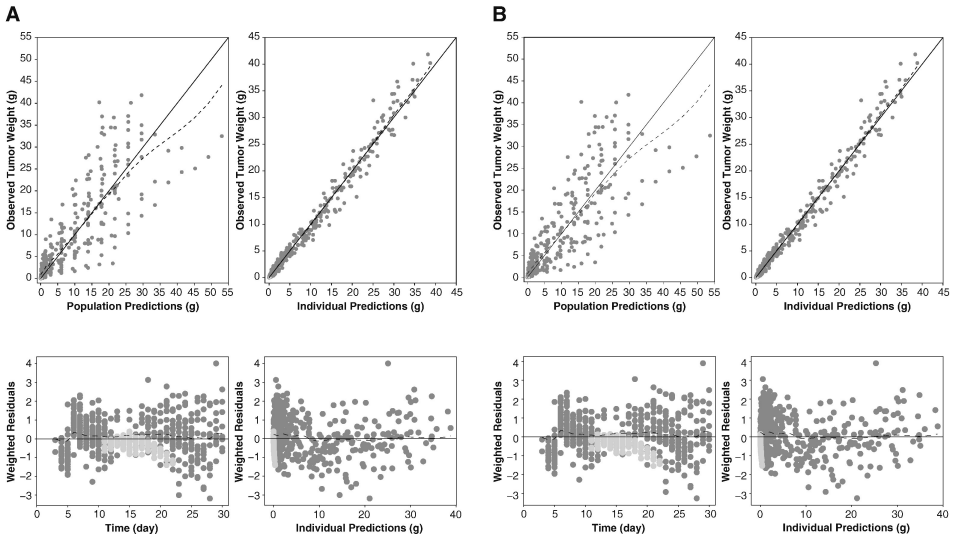

Figure 5.4: **Goodness-of-fit plots for the tumor weight.** Goodness-of-fit plots for the tumor weight using total plasma (A-four panels on the left side) or free tumor (B-four panels on the right side) concentrations. In the observed versus model predicted tumor weight plots (upper panels) the solid and dashed lines indicate the linear regression fit and identity line, respectively. In the panel below the residual plots are shown. The grey dots are the data, while the light grey dots represent the left censored data.

cially for those belonging to the control group, measures were possible only until 13 days post-inoculation, because the tumor grew faster and these animals had to be sacrificed. Still in Figure 5.4 it is possible to observe that the weighted residuals are randomly distributed around zero indicating the absence of model bias.
VPCs (Figure 5.5) indicate that the final model effectively explained the observed tumor weights.

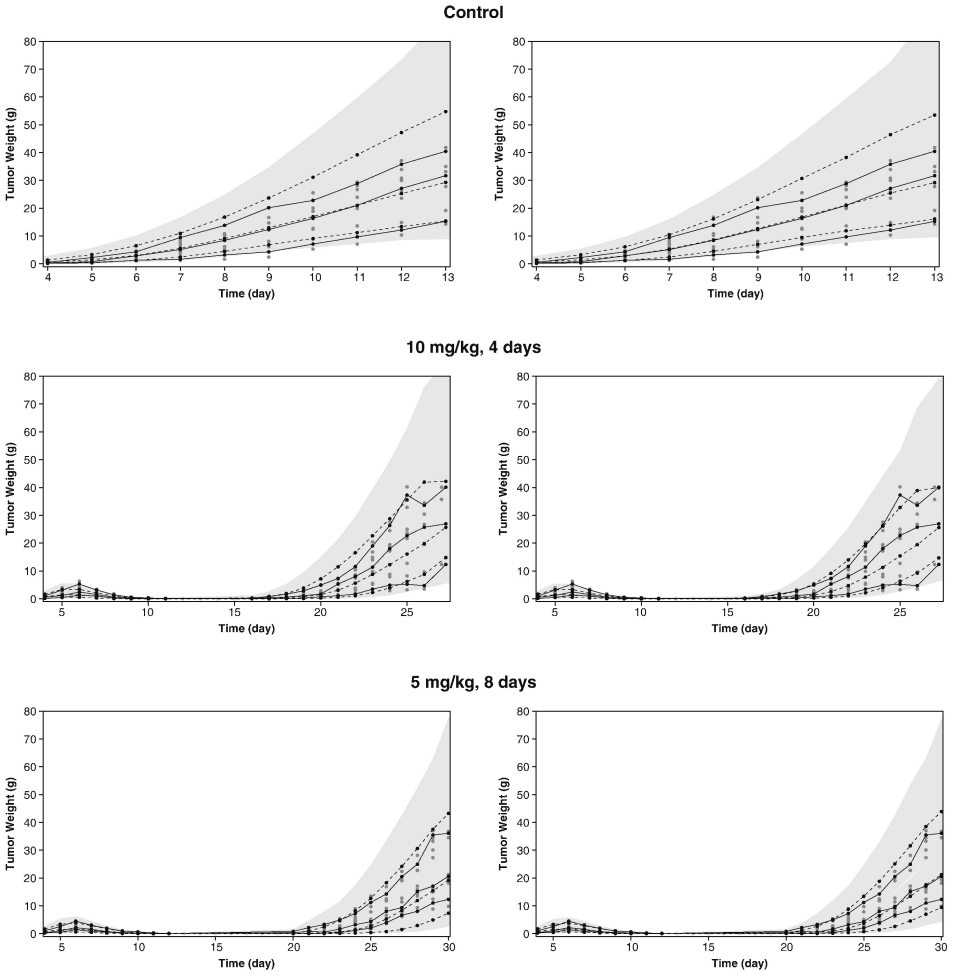

Figure 5.5: **VPC of the final PK/PD model.** VPC of the final PK/PD model stratified by group using total plasma (left panels) and free tumor (right panels) concentration based on 1000 simulated replicates of the original data. The solid and dashed lines show the 10^{th}, 50^{th} and 90^{th} percentiles of observed and simulated data, respectively; the grey shaded areas represent the 90% confidence interval for the corresponding model predicted percentile. The left censored data are indicated by the light grey dots.

	Estimate (RSE%)	
Parameter	Plasma[a]	Tumor[b]
Population median		
λ_0 [day^{-1}]	0.732 (2)	0.699 (2)
λ_1 [g·day^{-1}]	3.91 (11)	4.00 (11)
w_0 [g]	0.037 (12)	0.043 (11)
k_1 [day^{-1}]	1.63 (3)	1.62 (3)
k_{2max} [mL·μg^{-1}·day^{-1}]	12.6 (1)	25.8 (1)
IC_{50} [μg ·mL^{-1}]	1.07 (1)	1.08 (1)
IIV		
$\Omega(\lambda_0)$	0.087 (20)	0.073 (20)
$\Omega(\lambda_1)$	0.605 (15)	0.595 (14)
$\Omega(w_0)$	0.554 (15)	0.555 (15)
Residual variability		
b	0.404 (4)	0.403 (3)
c	0.5 fixed	0.5 fixed
AIC	1223.93	1188.17

Table 5.1: **Parameter estimates of the final PK/PD model.**

[a] Total plasma concentrations from the PK model; [b] free peripheral tumor concentrations from the PK model. Relative standard error = RSE% = (estimate/standard error) × 100; Ω: standard deviation of inter-individual variability (IIV) estimates; AIC: Akaike information criterion NA: not applicable. Model parameters are defined in the text.

5.4 Discussion

In this study, we used the PK/PD modeling for describing tumor growth and the anti-tumor effect of etoposide in tumor-bearing rats. PK model was obtained from a previous work and linked to the PD model using total plasma or free peripheral tumor concentration-time profiles.

Modeling started using Simeoni TGI model already published, with the difference that besides plasma concentrations also the tumor concentrations of etoposide were employed to explain the cytotoxic effect of the drug. However, despite the flexibility of the Simeoni TGI model, it was not able to describe experimental data when all the groups were considered (control, 5 mg/kg/day-8 days, 10 mg/kg/day-4 days) either using plasma or tumor concentration as PK input.

As previously referred, in the Simeoni model the decreasing of the tumor growth rate caused by the drug is directly proportional to the number of proliferating tumor cells (X_1) and the drug concentration via a proportionality constant k_2, which describes the potency of the drug. In the present study, however, this relation was not valid because it was observed that etoposide showed a schedule-dependent effect that resulted in a variable potency ($k_{2,variable}$).

The dependence on schedule observed in this work corroborates previously studies that demonstrated that the etoposide response has been evidently schedule dependent [169, 170, 171] in clinical studies. Slevin et al. [171] showed that patients with small-cell lung cancer receiving a 24-h infusion or the same dose divided over 5 days have positive response rates of 10% or 89%, respectively. Additionally, the schedule- dependent response of the epipodophyllotoxins such as etoposide (topoisomerase II inhibitor) has been related to the activity

of topo- isomerase II that it is variable during the cell cycle and also to the fast elimination of these drugs from the cell after the exposure, allowing cancer cells DNA repair. Accordingly, it is recommended in the literature the prolongation of the schedules of administration for these anticancer agents, using smaller daily doses, to improve the response [172, 173].

To model this schedule-dependent effect an inhibitory function was introduced in the Simeoni TGI model. Two new parameters were added - IC_{50} and k_{2max} - in order to describe the nonlinear relationship between concentration and effect. The rest of the model assumptions were similar to those originally presented for the Simeoni TGI model [75]. The Simeoni TGI-E_{max} model successfully described etoposide effect on tumor growth using different dosing schedules. The population approach allowed to correctly describing the drug effect for the individual animals, estimating at the same time a typical value and the interindividual variability.

The same PK/PD model was used to describe the relationship between etoposide concentration and tumor growth inhibition using different PK input - free intratumoral interstitial concentrations or total plasma concentrations-. The estimated k_{2max} was higher when free tumor concentrations were used, in accordance with the 82% lower drug exposure in tumor. This difference in k_{2max} (potency) depending on the PK input shows that total plasma concentration might not be a good surrogate for the pharmacologically active free tumor concentrations. When comparing antitumoral candidates using plasma concentrations as PK input, the PK/PD model can predict erroneous potency if the drugs have relevant differences in tumor penetration leading to inadequate selection of promising candidates.

The present study showed the development of a PK/PD model to

correlate etoposide effect using either total plasma or free intratumoral concentrations allowing the investigation of the importance of PK input data on PK/PD modeling. Considering that PK/PD modeling is currently used in drug development, this study points out the importance of knowing free intratumoral drug behavior when building PK/PD models for antitumor drugs.

5.5 Conclusion

In this study, the population PK/PD Simeoni TGI-E_{max} model developed adequately described the schedule-dependent effect of etoposide using total plasma and free interstitial tumor etoposide concentrations obtained in a W256-tumor bearing Wistar rat model. The results suggested that the use of free intratumoral concentrations as PK input for PK/PD modeling could provide a better understanding of the pharmaco-kinetics and pharmacodymamics relationship shading light into the reasons for drug inefficacy that the traditional PK/PD models based on plasma concentrations are unable to supply.

5.6 Acknowledgement

This work was supported by the National Counsel of Technological and Scientific Development (CNPq/Brazil) (project 477344/2011-9). Maiara Pigatto acknowledges CAPES Foundation/Brazil for PhD scholarship CAPES/Brazil and PDSE Program (Process #4929/14-4). The authors thank Dr. Sandra Coccuzzo Sampaio Vessoni from the Physiopathology Laboratory at Butantan Institute (Sao Paulo- SP, Brazil) who kindly donated the W-256 carcinosarcoma cells.

Chapter 6

Overall conclusions

The aim of this thesis was to investigate the suitability of a certain modeling strategy to address pharmacometric questions. The concept that no "one size fits all" approach can be applied to every pre-clinical and clinical program, irrespective of the characteristics of the individual drug, was defended thorough examples. This is particularly challenging towards organizations like pharmaceutical companies which are often entrenched in a low risk-low reward paradigm *(it has worked once, it will work again)*, based on individual experience rather than thorough screening of the different available methods.

The predictive performances of the WB-PBPK models, one of the most-promising tools in terms of predictive capabilities, were analyzed in Chapter 2. These models integrate physicochemical drug properties with information on organism anatomy an physiology, and are suitable for translational purposes by integrating information derived from animal experiments. For the case study investigated in this thesis, findings indicated that challenges still exist for prospective use of the approach with novel molecules, when full details of drug dis-

position is missing or differs between species. Conversely, when the WB-PBPK framework is used retrospectively, an accurate description of drug disposition was achieved. The model successfully described experimental data, well captured the observed IIV in the population under study and well predicted steady state drug level in the lung.

In some cases the PBPK model framework cannot be used, as in the oncology field. The incomplete physiologically characterization of the subjects with tumors is the major obstacle to the use of this approach. Consequently, even at the early phases of oncology drug discovery, different and less mechanistic modeling strategies are adopted. In Chapter 3 the modeling approaches applicable to anticancer drug discovery of approximately the last decade were illustrated. Nowadays, besides the standard PK/PD models directly describing tumor growth inhibitions, PK/PD models incorporating the interactions with the target were used to model the TGI. New concepts are spreding as, for examples, the carrying capacity for antiangiogenic compounds and the quantitative modeling of the pharmacological audit trials to support new targeted therapies.

In Chapter 4 it was examined if different modeling techniques lead to different results. A case study regarding the effect of the combination therapy between a standard cytotoxic and an antiangiogenic compound was investigated. The factors supposed to be responsible for a different result in terms of combination (negative, null or positive), i.e. the PD models, the preprocessing of data and the PK-or K-model were analyzed. No difference in the predicted effects of combination therapy were found.

In Chapter 5, the use of drug plasma concentration as a surrogate for drug concentrations in the biophase, i.e., the tumor, was investigated. Findings demonstrated that plasma concentration may not be

a good surrogate for pharmacologically active free tumor concentration. The maximal drug potency ($k_{2,max}$) is higher when free tumor concentrations were used, in accordance with the 82% lower drug exposure in tumor. Thus, comparing antitumoral candidates using plasma concentrations as PK input can form a problem when drugs have relevant differences in tumor penetration. Consequently, the erroneous predictions of candidate potency may lead to inadequate selection of promising candidates.

Appendix A

Supplementary information for Chapter 2[1]

A.1 Supplementary information for data simulation

The contents of this section are confidential

[1]The contents of this chapter are confidential

A.2 Supplementary results

A.2.1 Population predictions following the 1^{st} dose and at steady state

Population prediction following the first oral dose and at steady state were reported. Plasma concentration over time following the administration of 1000 mg (Figure A.1a) and 1200 mg of EMB (Figure A.1b)were reported.

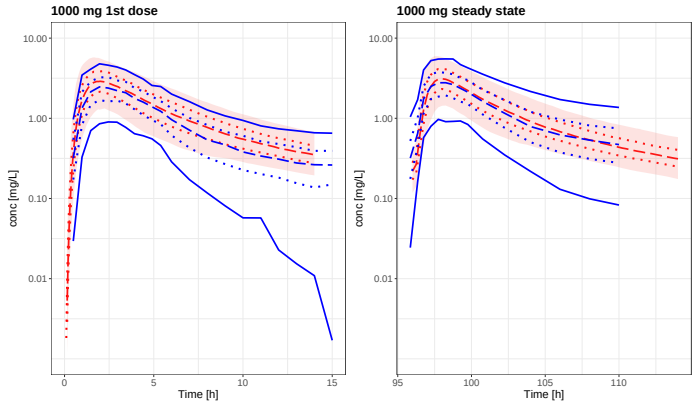

(a)

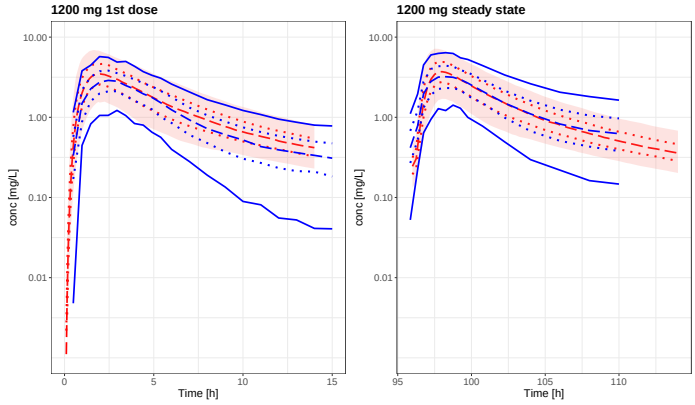

(b)

Figure A.1: **Scenario 6: population predictions of plasma EMB concentrations.** The red shaded areas represent the $5^{th} - 95^{th}$ percentiles of the PK-Sim population predicted plasma concentration profiles, the red dashed line and the red dotted lines represent the 50^{th}, 25^{th} and the 75^{th} precentiles, respectively. The blue continuous lines represent the $5^{th} - 95^{th}$ observed percentiles, the blue dashed line and the blue dotted lines represent the 50^{th}, 25^{th} and the 75^{th} precentiles, respectively. In Figure A.1a: prediction following the first EMB oral dose (1000 mg, left) and at steady state (right). In Figure A.1b: prediction following the first EMB oral dose (1200 mg, left) and at steady state (right).

A.2.2 Sensitivity analysis

Sensitivity analysis was performed in PK-Sim in the following way:

- sensitivity of LogP, TSspec and specific clearance was computed considering IV administration. Plasma AUC and Cmax were considered exposure metrics;
- sensitivity of Weibull dissolution time, Weibull dissolution shape and IPT was computed considering oral administration. Plasma AUC and Cmax were considered exposure metrics;
- sensitivity of LogP, TSspec and specific clearance, Weibull dissolution time, Weibull dissolution shape and IPT and lung effective permeability was computed considering oral administration. Lung exposure (lung AUC) and lung Cmax were considered exposure metrics.

Sensitivity analysis regarding drug plasma AUC and Cmax were reported only for 800 mg, since results were consistent for all the three doses (800, 1000 and 1200 mg) considered in this work.

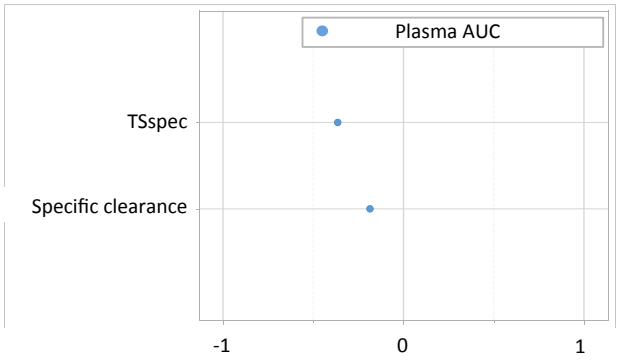

(a)

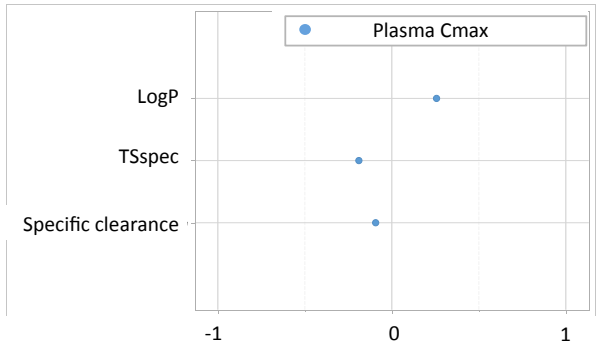

(b)

Figure A.2: **Sensitivity analysis following IV administration.**
Figure A.2a: sensitivity analysis considering AUC. Figure A.2b: sensitivity analysis considering Cmax.

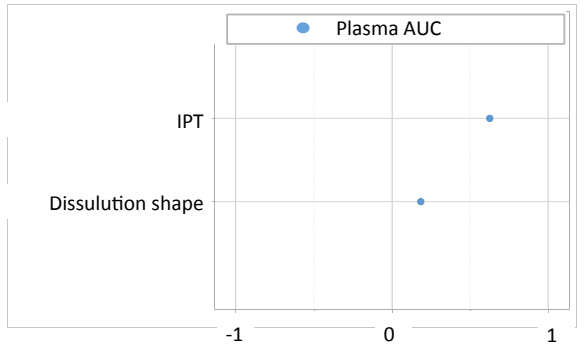

(a)

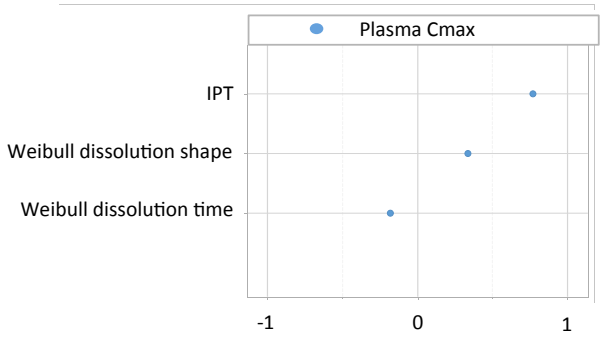

(b)

Figure A.3: **Sensitivity analysis following oral administration.**

Figure A.2a: sensitivity analysis considering AUC. Figure A.3b: sensitivity analysis considering Cmax.

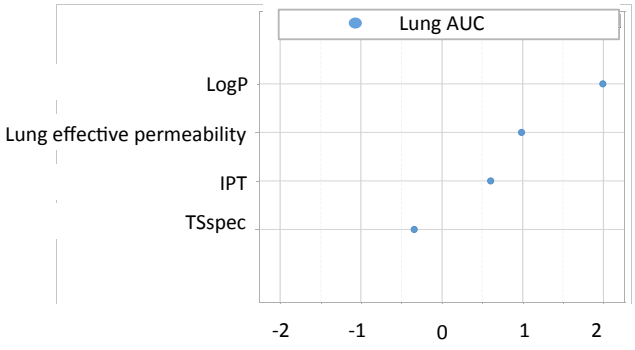

(a)

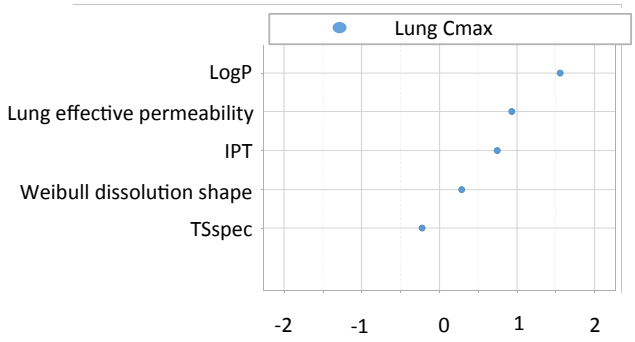

(b)

Figure A.4: **Sensitivity analysis on lung AUC and Cmax.** Figure A.4a: sensitivity analysis considering lung AUC. Figure A.4b: sensitivity analysis considering Cmax. The administered dose is 15 mg/kg.

Appendix B

Supplementary Information for Chapter 4

B.1 Materials and Methods

B.1.1 Adapted Rocchetti TGI model with K

The modified Rocchetti model with K was reported here below Eq. B.1. Please note that for sake of brevity, only the model for the null-interaction hypothesis was reported. The models used to describe the action of Sunitinib and Irinotecan as single agents could be derived by superimposing C(t) and S(t) equal to zero, respectively.

$$
\begin{aligned}
&\frac{dC_{eff}(t)}{dt} = k_{eff} \cdot S(t) - k_{eff} \cdot C_{eff}(t) \\
&\frac{dX_1(t)}{dt} = \frac{\lambda_0 X_1(t)}{\left[1 + \left(\frac{\lambda_0}{\lambda_1} \cdot W(t)\right)^{\psi}\right]^{\frac{1}{\psi}}} \cdot \left(1 - \frac{E_{max} \cdot C_{eff}(t)}{IC_{eff,50} + C_{eff}(t)}\right) - k_2 \cdot C(t) \cdot Z_1(t) \\
&\frac{dX_2(t)}{dt} = k_2 \cdot C(t) \cdot X_1(t) - k_1 \cdot X_2(t) \\
&\frac{dX_3(t)}{dt} = k_1 \cdot X_2(t) - k_1 \cdot X_3(t) \\
&\frac{dX_4(t)}{dt} = k_1 \cdot X_3(t) - k_1 \cdot X_4(t) \\
&W(t) = X_1(t) + X_2(t) + X_3(t) + X_4(t) \\
&C_{eff}(t=0) = 0 \qquad X_1(t=0) = w_0 \qquad X_{2,3,4}(t=0) = 0 \\
&\frac{dS(t)}{dt} = -p_S \cdot S(t) \qquad S(t=T_S) = 1 \\
&\frac{dC(t)}{dt} = -p_C \cdot C(t) \qquad C(t=T_C) = 1
\end{aligned}
\tag{B.1}
$$

B.1.2 Adapted Ouerdani TGI model with PK

The modified Ouerdani model with PK was reported here below Eq. B.2. Please note that for sake of brevity, only the model for the null-interaction hypothesis was reported. The models used to describe the action of Sunitinib and Irinotecan as single agents could be derived by superimposing $c_B(t)$ and $c_A(t)$ equal to zero, respectively.

$$
\begin{aligned}
&\frac{dV_1(t)}{dt} = \lambda \cdot P \cdot \left(1 - \frac{V}{K}\right) - \beta_C \cdot c_B(t) \cdot V_1(t), \qquad V_1(t=0) = V_0 \\
&\frac{dV_2(t)}{dt} = \beta_C \cdot c_B(t) \cdot V_1(t) - k_c \cdot V_2(t), \qquad V_2(t=0) = 0 \\
&\frac{dV_3(t)}{dt} = k_c \cdot V_2(t) - k_c \cdot V_3(t), \qquad V_3(t=0) = 0 \\
&\frac{dV_4(t)}{dt} = k_c \cdot V_3(t) - k_c \cdot V_4(t), \qquad V_4(t=0) = 0 \\
&\frac{dK(t)}{dt} = b \cdot V_1(t)^{2/3} - \beta_S \cdot c_A(t) \cdot K(t), \qquad K(t=0) = K_0 \\
&V(t) = V_1(t) + V_2(t) + V_3(t) + V_4(t)
\end{aligned}
\tag{B.2}
$$

where $c_B(t)$ and $c_A(t)$ are the plasma concentrations profiles over time of Irinotecan and Sunitinib modeled with a two-compartmental model and a one-compartmental model with absorption, respectively.

Bibliography

[1] The guardian. The price of health: the cost of developing new medicines. https://www.theguardian.com/healthcare-network/2016/mar/30/new-drugs-development-costs-pharma, 2016.

[2] S.F. Marshall, R. Burghaus, V. Cosson, S.Y.A. Cheung, M. Chenel, O. Della Pasqua, N. Frey, B. Hamren, L. Harnisch, F. Ivanow, et al. Good practices in model-informed drug discovery and development: practice, application, and documentation. *CPT: pharmacometrics & systems pharmacology*, 5(3):93–122, 2016.

[3] L. Kuepfer, J. Lippert, and T. Eissing. Multiscale mechanistic modeling in pharmaceutical research and development. In *Advances in Systems Biology*, pages 543–561. Springer, 2012.

[4] FDA. https://www.fda.gov/ForPatients/Approvals/Drugs/ucm405622.htm.

[5] R.L. Lalonde, K.G. Kowalski, M.M. Hutmacher, W. Ewy, D.J. Nichols, P.A. Milligan, B.W. Corrigan, P.A. Lockwood, S.A.

Marshall, L.J. Benincosa, et al. Model-based drug development. *Clinical Pharmacology & Therapeutics*, 82(1):21–32, 2007.

[6] P.A. Milligan, M.J. Brown, B. Marchant, S.W. Martin, P.H. Graaf, N. Benson, G. Nucci, D.J. Nichols, R.A. Boyd, J.W. Mandema, et al. Model-based drug development: a rational approach to efficiently accelerate drug development. *Clinical Pharmacology & Therapeutics*, 93(6):502–514, 2013.

[7] Pricewaterhouse Coopers. Pharma 2005: Silicon rally: The race to e-r&d. PWC, 2005.

[8] E. Manolis, S. Rohou, R. Hemmings, T. Salmonson, M. Karlsson, and P.A. Milligan. The role of modeling and simulation in development and registration of medicinal products: output from the efpia/ema modeling and simulation workshop. *CPT: pharmacometrics & systems pharmacology*, 2(2):1–4, 2013.

[9] FDA. `https://www.fda.gov/downloads/ScienceResearch/SpecialTopics/CriticalPathInitiative/CriticalPathOpportunitiesReports/ucm077262.pdf`.

[10] FDA. `https://www.fda.gov/downloads/ScienceResearch/SpecialTopics/RegulatoryScience/UCM268225.pdf`.

[11] J.V.S. Gobburu and L.J. Lesko. Quantitative disease, drug, and trial models. *Annual review of pharmacology and toxicology*, 49:291–301, 2009.

[12] B. Meibohm and H. Derendorf. Basic concepts of pharmacokinetic/pharmacodynamic (pk/pd) modelling. *International journal of clinical pharmacology and therapeutics*, 35(10):401–413, 1997.

[13] P. Jacqmin, E. Snoeck, E.A. Van Schaick, R. Gieschke, P. Pillai, J.L. Steimer, and P. Girard. Modelling response time profiles in the absence of drug concentrations: definition and performance evaluation of the k–pd model. *Journal of pharmacokinetics and pharmacodynamics*, 34(1):57–85, 2007.

[14] Z.P. Parra-Guillen, P. Berraondo, E. Grenier, B. Ribba, and I.F. Troconiz. Mathematical model approach to describe tumour response in mice after vaccine administration and its applicability to immune-stimulatory cytokine-based strategies. *The AAPS journal*, 15(3):797–807, 2013.

[15] H. W. Haggard. The absorption, distribution, and elimination of ethyl ether. *Survey of Anesthesiology*, 1(5):561, 1957.

[16] F. P. Theil, T. W. Guentert, S. Haddad, and P. Poulin. Utility of physiologically based pharmacokinetic models to drug development and rational drug discovery candidate selection. *Toxicology letters*, 138(1):29–49, 2003.

[17] J. C. Ramsey and M. E. Andersen. A physiologically based description of the inhalation pharmacokinetics of styrene in rats and humans. *Toxicology and applied pharmacology*, 73(1):159–175, 1984.

[18] G. W. Drach. Prostatitis: Man's hidden infection. *The Urologic clinics of North America*, 2(3):499–520, 1975.

[19] M. Müller, A. dela Peña, and H. Derendorf. Issues in pharmacokinetics and pharmacodynamics of anti-infective agents: distribution in tissue. *Antimicrobial agents and chemotherapy*, 48(5):1441–1453, 2004.

[20] C. Joukhadar, M. Frossard, B. X. Mayer, M. Brunner, N. Klein, P. Siostrzonek, H. G. Eichler, and M. Müller. Impaired target site penetration of β-lactams may account for therapeutic failure in patients with septic shock. *Critical care medicine*, 29(2):385–391, 2001.

[21] World Health Organization. *Global tuberculosis report 2016*, 2016.

[22] V. Dartois. The path of anti-tuberculosis drugs: from blood to lesions to mycobacterial cells. *Nature Reviews Microbiology*, 12(3):159–167, 2014.

[23] J. B. Bass Jr, L. S. Farer, P. C. Hopewell, R. O'Brien, R. F. Jacobs, F. Ruben, D. E. Snider Jr, and G. Thornton. Treatment of tuberculosis and tuberculosis infection in adults and children. american thoracic society and the centers for disease control and prevention. *American journal of respiratory and critical care medicine*, 149(5):1359–1374, 1994.

[24] C. S. Lee, D. C. Brater, J. G. Gambertoglio, and L. Z. Benet. Disposition kinetics of ethambutol in man. *Journal of pharmacokinetics and biopharmaceutics*, 8(4):335–346, 1980.

[25] R Core Team. *R: A Language and Environment for Statistical Computing*. R Foundation for Statistical Computing, Vienna, Austria, 2015.

[26] M. Lavielle. *mlxR: Simulation of Longitudinal Data*, 2016. R package version 3.0.3.

[27] S. Jönsson, A. Davidse, J. Wilkins, J. S. Van der Walt, U. S. H. Simonsson, M. O. Karlsson, P. Smith, and H. McIlleron. Population pharmacokinetics of ethambutol in south african tu-

berculosis patients. *Antimicrobial agents and chemotherapy*, 55(9):4230–4237, 2011.

[28] S. Strauch, E. Jantratid, M. Stahl, L. Rägo, and J. B. Dressman. The biowaiver procedure: its application to antituberculosis products in the who prequalification programme. *Journal of pharmaceutical sciences*, 100(3):822–830, 2011.

[29] J. Xu, H. Jin, H. Zhu, M. Zheng, B. Wang, C. Liu, M. Chen, L. Zhou, W. Zhao, L. Fu, et al. Oral bioavailability of rifampicin, isoniazid, ethambutol, and pyrazinamide in a 4-drug fixed-dose combination compared with the separate formulations in healthy chinese male volunteers. *Clinical therapeutics*, 35(2):161–168, 2013.

[30] H. F. Wang, R. Wang, M. O'Gorman, P. Crownover, A. Naqvi, and I. Jafri. Bioequivalence of fixed-dose combination myrin®-p forte and reference drugs in loose combination. *The International Journal of Tuberculosis and Lung Disease*, 17(12):1596–1601, 2013.

[31] J. E. Conte, J. A. Golden, J. Kipps, E. T. Lin, and E. Zurlinden. Effects of aids and gender on steady-state plasma and intrapulmonary ethambutol concentrations. *Antimicrobial agents and chemotherapy*, 45(10):2891–2896, 2001.

[32] S. B. Lakshminarayana, T. B. Huat, P. C. Ho, U. H. Manjunatha, V. Dartois, T. Dick, and S. P. S. Rao. Comprehensive physicochemical, pharmacokinetic and activity profiling of anti-tb agents. *Journal of Antimicrobial Chemotherapy*, 70(3):857–867, 2014.

[33] P. Costa and J. M. S. Lobo. Modeling and comparison of dissolution profiles. *European journal of pharmaceutical sciences*, 13(2):123–133, 2001.

[34] J. A. Goldsmith, N. Randall, and S. D. Ross. On methods of expressing dissolution rate data. *Journal of Pharmacy and Pharmacology*, 30(1):347–349, 1978.

[35] T Dekker, editor. *Proceedings of WHO workshop on Quality, good manufacturing practice and bioequivalence with a focus on antituberculotics: Comparative dissolution testing and application*. Geneva: World Health Organization, 5-9 November 2007. `http://slideplayer.com/slide/8756294/`.

[36] Open system pharmacology suite community. *Open system pharmacology suite manual*, February 2017. version 7.0.

[37] T. Rodgers and M. Rowland. Mechanistic approaches to volume of distribution predictions: understanding the processes. *Pharmaceutical research*, 24(5):918–933, 2007.

[38] P. Poulin, K. Schoenlein, and F. P. Theil. Prediction of adipose tissue: plasma partition coefficients for structurally unrelated drugs. *Journal of pharmaceutical sciences*, 90(4):436–447, 2001.

[39] P. Poulin and F. P. Theil. A priori prediction of tissue: Plasma partition coefficients of drugs to facilitate the use of physiologically-based pharmacokinetic models in drug discovery. *Journal of pharmaceutical sciences*, 89(1):16–35, 2000.

[40] T. Rodgers, D. Leahy, and M. Rowland. Physiologically based pharmacokinetic modeling 1: Predicting the tissue distribution of moderate-to-strong bases. *Journal of pharmaceutical sciences*, 94(6):1259–1276, 2005.

[41] T. Rodgers and M. Rowland. Physiologically based pharmacokinetic modelling 2: predicting the tissue distribution of acids, very weak bases, neutrals and zwitterions. *Journal of pharmaceutical sciences*, 95(6):1238–1257, 2006.

[42] L. M. Berezhkovskiy. Volume of distribution at steady state for a linear pharmacokinetic system with peripheral elimination. *Journal of pharmaceutical sciences*, 93(6):1628–1640, 2004.

[43] W. Schmitt. General approach for the calculation of tissue to plasma partition coefficients. *Toxicology in Vitro*, 22(2):457–467, 2008.

[44] S. Willmann, J. Lippert, and W. Schmitt. From physicochemistry to absorption and distribution: predictive mechanistic modelling and computational tools. *Expert opinion on drug metabolism & toxicology*, 1(1):159–168, 2005.

[45] S. Willmann, J. Lippert, M. Sevestre, J. Solodenko, F. Fois, and W. Schmitt. Pk-sim®: a physiologically based pharmacokinetic 'whole-body'model. *Biosilico*, 1(4):121–124, 2003.

[46] A. Loidl-Stahlhofen, T. Hartmann, M. Schöttner, C. Röhring, H. Brodowsky, J. Schmitt, and J. Keldenich. Multilamellar liposomes and solid-supported lipid membranes (transil): screening of lipid-water partitioning toward a high-throughput scale. *Pharmaceutical research*, 18(12):1782–1788, 2001.

[47] L. F. Prescott. *Novel drug delivery and its therapeutic application*. John Wiley & Sons, 1989.

[48] J. Worsøe, L. Fynne, T. Gregersen, V. Schlageter, L. A Christensen, J. F. Dahlerup, N. J. M. Rijkhoff, S. Laurberg, and K. Krogh. Gastric transit and small intestinal transit time and

motility assessed by a magnet tracking system. *BMC gastroenterology*, 11(1):145, 2011.

[49] L. Gaohua, J. Wedagedera, B. G. Small, L. Almond, K. Romero, D. Hermann, D. Hanna, M. Jamei, and I. Gardner. Development of a multicompartment permeability-limited lung pbpk model and its application in predicting pulmonary pharmacokinetics of antituberculosis drugs. *CPT: pharmacometrics & systems pharmacology*, 4(10):605–613, 2015.

[50] Drugbank. Ethambutol. `www.drugbank.ca`, 2017.

[51] C. S. Lee, J. G. Gambertoglio, D. C. Brater, and L. Z. Benet. Kinetics of oral ethambutol in the normal subject. *Clinical Pharmacology & Therapeutics*, 22(5part1):615–621, 1977.

[52] T. Eissing, L. Kuepfer, C. Becker, M. Block, K. Coboeken, T. Gaub, L. Goerlitz, J. Jaeger, R. Loosen, B. Ludewig, et al. A computational systems biology software platform for multiscale modeling and simulation: integrating whole-body physiology, disease biology, and molecular reaction networks. *Frontiers in physiology*, 2:4, 2011.

[53] K. Thelen, K. Coboeken, S. Willmann, R. Burghaus, J.B. Dressman, and J. Lippert. Evolution of a detailed physiological model to simulate the gastrointestinal transit and absorption process in humans, part 1: oral solutions. *Journal of pharmaceutical sciences*, 100(12):5324–5345, 2011.

[54] L. Kuepfer, C. Niederalt, T. Wendl, J.F. Schlender, S. Willmann, J. Lippert, M. Block, T. Eissing, and D. Teutonico. Applied concepts in pbpk modeling: How to build a pbpk/pd model. *CPT: Pharmacometrics & Systems Pharmacology*, 5(10):516–531, 2016.

[55] R. C. Milan-Segovia, A. M. Dominguez-Ramirez, H. Jung-Cook, M. Magana-Aquino, M. C. Romero-Mendez, S. E. Medellin-Garibay, M. Vigna-Perez, and S. Romano-Moreno. Relative bioavailability of rifampicin in a three-drug fixed-dose combination formulation. *The International Journal of Tuberculosis and Lung Disease*, 14(11):1454–1460, 2010.

[56] S. Agrawal, I. Singh, K. J. Kaur, S. R. Bhade, C. L. Kaul, and R. Panchagnula. Comparative bioavailability of rifampicin, isoniazid and pyrazinamide from a four drug fixed dose combination with separate formulations at the same dose levels. *International journal of pharmaceutics*, 276(1):41–49, 2004.

[57] I. Kola and J. Landis. Opinion: Can the pharmaceutical industry reduce attrition rates? *Nature reviews. Drug discovery*, 3(8):711, 2004.

[58] P. Workman. Auditing the pharmacological accounts for hsp90 molecular chaperone inhibitors: Unfolding the relationship between pharmacokinetics and pharmacodynamics1. *Molecular cancer therapeutics*, 2(2):131–138, 2003.

[59] T. A. Yap, S. K. Sandhu, P. Workman, and J. S. De Bono. Envisioning the future of early anticancer drug development. *Nature reviews. Cancer*, 10(7):514, 2010.

[60] L. R. Kelland. "of mice and men": values and liabilities of the athymic nude mouse model in anticancer drug development. *European Journal of Cancer*, 40(6):827–836, 2004.

[61] M. G. Hollingshead. Antitumor efficacy testing in rodents. *JNCI: Journal of the National Cancer Institute*, 100(21):1500–1510, 2008.

[62] J. Jung. Human tumor xenograft models for preclinical assessment of anticancer drug development. *Toxicological research*, 30(1):1, 2014.

[63] M. Liu and D. Hicklin. Human tumor xenograft efficacy models. In *Tumor Models in Cancer Research*, pages 99–124. Springer, 2011.

[64] B. Gorelik, I. Ziv, R. Shohat, M. Wick, W.D. Hankins, D. Sidransky, and Z. Agur. Efficacy of weekly docetaxel and bevacizumab in mesenchymal chondrosarcoma: a new theranostic method combining xenografted biopsies with a mathematical model. *Cancer research*, 68(21):9033–9040, 2008.

[65] A. Bernard, H. Kimko, D. Mital, and I. Poggesi. Mathematical modeling of tumor growth and tumor growth inhibition in oncology drug development. *Expert opinion on drug metabolism & toxicology*, 8(9):1057–1069, 2012.

[66] M. Simeoni, G. De Nicolao, P. Magni, M. Rocchetti, and I. Poggesi. Modeling of human tumor xenografts and dose rationale in oncology. *Drug Discovery Today: Technologies*, 10(3):e365–e372, 2013.

[67] B. Ribba, N.H. Holford, P. Magni, I. Trocóniz, I. Gueorguieva, P. Girard, C. Sarr, M. Elishmereni, C. Kloft, and L. E. Friberg. A review of mixed-effects models of tumor growth and effects of anticancer drug treatment used in population analysis. *CPT: pharmacometrics & systems pharmacology*, 3(5):1–10, 2014.

[68] S. Benzekry, C. Lamont, A. Beheshti, A. Tracz, J. M. L. Ebos, L. Hlatky, and P. Hahnfeldt. Classical mathematical models for description and prediction of experimental tumor growth. *PLoS computational biology*, 10(8):e1003800, 2014.

[69] S. S. Carroll, J. Inglese, S. Mao, and D. B. Olsen. Drug screening: Assay development issues. *Molecular Cancer Therapeutics: Strategies for Drug Discovery and Development*, pages 119–140, 2004.

[70] M. Germani, P. Magni, G. De Nicolao, I. Poggesi, A. Marsiglio, D. Ballinari, and M. Rocchetti. In vitro cell growth pharmacodynamic studies: a new nonparametric approach to determining the relative importance of drug concentration and treatment time. *Cancer chemotherapy and pharmacology*, 52(6):507–513, 2003.

[71] J. E Kalns, N. J Millenbaugh, M. G. Wientjes, and J. L. S. Au. Design and analysis of in vitro antitumor pharmacodynamic studies. *Cancer research*, 55(22):5315–5322, 1995.

[72] L. M. Levasseur, H. K. Slocum, Y. M. Rustum, and W. R. Greco. Modeling of the time-dependency of in vitro drug cytotoxicity and resistance. *Cancer Research*, 58(24):5749–5761, 1998.

[73] S.N. Gardner. A mechanistic, predictive model of dose-response curves for cell cycle phase-specific and-nonspecific drugs. *Cancer research*, 60(5):1417–1425, 2000.

[74] F. Del Bene, M. Germani, G. De Nicolao, P. Magni, C.E. Re, D. Ballinari, and M. Rocchetti. A model-based approach to the in vitro evaluation of anticancer activity. *Cancer chemotherapy and pharmacology*, 63(5):827–836, 2009.

[75] M. Simeoni, P. Magni, C. Cammia, G. De Nicolao, V. Croci, E. Pesenti, M. Germani, I. Poggesi, and M. Rocchetti. Predictive pharmacokinetic-pharmacodynamic modeling of tumor growth kinetics in xenograft models after administration of anticancer agents. *Cancer research*, 64(3):1094–1101, 2004.

[76] D. Moreno, I.F. Trocóniz, M. Enguita, E. Bandrés, J. García-Foncillas, and M. Garrido. Semi-mechanistic description of the in-vitro antiproliferative effect of different antitumour agents. *Journal of Pharmacy and Pharmacology*, 60(1):77–82, 2008.

[77] B.S. Cummings and R.G. Schnellmann. Cisplatin-induced renal cell apoptosis: caspase 3-dependent and-independent pathways. *Journal of Pharmacology and Experimental Therapeutics*, 302(1):8–17, 2002.

[78] H. Lin, C.B. Landersdorfer, D. London, R. Meng, C. Lim, C. Lin, S. Lin, H. Tang, D. Brown, B. Van Scoy, et al. Pharmacodynamic modeling of anti-cancer activity of tetraiodothyroacetic acid in a perfused cell culture system. *PLoS computational biology*, 7(2):e1001073, 2011.

[79] J.B. Bulitta, N.S. Ly, J.C. Yang, A. Forrest, W.J. Jusko, and B.T. Tsuji. Development and qualification of a pharmacodynamic model for the pronounced inoculum effect of ceftazidime against pseudomonas aeruginosa. *Antimicrobial agents and chemotherapy*, 53(1):46–56, 2009.

[80] M. Li, H. Li, X. Cheng, X. Wang, L. Li, T. Zhou, and W. Lu. Preclinical pharmacokinetic/pharmacodynamic models to predict schedule-dependent interaction between erlotinib and gemcitabine. *Pharmaceutical research*, 30(5):1400–1408, 2013.

[81] G. Koch, A. Walz, G. Lahu, and J. Schropp. Modeling of tumor growth and anticancer effects of combination therapy. *Journal of pharmacokinetics and pharmacodynamics*, 36(2):179–197, 2009.

[82] X. Miao, G. Koch, R.M. Straubinger, and W.J. Jusko. Pharmacodynamic modeling of combined chemotherapeutic effects predicts synergistic activity of gemcitabine and trabectedin in

pancreatic cancer cells. *Cancer chemotherapy and pharmacology*, 77(1):181–193, 2016.

[83] E.D. Lobo and J.P. Balthasar. Pharmacodynamic modeling of chemotherapeutic effects: application of a transit compartment model to characterize methotrexate effects in vitro. *The AAPS Journal*, 4(4):212–222, 2002.

[84] L. Bueno, D.P. de Alwis, C. Pitou, J. Yingling, M. Lahn, S. Glatt, and I.F. Trocóniz. Semi-mechanistic modelling of the tumour growth inhibitory effects of ly2157299, a new type i receptor tgf-β kinase antagonist, in mice. *European journal of cancer*, 44(1):142–150, 2008.

[85] A.K. Laird. Dynamics of tumour growth. *British journal of cancer*, 18(3):490, 1964.

[86] A.K. Laird. Dynamics of tumour growth: comparison of growth rates and extrapolation of growth curve to one cell. *British Journal of Cancer*, 19(2):278, 1965.

[87] W.J. Jusko. Pharmacodynamics of chemotherapeutic effects: Dose-time-response relationships for phase-nonspecific agents. *Journal of pharmaceutical sciences*, 60(6):892–895, 1971.

[88] W.J. Jusko. A pharmacodynamic model for cell-cycle-specific chemotherapeutic agents. *Journal of Pharmacokinetics and Pharmacodynamics*, 1(3):175–200, 1973.

[89] J. Yang, D.E. Mager, and R.M. Straubinger. Comparison of two pharmacodynamic transduction models for the analysis of tumor therapeutic responses in model systems. *The AAPS journal*, 12(1):1–10, 2010.

[90] M. Rocchetti, M. Simeoni, E. Pesenti, G. De Nicolao, and I. Poggesi. Predicting the active doses in humans from animal studies: a novel approach in oncology. *European Journal of Cancer*, 43(12):1862–1868, 2007.

[91] P.L. Bonate. Modeling tumor growth in oncology. In *Pharmacokinetics in drug development*, pages 1–19. Springer, 2011.

[92] *Modeling drug effects and resistance development on tumor growth dynamics*, 2007.

[93] R.M. Pigatto, M.C. Roman, L. Carrara, A. Buffon, P. Magni, and T. Dalla Costa. Pharmacokinetic/pharmacodynamic modeling of etoposide tumor growth inhibitory effect in walker-256 tumor-bearing rat model using free intratumoral drug concentrations. *European Journal of Pharmaceutical Sciences*, 97:70–78, 2017.

[94] P. Hahnfeldt, D. Panigrahy, J. Folkman, and L. Hlatky. Tumor development under angiogenic signaling. *Cancer research*, 59(19):4770–4775, 1999.

[95] A. Ouerdani, H. Struemper, A.B. Suttle, D. Ouellet, and B. Ribba. Preclinical modeling of tumor growth and angiogenesis inhibition to describe pazopanib clinical effects in renal cell carcinoma. *CPT: pharmacometrics & systems pharmacology*, 4(11):660–668, 2015.

[96] S. Wilson, M. Tod, A. Ouerdani, A. Emde, Y. Yarden, A. Adda Berkane, S. Kassour, M.X. Wei, G. Freyer, B. You, et al. Modeling and predicting optimal treatment scheduling between the antiangiogenic drug sunitinib and irinotecan in preclinical settings. *CPT: pharmacometrics & systems pharmacology*, 4(12):720–727, 2015.

[97] B. Ribba, E. Watkin, M. Tod, P. Girard, E. Grenier, B. You, E. Giraudo, and G. Freyer. A model of vascular tumour growth in mice combining longitudinal tumour size data with histological biomarkers. *European Journal of Cancer*, 47(3):479–490, 2011.

[98] N. Terranova, M. Germani, F. Del Bene, and P. Magni. A predictive pharmacokinetic–pharmacodynamic model of tumor growth kinetics in xenograft mice after administration of anticancer agents given in combination. *Cancer chemotherapy and pharmacology*, 72(2):471–482, 2013.

[99] M. Rocchetti, F. Del Bene, M. Germani, F. Fiorentini, I. Poggesi, E. Pesenti, P. Magni, and G. De Nicolao. Testing additivity of anticancer agents in pre-clinical studies: a pk/pd modelling approach. *European Journal of Cancer*, 45(18):3336–3346, 2009.

[100] M. Rocchetti, M. Germani, F. Del Bene, I. Poggesi, P. Magni, E. Pesenti, and G. De Nicolao. Predictive pharmacokinetic–pharmacodynamic modeling of tumor growth after administration of an anti-angiogenic agent, bevacizumab, as single-agent and combination therapy in tumor xenografts. *Cancer chemotherapy and pharmacology*, 71(5):1147–1157, 2013.

[101] M. Danhof, G. Alvan, S.G. Dahl, J. Kuhlmann, and G. Paintaud. Mechanism-based pharmacokinetic–pharmacodynamic modeling—a new classification of biomarkers. *Pharmaceutical research*, 22(9):1432–1437, 2005.

[102] S.A.G. Visser, M. Aurell, R.D.O. Jones, V.J.A. Schuck, A. Egnell, S.A. Peters, L. Brynne, J.W.T. Yates, R. Jansson-Löfmark, B. Tan, et al. Model-based drug discovery: implementation and impact. *Drug discovery today*, 18(15):764–775, 2013.

[103] N.L. Dayneka, V. Garg, and W.J. Jusko. Comparison of four basic models of indirect pharmacodynamic responses. *Journal of Pharmacokinetics and Pharmacodynamics*, 21(4):457–478, 1993.

[104] P. Ten Dijke, M.J. Goumans, F. Itoh, and S. Itoh. Regulation of cell proliferation by smad proteins. *Journal of cellular physiology*, 191(1):1–16, 2002.

[105] A. Sharma and W.J. Jusko. Characteristics of indirect pharmacodynamic models and applications to clinical drug responses. *British journal of clinical pharmacology*, 45(3):229–239, 1998.

[106] Amarnath Sharma, William F Ebling, and William J Jusko. Precursor-dependent indirect pharmacodynamic response model for tolerance and rebound phenomena. *Journal of pharmaceutical sciences*, 87(12):1577–1584, 1998.

[107] L. Salphati, H. Wong, M. Belvin, D. Bradford, K. A Edgar, W.W. Prior, D. Sampath, and J.J. Wallin. Pharmacokinetic-pharmacodynamic modeling of tumor growth inhibition and biomarker modulation by the novel phosphatidylinositol 3-kinase inhibitor gdc-0941. *Drug Metabolism and Disposition*, 38(9):1436–1442, 2010.

[108] J.A. Engelman. Targeting pi3k signalling in cancer: opportunities, challenges and limitations. *Nature reviews. Cancer*, 9(8):550, 2009.

[109] M.L. Sardu, I. Poggesi, and G. De Nicolao. Biomarker-versus drug-driven tumor growth inhibition models: an equivalence analysis. *Journal of pharmacokinetics and pharmacodynamics*, 42(6):611–626, 2015.

[110] Xi-wei Ji, Shuang-min Ji, Run-tao Li, Ke-hua Wu, Xiao Zhu, Wei Lu, and Tian-yan Zhou. Pharmacokinetic-pharmacodynamic modeling of the antitumor effect of tm208 and egfr-tki resistance in human breast cancer xenograft mice. *Acta Pharmacologica Sinica*, 37(6):825, 2016.

[111] M.I. Titze, O. Schaaf, M.H. Hofmann, M.P. Sanderson, S.K. Zahn, J. Quant, and T. Lehr. A comprehensive pharmacokinetic/pharmacodynamics analysis of the novel igf1r/insr inhibitor bi 893923 applying in vitro, in vivo and in silico modeling techniques. *Cancer chemotherapy and pharmacology*, 77(6):1303–1314, 2016.

[112] J.M. Harrold, R.M. Straubinger, and D.E. Mager. Combinatorial chemotherapeutic efficacy in non-hodgkin lymphoma can be predicted by a signaling model of cd20 pharmacodynamics. *Cancer research*, 72(7):1632–1641, 2012.

[113] G. Levy. Pharmacologic target-mediated drug disposition. *Clinical Pharmacology & Therapeutics*, 56(3):248–252, 1994.

[114] I. Poggesi, G. de Nicolao, M. Germani, and M. Rocchetti. Re: Antitumor efficacy testing in rodents. *JNCI: Journal of the National Cancer Institute*, 101(22):1592–1593, 2009.

[115] S. Yamazaki, J. Skaptason, D. Romero, J.H. Lee, H.Y. Zou, J.G. Christensen, J.R. Koup, B.J. Smith, and T. Koudriakova. Pharmacokinetic-pharmacodynamic modeling of biomarker response and tumor growth inhibition to an orally available cmet kinase inhibitor in human tumor xenograft mouse models. *Drug Metabolism and Disposition*, 36(7):1267–1274, 2008.

[116] S. Yamazaki, P. Vicini, Z. Shen, H.Y. Zou, J. Lee, Q. Li, J.G. Christensen, B.J. Smith, and B. Shetty. Pharmacoki-

netic/pharmacodynamic modeling of crizotinib for anaplastic lymphoma kinase inhibition and antitumor efficacy in human tumor xenograft mouse models. *Journal of Pharmacology and Experimental Therapeutics*, 340(3):549–557, 2012.

[117] S. Yamazaki, J.L. Lam, H.Y. Zou, H. Wang, T. Smeal, and P. Vicini. Mechanistic understanding of translational pharmacokinetic-pharmacodynamic relationships in nonclinical tumor models: a case study of orally available novel inhibitors of anaplastic lymphoma kinase. *Drug Metabolism and Disposition*, 43(1):54–62, 2015.

[118] S. Yamazaki, L. Nguyen, S. Vekich, Z. Shen, M.J. Yin, P.P. Mehta, P.P. Kung, and P. Vicini. Pharmacokinetic-pharmacodynamic modeling of biomarker response and tumor growth inhibition to an orally available heat shock protein 90 inhibitor in a human tumor xenograft mouse model. *Journal of Pharmacology and Experimental Therapeutics*, 338(3):964–973, 2011.

[119] S. Yamazaki. Translational pharmacokinetic-pharmacodynamic modeling from nonclinical to clinical development: a case study of anticancer drug, crizotinib. *The AAPS journal*, 15(2):354–366, 2013.

[120] M. Stroh, D.G. Duda, C.H. Takimoto, S. Yamazaki, and P. Vicini. Translation of anticancer efficacy from nonclinical models to the clinic. *CPT: pharmacometrics & systems pharmacology*, 3(8):1–4, 2014.

[121] G. Segre. Kinetics of interaction between drugs and biological systems. *Il Farmaco; edizione scientifica*, 23(10):907–918, 1968.

[122] L.B. Sheiner, D.R. Stanski, S. Vozeh, R.D. Miller, and J. Ham. Simultaneous modeling of pharmacokinetics and pharmacodynamics: application to d-tubocurarine. *Clinical Pharmacology & Therapeutics*, 25(3):358–371, 1979.

[123] S. Wang, Q. Zhou, and J.M. Gallo. Demonstration of the equivalent pharmacokinetic/pharmacodynamic dosing strategy in a multiple-dose study of gefitinib. *Molecular cancer therapeutics*, 8(6):1438–1447, 2009.

[124] C. Tanaka, T. O'Reilly, J.M. Kovarik, N. Shand, K. Hazell, I. Judson, E. Raymond, S. Zumstein-Mecker, C. Stephan, A. Boulay, et al. Identifying optimal biologic doses of everolimus (rad001) in patients with cancer based on the modeling of preclinical and clinical pharmacokinetic and pharmacodynamic data. *Journal of Clinical Oncology*, 26(10):1596–1602, 2008.

[125] E.F. Choo, M. Belvin, J. Boggs, Y. Deng, K.P. Hoeflich, J. Ly, M. Merchant, C. Orr, E. Plise, K. Robarge, et al. Preclinical disposition of gdc-0973 and prospective and retrospective analysis of human dose and efficacy predictions. *Drug Metabolism and Disposition*, 40(5):919–927, 2012.

[126] D.K. Shah, N. Haddish-Berhane, and A. Betts. Bench to bedside translation of antibody drug conjugates using a multiscale mechanistic pk/pd model: a case study with brentuximab-vedotin. *Journal of pharmacokinetics and pharmacodynamics*, 39(6):643–659, 2012.

[127] H. Wong, E.F. Choo, B. Alicke, X. Ding, H. La, E. McNamara, F.-P. Theil, J. Tibbitts, L. S Friedman, C.E.C.A. Hop, et al. Anti-tumor activity of targeted and cytotoxic agents in murine subcutaneous tumor models correlates with clinical response. *Clinical Cancer Research*, pages clincanres–0738, 2012.

[128] N. Haddish-Berhane, D.K. Shah, D. Ma, M. Leal, H.P. Gerber, P. Sapra, H.A. Barton, and A.M. Betts. On translation of antibody drug conjugates efficacy from mouse experimental tumors to the clinic: a pk/pd approach. *Journal of pharmacokinetics and pharmacodynamics*, 40(5):557–571, 2013.

[129] Z. P Parra-Guillen, P. Berraondo, B. Ribba, and I.F. Trocóniz. Modeling tumor response after combined administration of different immune-stimulatory agents. *Journal of Pharmacology and Experimental Therapeutics*, 346(3):432–442, 2013.

[130] N.L. Jumbe, Y. Xin, D. D Leipold, L. Crocker, D. Dugger, E. Mai, M.X. Sliwkowski, P.J. Fielder, and J. Tibbitts. Modeling the efficacy of trastuzumab-dm1, an antibody drug conjugate, in mice. *Journal of pharmacokinetics and pharmacodynamics*, 37(3):221–242, 2010.

[131] Alison M Betts, Nahor Haddish-Berhane, John Tolsma, Paul Jasper, Lindsay E King, Yongliang Sun, Subramanyam Chakrapani, Boris Shor, Joseph Boni, and Theodore R Johnson. Preclinical to clinical translation of antibody-drug conjugates using pk/pd modeling: a retrospective analysis of inotuzumab ozogamicin. *The AAPS journal*, 18(5):1101–1116, 2016.

[132] H. Wong, M. Belvin, S. Herter, K. P Hoeflich, L. J Murray, L. Wong, and E.F. Choo. Pharmacodynamics of 2-{4-[(1E)-1-(hydroxyimino)-2, 3-dihydro-1H-inden-5-yl]-3-(pyridine-4-yl)-1H-pyrazol-1-yl} ethan-1-ol (gdc-0879), a potent and selective b-raf kinase inhibitor: understanding relationships between systemic concentrations, phosphorylated mitogen-activated protein kinase kinase 1 inhibition, and efficacy. *Journal of Pharmacology and Experimental Therapeutics*, 329(1):360–367, 2009.

[133] S. Yamazaki, J. L Lam, H.Y. Zou, H. Wang, T. Smeal, and P. Vicini. Translational pharmacokinetic-pharmacodynamic modeling for an orally available novel inhibitor of anaplastic lymphoma kinase and c-ros oncogene 1. *Journal of Pharmacology and Experimental Therapeutics*, 351(1):67–76, 2014.

[134] G. Lestini, F. Mentré, and P. Magni. Optimal design for informative protocols in xenograft tumor growth inhibition experiments in mice. *The AAPS journal*, 18(5):1233–1243, 2016.

[135] P.B. Pierrillas, M. Tod, M. Amiel, M. Chenel, and E. Henin. Improvement of parameter estimations in tumor growth inhibition models on xenografted animals: a novel method to handle the interval censoring caused by measurement of smaller tumors. *The AAPS journal*, 18(2):404–415, 2016.

[136] P.B. Pierrillas, M. Tod, M. Amiel, M. Chenel, and E. Henin. Improvement of parameter estimations in tumor growth inhibition models on xenografted animals: handling sacrifice censoring and error caused by experimental measurement on larger tumor sizes. *The AAPS journal*, 18(5):1262–1272, 2016.

[137] M. Block. Physiologically based pharmacokinetic and pharmacodynamic modeling in cancer drug development: status, potential and gaps. *Expert opinion on drug metabolism & toxicology*, 11(5):743–756, 2015.

[138] S. Cheeti, N. R Budha, S. Rajan, M.J. Dresser, and J.Y. Jin. A physiologically based pharmacokinetic (pbpk) approach to evaluate pharmacokinetics in patients with cancer. *Biopharmaceutics & drug disposition*, 34(3):141–154, 2013.

[139] R.S. Kerbel. Antiangiogenic therapy: a universal chemosensitization strategy for cancer? *Science*, 312(5777):1171–1175, 2006.

[140] http://www.oncologiarimini.it/wp-content/uploads/2010/02/Farmaci-Antiblastici.pdf.

[141] *Modelling the effect of Sunitinib given alone and in combination with CPT-11 on the tumor growth in xenografted mice*, 2015.

[142] J.Ö. Haznedar, S. Patyna, C. L. Bello, G. W. Peng, W. Speed, X. Yu, Q. Zhang, J. Sukbuntherng, D. J. Sweeny, L. Antonian, et al. Single-and multiple-dose disposition kinetics of sunitinib malate, a multitargeted receptor tyrosine kinase inhibitor: comparative plasma kinetics in non-clinical species. *Cancer chemotherapy and pharmacology*, 64(4):691–706, 2009.

[143] C.E. Garnett, J. Y. Lee, and J.V.S. Gobburu. Contribution of modeling and simulation in the regulatory review and decision-making: Us fda perspective. In *Clinical Trial Simulations*, pages 37–57. Springer, 2011.

[144] J.V.S. Gobburu. Pharmacometrics 2020. *The Journal of Clinical Pharmacology*, 50(S9), 2010.

[145] S. Jönsson, A. Henningsson, M. Edholm, and T. Salmonson. Contribution of modeling and simulation studies in the regulatory review: a european regulatory perspective. In *Clinical Trial Simulations*, pages 15–36. Springer, 2011.

[146] B.C. Bender, E. Schindler, and L.E. Friberg. Population pharmacokinetic–pharmacodynamic modelling in oncology: a tool for predicting clinical response. *British journal of clinical pharmacology*, 79(1):56–71, 2015.

[147] L.E. Friberg. *Pharmacokinetic-Pharmacodynamic Modelling of Anticancer Drugs: Haematological Toxicity and Tumour Response in Hollow Fibres*. PhD thesis, Acta Universitatis Upsaliensis, 2003.

[148] C.H. Van Kesteren, R.A.A. Mathôt, J.H. Beijnen, and J.H.M. Schellens. Pharmacokinetic–pharmacodynamic guided trial design in oncology. *Investigational new drugs*, 21(2):225–241, 2003.

[149] D.R. Mould, A.C. Walz, T. Lave, J.P. Gibbs, and B. Frame. Developing exposure/response models for anticancer drug treatment: special considerations. *CPT: pharmacometrics & systems pharmacology*, 4(1):12–27, 2015.

[150] B. Ribba, G. Kaloshi, M. Peyre, D. Ricard, V. Calvez, M. Tod, B. Čajavec-Bernard, A. Idbaih, D. Psimaras, L. Dainese, et al. A tumor growth inhibition model for low-grade glioma treated with chemotherapy or radiotherapy. *Clinical Cancer Research*, 18(18):5071–5080, 2012.

[151] A. Lindauer, P. Di Gion, F. Kanefendt, D. Tomalik-Scharte, M. Kinzig, M. Rodamer, F. Dodos, F. Sörgel, U. Fuhr, and U. Jaehde. Pharmacokinetic/pharmacodynamic modeling of biomarker response to sunitinib in healthy volunteers. *Clinical Pharmacology & Therapeutics*, 87(5):601–608, 2010.

[152] L.E. Friberg, A. Henningsson, H. Maas, L. Nguyen, and M.O. Karlsson. Model of chemotherapy-induced myelosuppression with parameter consistency across drugs. *Journal of clinical oncology*, 20(24):4713–4721, 2002.

[153] A.L. Quartino, L.E. Friberg, and M.O. Karlsson. A simultaneous analysis of the time-course of leukocytes and neutrophils following docetaxel administration using a semi-mechanistic myelosuppression model. *Investigational new drugs*, 30(2):833–845, 2012.

[154] M. Rocchetti, I. Poggesi, M. Germani, F. Fiorentini, C. Pellizzoni, P. Zugnoni, E. Pesenti, M. Simeoni, and G. De Nicolao. A pharmacokinetic-pharmacodynamic model for predicting

tumour growth inhibition in mice: A useful tool in oncology drug development. *Basic & clinical pharmacology & toxicology*, 96(3):265–268, 2005.

[155] J.M. Gallo. Pharmacokinetic/pharmacodynamic-driven drug development. *Mount Sinai Journal of Medicine: A Journal of Translational and Personalized Medicine*, 77(4):381–388, 2010.

[156] R.H. Grantab and I.F. Tannock. Penetration of anticancer drugs through tumour tissue as a function of cellular packing density and interstitial fluid pressure and its modification by bortezomib. *BMC cancer*, 12(1):214, 2012.

[157] Y.H. Wei, L.Z. Xu, L. Liu, Q. Shen, and F.Z. Li. Microdialysis: a technique for pharmacokinetic-pharmacodynamic studies of oncological drugs. *Current pharmaceutical biotechnology*, 10(6):631–640, 2009.

[158] Q. Zhou and J.M. Gallo. In vivo microdialysis for pk and pd studies of anticancer drugs. *The AAPS journal*, 7(3):E659–E667, 2005.

[159] M. Hunz, A. Jetter, M. Warm, E. Pantke, M. Tuscher, G. Hempel, U. Jaehde, M. Untch, C. Kurbacher, and U. Fuhr. Plasma and tissue pharmacokinetics of epirubicin and paclitaxel in patients receiving neoadjuvant chemotherapy for locally advanced primary breast cancer. *Clinical Pharmacology & Therapeutics*, 81(5):659–668, 2007.

[160] S.N. Sani, K. Henry, M. Böhlke, J. Kim, A. Stricker-Krongrad, and T.J. Maher. The effects of drug transporter inhibitors on the pharmacokinetics and tissue distribution of methotrexate in normal and tumor-bearing mice: a microdialysis study. *Cancer chemotherapy and pharmacology*, 66(1):159–169, 2010.

[161] I. Fuso Nerini, L. Morosi, M. Zucchetti, A. Ballerini, R. Giavazzi, and M. D'incalci. Intratumor heterogeneity and its impact on drug distribution and sensitivity. *Clinical Pharmacology & Therapeutics*, 96(2):224–238, 2014.

[162] J. Sharma, H. Lv, and J.M. Gallo. Intratumoral modeling of gefitinib pharmacokinetics and pharmacodynamics in an orthotopic mouse model of glioblastoma. *Cancer research*, 73(16):5242–5252, 2013.

[163] P. Colin, L. De Smet, C. Vervaet, J.P. Remon, W. Ceelen, J. Van Bocxlaer, K. Boussery, and A. Vermeulen. A model based analysis of ipec dosing of paclitaxel in rats. *Pharmaceutical research*, 31(10):2876–2886, 2014.

[164] M.L. Slevin. The clinical pharmacology of etoposide. *Cancer*, 67(S1):319–329, 1991.

[165] G. Toffoli, G. Corona, R. Sorio, I. Robieux, B. Basso, A.M. Colussi, and M. Boiocchi. Population pharmacokinetics and pharmacodynamics of oral etoposide. *British journal of clinical pharmacology*, 52(5):511–519, 2001.

[166] S. Kaul, L.N. Igwemezie, D.J. Stewart, S.Z. Fields, M. Kosty, N. Levithan, R. Bukowski, D. Gandara, G. Goss, and P. O'Dwyer. Pharmacokinetics and bioequivalence of etoposide following intravenous administration of etoposide phosphate and etoposide in patients with solid tumors. *Journal of clinical oncology*, 13(11):2835–2841, 1995.

[167] M.C. Pigatto, B.V. de Araujo, B.G.S. Torres, S. Schmidt, P. Magni, and T. Dalla Costa. Population pharmacokinetic modeling of etoposide free concentrations in solid tumor. *Pharmaceutical research*, 33(7):1657–1670, 2016.

[168] Friederick. Acuc guidelines involving experimental neoplasia proposals in mice and rats. `https://ncifrederick.cancer.gov/Lasp/Acuc/Frederick/Media/Documents/ACUC14.pdf`, 2012.

[169] P. Dombernowsky and N.I. Nissen. Schedule dependency of yhe antileukemic activity of the podophyllotoxin-derivative vp16-213(nsc-141540) in l1210 leukemia. *APMIS*, 81(5):715–724, 1973.

[170] W.M. Liu and S.P. Joel. The schedule-dependent effects of etoposide in leukaemic cell lines: a function of concentration and duration. *Cancer chemotherapy and pharmacology*, 51(4):291–296, 2003.

[171] M.L. Slevin, P.I. Clark, S.P. Joel, S. Malik, R.J. Osborne, W.M. Gregory, D.G. Lowe, R.H. Reznek, and P.F. Wrigley. A randomized trial to evaluate the effect of schedule on the activity of etoposide in small-cell lung cancer. *Journal of Clinical Oncology*, 7(9):1333–1340, 1989.

[172] K.R. Hande. The importance of drug scheduling in cancer chemotherapy: etoposide as an example. *The oncologist*, 1(4):234–239, 1996.

[173] S.P. Joel and M.L. Slevin. Schedule-dependent topoisomerase ii-inhibiting drugs. *Cancer chemotherapy and pharmacology*, 34:S84–S88, 1994.

[174] T. Iwatsubo, H. Suzuki, and Y. Sugiyama. Prediction of species differences (rats, dogs, humans) in thein vivo metabolic clearance of ym796 by the liver fromin vitro data. *Journal of Pharmacology and Experimental Therapeutics*, 283(2):462–469, 1997.

[175] Y. Naritomi, S. Terashita, A. Kagayama, and Y. Sugiyama. Utility of hepatocytes in predicting drug metabolism: comparison of hepatic intrinsic clearance in rats and humans in vivo and in vitro. *Drug Metabolism and Disposition*, 31(5):580–588, 2003.

List of publications

Articles in peer reviewed journals

- L. Carrara, S.M. Lavezzi, E. Borella, G. De Nicolao, P. Magni, I. Poggesi. Current mathematical models for cancer drug discovery. *Expert opinion on drug discovery,* 12(8): 785-799, 2017.

- S.M. Lavezzi, E. Borella, L. Carrara, G. De Nicolao, P. Magni, I. Poggesi. Current mathematical models for cancer drug development. *Expert opinion on drug discovery,* 13(1):5-21, 2018.

- M.K. Smith, S. Moodie, R. Bizzotto, E. Blaudez, E. Borella, L. Carrara, P. Chan, M. Chenel, E. Comets, R. Gieschke, K. Harling, L. Harnisch, N. Hartung, A. Hooker, M.O. Karlsson, R. Kaye, C. Kloft, N. Kokash, M. Lavielle, G. Lestini, P. Magni, A. Mari, F. Mentre, C. Muselle, R. Nordgren, H. Nyberg, Z.P. Parra-Guillen, L. Pasotti, N. Rode-Kristensen, M.L. Sardu, G. Smith, M.J. Swat, N. Terranova, G. Yngman, F. Yvon, N. Holford. Model Description Language (MDL): A standard for modelling and simulation. *CPT:PSP,* 6(10):647-659, 2017.

- M.C. Pigatto, R.M. Roman, L. Carrara, A. Buffon, P. Magni, T. Dalla Costa. Pharmacokinetic/pharmacodynamic modeling of etoposide tumor growth inhibitory effect in Walker-256 tumor-bearing rat model using free intratumoral drug concentrations. *European Journal of Pharmaceutical Sciences,* 97:70-78, 2017.

Contributions to conference proceedings

- L. Carrara, P. Magni, D. Teutonico, O. Della Pasqua, F. Kloprogge. Which data are necessary to build a WB-PBPK model that accurately predicts exposure in the lung? A case study using ethambutol for tuberculosis treatment. *Proceedings of the PAGE Meeting.* June 6-9, 2017, Budapest (Hungary).

- E. Borella, L. Carrara, S.M. Lavezzi, I. Massaiu, E. Sauta, E.M. Tosca, F. Vitali, S. Zucca, L. Pasotti, G. De Nicolao, P. Magni. Methods and tools for multiscale modelling in Systems Pharmacology: a review. *Proceedings of the PAGE Meeting,* June 7-10, 2016, Lisboa (Portugal).

- M.K. Smith, S. Moodie, R. Bizzotto, E. Blaudez, E. Borella, L. Carrara, P. Chan, M. Chenel, E. Comets, R. Gieschke, K. Harling, L. Harnisch, N. Hartung, A. Hooker, M.O. Karlsson, R. Kaye, C. Kloft, N. Kokash, M. Lavielle, P. Magni, A. Mari, F. Mentre, C. Muselle, R. Nordgren, H. Nyberg, Z.P. Parra-Guillen, L. Pasotti, N. Rode-Kristensen, G. Smith, M.J. Swat, N. Terranova, F. Yvon, N. Holford. Model Description Language (MDL) - a standard for model communication and interoperability. *Proceedings of the PAGE Meeting,* June 7-10, 2016, Lisboa (Portugal).

- L. Carrara, B. Ribba, M. Tod, M. Wei, B. You, G. Freyer, P.

Magni. Modelling the effect of Sunitinib given alone and in combination with CPT-11 on the tumor growth in xenografted mice. *Proceedings of the PAGE Meeting,* June 2-5, 2015, Hersonisson (Crete).

- E. Borella, L. Carrara, S.M. Lavezzi, E. Mezzalana, L. Pasotti, G. De Nicolao, P. Magni. Evaluation of software tools for Bayesian estimation on population models with count and continuous data. *Proceedings of the PAGE Meeting,* June 2-5, 2015, Hersonisson (Crete).

- M. Pigatto, R.M. Roman, L. Carrara P. Magni, T. Dalla Costa. PK/PD modeling of tumor growth inhibition after etoposide administration in vitro and to tumor-bearing rats. *Proceedings of the PAGE Meeting,* June 2-5, 2015, Hersonisson (Crete).